P
2mt

NASA TECHNICAL NOTE

NASA TN D-7547

D-7547

SATELLITE VIEWS OF HURRICANE CAMILLE

by William E. Shenk and Edward B. Rodgers

Goddard Space Flight Center
Greenbelt, Md. 20771

NATIONAL AERONAUTICS AND SPACE ADMINISTRATION • WASHINGTON, D. C. • APRIL 1974

1. Report No.	2. Government Accession No.	3. Recipient's Catalog No.
D-7547		

4. Title and Subtitle	5. Report Date
Satellite Views of Hurricane Camille	APRIL 1974
	6. Performing Organization Code: 650

7. Author(s)	8. Performing Organization Report No.
William E. Shenk and Edward B. Rodgers	G-7405

9. Performing Organization Name and Address	10. Work Unit No.
Goddard Space Flight Center Greenbelt, Maryland 20771	039-23-01-01
	11. Contract or Grant No.
	13. Type of Report and Period Covered: Technical Note
12. Sponsoring Agency Name and Address National Aeronautics and Space Administration Washington, D. C. 20546	14. Sponsoring Agency Code

15. Supplementary Notes

16. Abstract

Three periods within the life cycle of Hurricane Camille (1969) are studied with radiometric and camera measurements from Nimbus-3 and camera information from ATS-3 in conjunction with conventional information. These periods are the deepening phase, the interaction of Camille with midlatitude westerlies, and the excessive rain producing period when the cyclone was over the central Appalachian Mountains. Just prior to significant deepening, the Nimbus-3 Medium Resolution Infrared Radiometer (MRIR) showed that a pronounced feeder band had formed southeast of the center which was associated with the rapid transport of moisture into the storm circulation. During the rapid deepening phase the MRIR measurements indicated the development of large-scale subsidence throughout the troposphere northwest of the center. When Camille was over the lower Mississippi Valley it acted as an obstruction to the environmental wind. A region of widespread subsidence was created west and north of the cyclone center. Increased cloud-top elevations, back to the levels reached when Camille was an intense cyclone over the Gulf of Mexico, were estimated from the Nimbus-3 High Resolution Infrared Radiometer (HRIR) measurements on August 20, 1969, when Camille produced rains of major flood proportions near the east slopes of the Appalachians in central Virginia.

17. Key Words (Selected by Author(s))	18. Distribution Statement
Hurricane analysis; Radiation measurements; Geophysics; Meteorology	Unclassified—Unlimited Cat. 20

19. Security Classif. (of this report)	20. Security Classif. (of this page)	21. No. of Pages	22. Price*
Unclassified	Unclassified	43	$4.00

*For sale by the National Technical Information Service, Springfield, Virginia 22151.

CONTENTS

SATELLITE VIEWS OF HURRICANE CAMILLE

William E. Shenk
Goddard Space Flight Center
and
Edward B. Rodgers
Environmental Research and Technology, Inc.

INTRODUCTION

From a meteorological point of view, Hurricane Camille was the most important Atlantic hurricane of record (Reference 1). As it crossed the Gulf Coast the highest storm tides on record were produced (7.5 m (24.6 ft)). No recording anemometer equipment was able to survive in the area of maximum winds as the cyclone moved ashore. Velocities approaching 175 kn were estimated from an appraisal of the damage within a few hundred yards of the coast. The minimum central pressure of 905 mbar was second only to the Florida Keys storm of 1935 (892 mbar) for Atlantic hurricanes. Whereas the Florida Keys storm probably had higher maximum winds than Camille, the diameter of hurricane winds was less than 100 km (62 miles) as compared to 160 to 240 km (100 to 150 miles) for Camille.

Camille began to develop near the island of Grand Cayman from a tropical disturbance which moved westward across the Atlantic from the African Coast (Figure 1). The cyclone deepened rapidly as it passed over the western tip of Cuba into the Gulf, and it reached maximum intensity by 0000 GMT on August 17, 1969. This intensity was maintained with little apparent fluctuation as observed by reconnaissance aircraft until the center reached the coast at 0430 GMT on August 18. Within 12 hours the winds had decreased to less than hurricane strength as the cyclone moved northward through Mississippi. For the next 36 hours the remains moved north, then east, with the winds and rains diminishing in the typical history of a tropical cyclone moving away from its moisture source. Suddenly, excessive rainfall began over the central Appalachians in response to an injection of extremely moist air at low levels, an unstable lapse rate, and topography (Reference 2). This portion of Camille's history is similar to that of Hurricane Diane in 1955 that produced massive flooding in New England after Diane had weakened considerably when it moved across the Carolinas and Virginia. Camille briefly regained tropical storm strength after moving eastward off the Atlantic Coast near Norfolk, but interaction with a cold front caused the cyclone to become extratropical.

Throughout the important phases of Camille's life cycle the storm was observed by meteorological satellites such as Nimbus-3, ATS-3, and operational satellites. This outstanding coverage, along with conventional measurements, permitted the examination in some detail of three important events in the history of Camille which were: (a) the rapid deepening phase; (b) the interaction with the midlatitude westerlies as the cyclone moved inland; and (c) the development of the heavy rains over the central Appalachians.

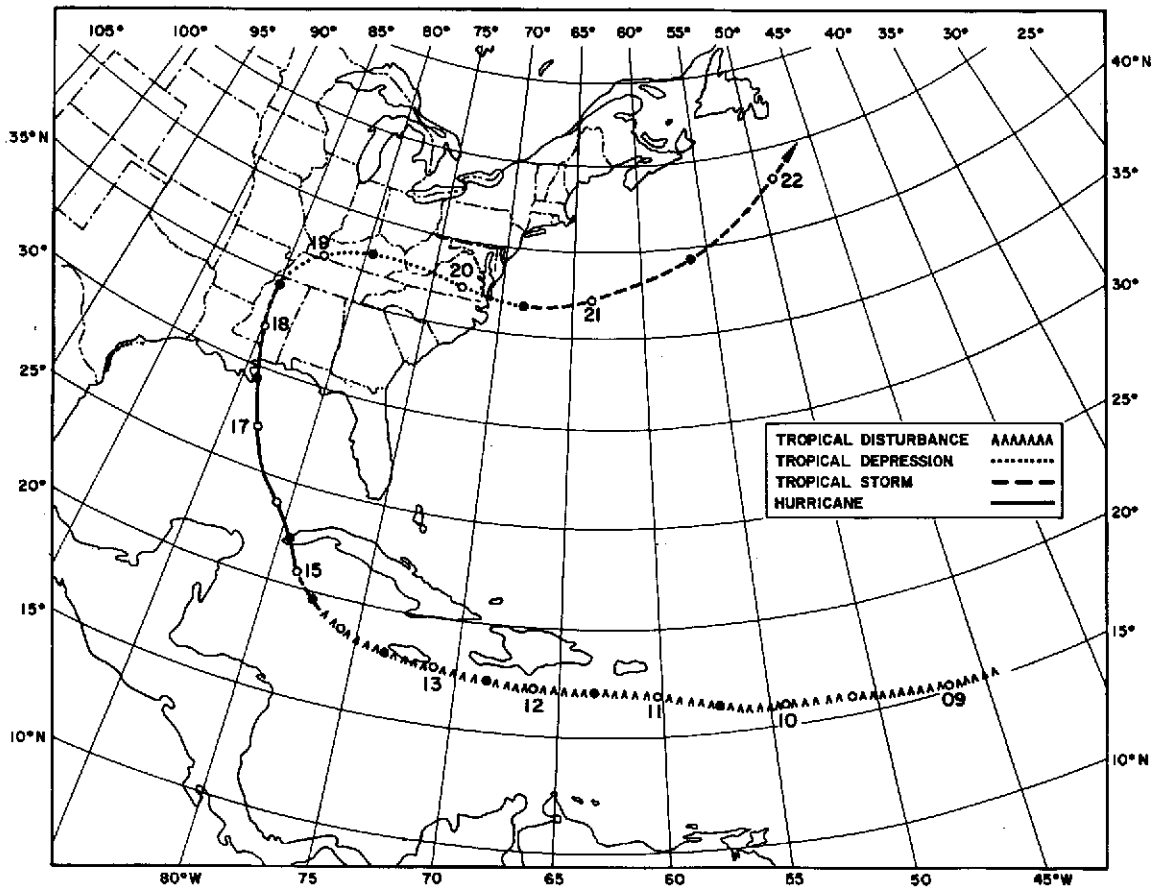

Figure 1. Track and development stages of Hurricane Camille from August 9 to 22, 1969. (Extracted from Monthly Weather Review, Vol. 98, No. 4, April 1970, p. 294.)

AVAILABLE DATA AND MAPPING PROCEDURES

Radiometric measurements with a 55-km subsatellite-track spatial resolution were taken at 12-hr intervals by the Nimbus-3 Medium Resolution Infrared Radiometer (MRIR) in five spectral regions. Four of these were spectrally located at 0.2 to 4.0 μm, 6.5 to 7.0 μm, 10 to 11 μm, and 20 to 23 μm. The first channel measures nearly all of the reflected energy, the third is in an infrared atmospheric window, and the second and fourth measure the emitted energy in regions of moderate to strong water vapor absorption. Figure 2 shows the layers of a mean tropical cloudless atmosphere that contribute to the sensed radiance in each of the three infrared spectral intervals. The emission in the 6.5- to 7.0-μm region primarily comes from the upper troposphere, whereas the 20- to 23-μm emission emanates mostly from the middle troposphere, and the 10- to 11-μm radiance nearly all comes from the surface and lower troposphere.

Nimbus-3 High Resolution Infrared Radiometer (HRIR) nighttime emission measurements were made at 3.5 to 4.1 μm with a 9-km subsatellite-track spatial resolution. Further

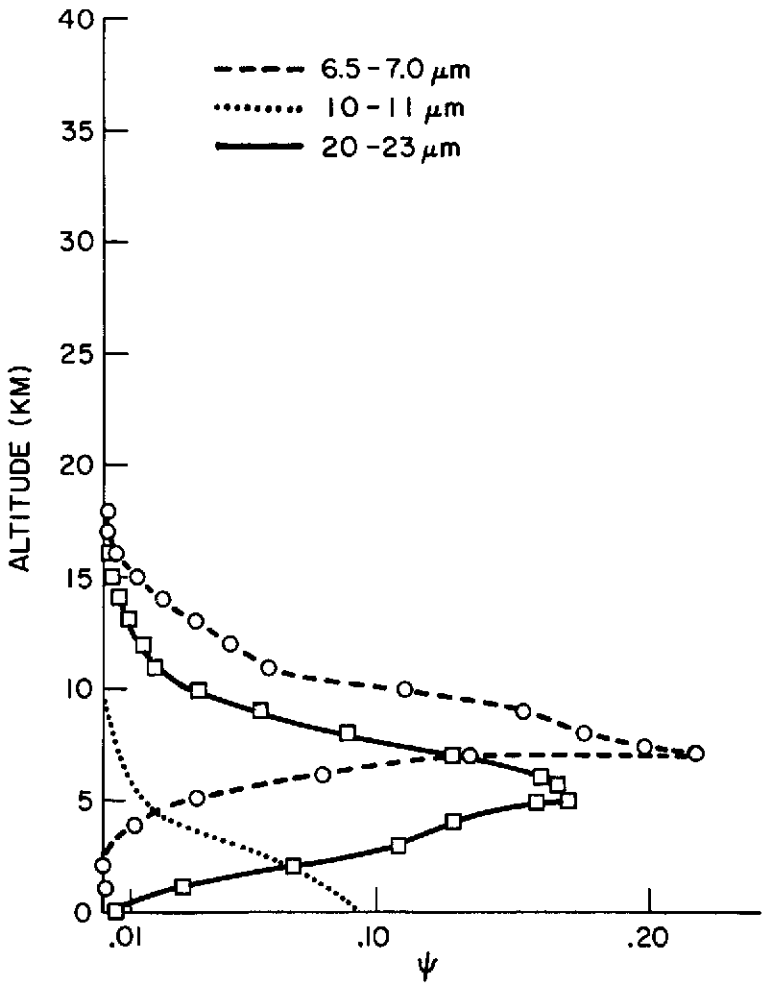

Figure 2. Weighting function (ψ) curves (ψ units are w/cm^2 ster cm^{-1} km normalized to unity) determined from radiative transfer theory based on a mean tropical atmosphere for three Nimbus MRIR channels (6.5 to 7.0 μm, 10 to 11 μm, and 20 to 23 μm).

details of the Nimbus-3 satellite and the instrumentation is provided in the Nimbus-3 Users' Guide (Reference 3).

Visible measurements were obtained at 11-min intervals from the Multicolor Spin Scan Cloud Camera (MSSCC) on ATS-3. Due to the frequent observations, it was possible to track the motions of individual cloud elements to determine the wind. The clouds were classified as high or low, depending on their appearance and motion; the high clouds most likely indicating the air motion near 200 mbar and the low clouds near 850 mbar. Some middle clouds may have inadvertently been included, especially in the high-cloud sample. Hubert and Whitney (Reference 4) have discussed cloud motion-wind accuracies from ATS data. More information on the ATS-3 satellite and the MSSCC can be found in the ATS Users' Guide and catalog publication series.

Conventional radiosonde and surface observations were obtained every 12 hours from 0000 GMT on August 14 to 1200 GMT on August 20, 1969. The radiosonde information was analyzed over the Gulf of Mexico, the Caribbean, and the United States at the standard pressure levels (850, 700, 500, 300, and 200 mbar), except for the observations of 1200 GMT on August 18 and 0000 GMT on August 19. At these times, charts were constructed over the United States every 50 mbar from the surface to 100 mbar and at the 70-, 50-, 30-, and 20-mbar levels. This permitted a more detailed examination of Camille and its interaction with the westerlies after the cyclone had moved inland.

The Nimbus radiation measurements were mapped in the stereographic horizon map projection (Reference 5) where the center of Camille was always placed at the center of the map. Thus, Camille was mapped (but not viewed) in the same perspective throughout the period of interest. A correction was applied to the measurements from the water vapor channels (6.5 to 7.0 μm and 20 to 23 μm) to compensate for limb-darkening effects.* The correction varied from zero to several degrees Kelvin for equivalent blackbody temperatures (T_{BB}'s) measured at a nadir angle of 50° (the maximum allowed).

RESULTS

Rapid Deepening Phase

The first significant event in the life of Camille was the rapid deepening that occurred before and after the cyclone center passed over the western tip of Cuba. An interpretation of the time history of the minimum central pressure curve is shown in Figure 3. There is a suggestion of two periods of deepening. The first primarily occurred between 1200 GMT on August 14 and 15. Four closely spaced reconnaissance aircraft reports centered at about 1200 GMT on August 15 all reported a minimum pressure of about 965 mbar. Shortly thereafter the center crossed the southern coast of Cuba near the western tip. It took approximately 3 hours for the eye to move to the northern coast. During this time the shape of the minimum pressure curve is more uncertain, but since most of the cyclone's circulation remained over the water it is likely that the rise, if any, in the central pressure was small.

There were no reconnaissance penetrations of the eye for 18 hours after Camille left the Cuban Coast. At 0500 GMT on August 16 Nimbus-3 passed overhead with an almost vertical view of the storm.

Figure 4 depicts the cloud shield of Camille with HRIR measurements (1:2,000,000 map scale) 4 hours after the center moved off the Cuban Coast. Two features suggest that further deepening had begun. First is the appearance of a well-defined eye as indicated by T_{BB}'s as high as 287 K (the insert in Figure 4 depicts a small area near the center mapped at 1:500,000). This measurement could have been caused by either near transparent cirrus

*V. V. Salomonson, personal communication, 1972.

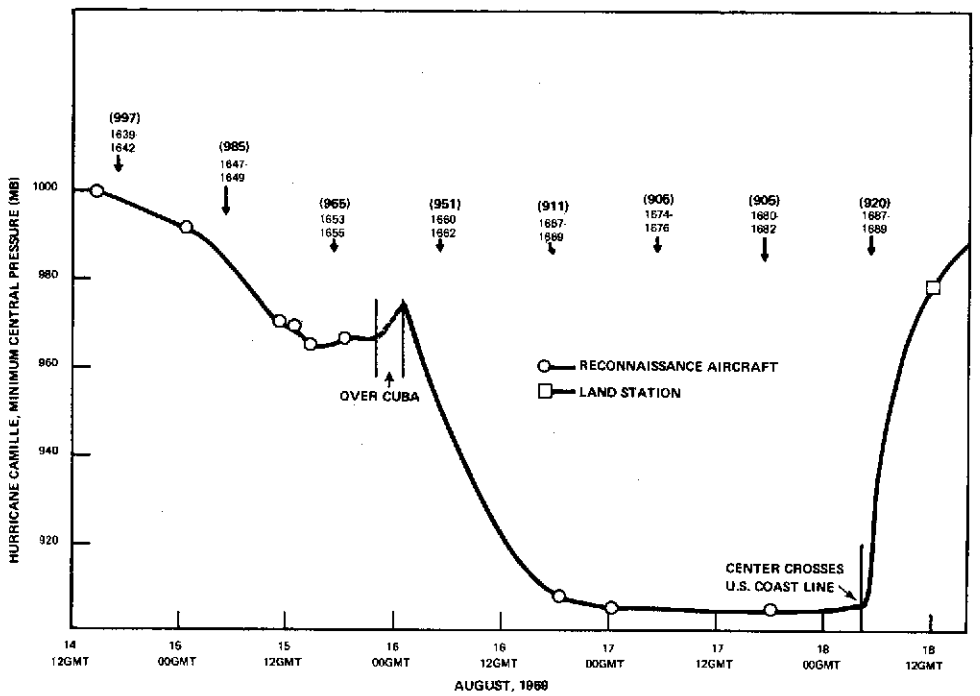

Figure 3. A trace of the minimum central pressure for Hurricane Camille from 1200 GMT on August 14 to 1800 GMT on August 18, 1969. The estimated central pressures and the Nimbus-3 orbit numbers are shown above each of the arrows that indicates the time of a Nimbus-3 overpass.

and/or low clouds, or a partially filled radiometer field of view with any of the above cloud combinations. Second, a ring of very low T_{RR}'s ($\leqslant 210$ K), indicating the opaque storm cloudiness, surrounds the eye except to the west. This ring represents the highest clouds associated with the wall cloud where the lowest (and probably the weakest) portion is on the west side.

With the satellite evidence of a nearly clear eye (in the radiometric sense) and a strong wall cloud that almost encircled the eye, the rapid deepening was shown in Figure 3 to commence immediately after the storm moved off the Cuban Coast. No reconnaissance reports were available until 1800 GMT on August 16 when Camille had reached severe status, an intensity that the aircraft central pressure measurements would indicate was maintained until the cyclone crossed the U. S. coastline. Thereafter, the central pressure rose rapidly; the Jackson, Mississippi, minimum pressure was 978 mbar as the center passed about 35 km east of the station at 1200 GMT on August 18.

Perhaps the best day and night satellite observations of Camille during the rapid deepening phase were made by the Nimbus-3 MRIR. By examining the information from the three infrared channels at 12-hr intervals and the visible channel data every 24 hours, it was anticipated that the changes in the structure of Camille as it became a severe cyclone could

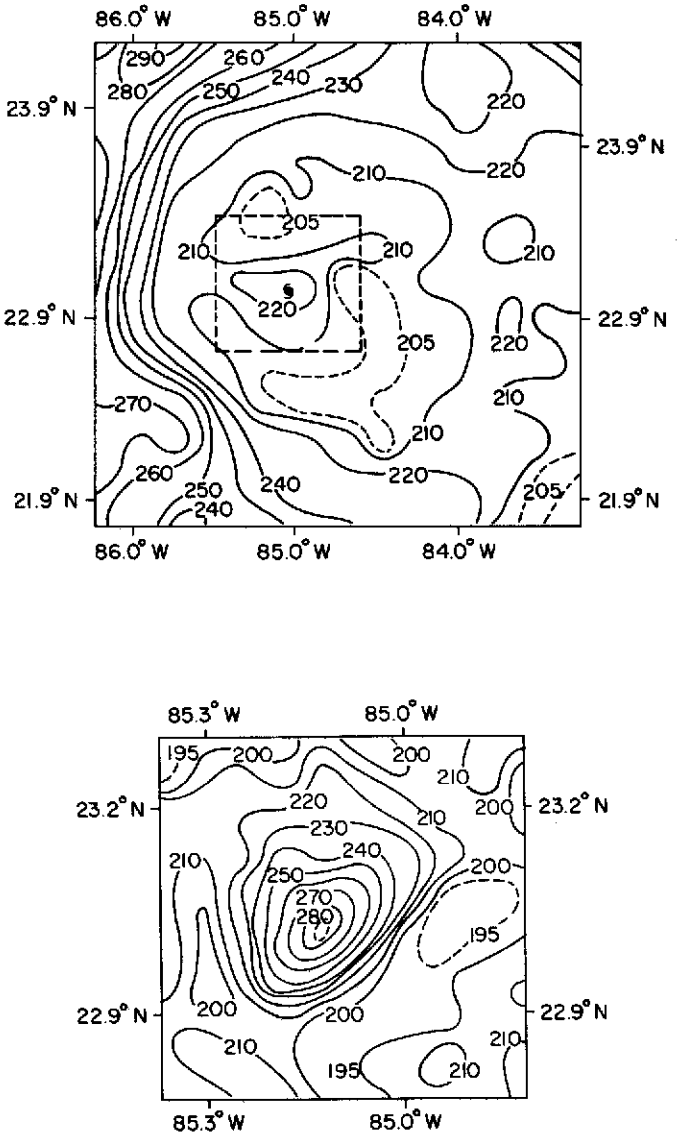

Figure 4. Two views of the interior portion of the cloud structure of Hurricane Camille at 0500 GMT on August 16, 1969, as depicted by the 3.5- to 4.1-μm equivalent blackbody temperatures (T_{BB}'s) from the Nimbus-3 HRIR. The top picture was mapped at a 1:2 million scale while the insert over the eye seen in the bottom picture (the area within the dashed box in the top picture) was mapped at a 1:500,000 scale.

be determined. The daytime observations were combined with the ATS-3 cloud motions to obtain a more complete picture of the circulation.

August 14, 1969

On August 14, Camille advanced from a tropical disturbance to a tropical storm. The first MRIR observations were taken between 0300 and 0700 GMT on August 14 (a composite of three orbits) and Figure 5 shows the 10- to 11-μm T_{BB}'s over a large region surrounding the center at 18° N, 80° W. Already the cyclone cloud pattern exhibits a definite spiral configuration. However, there appear to be only two small regions to the east of the center where deep convection is occurring. The deep convection associated with the intertropical convergence zone (ITCZ) is seen to extend from the ITCZ toward Camille. Another band of intense cloudiness about 1000 km north of Camille is connected with a strong easterly wave approaching Florida. A feeder band with clouds reaching the middle and upper troposphere is located to the southeast and the south of the cyclone center. In the semicircle to the west of the center there is a large region where 10- to 11-μm T_{BB}'s are $\geqslant$ 290 K with some as high as 295 K, which, when corrected for the effects of a tropical atmosphere by adding 6 to 8 K, are very close to the 302- to 304-K sea surface temperatures reported by ships. Other large areas of $\geqslant$ 290-K T_{BB}'s are found northeast and northwest of Camille well away from the cyclone circulation. These high T_{BB}'s indicate that the amount and/or the vertical development of low level cumulus was being suppressed, probably due to subsidence in the lower troposphere.

This method of inferring subsidence has the limitation that once the clouds have been substantially suppressed or eliminated there is no further information on the strength of the subsidence. Once the clouds are gone it is not possible to use cloud tracking from geosynchronous satellite measurements to implement kinematic techniques of calculating the vertical motion. However, the information from the water vapor channels offers a possible method for inferring subsidence in clear air in the middle and upper troposphere. This is possible because the emission will come from lower in the atmosphere as the temperature and dewpoint spread increases, and therefore the T_{BB}'s will also increase. These regions of dry air, characterized by high 6.5- to 7.0-μm T_{BB}'s, are associated either with areas of subsidence or horizontal advection (Reference 6). Subsidence is indicated when a local change in clear air T_{BB} to a higher measurement has occurred where the possibility of the advection of the dry air was small. Even in the advection case, the vertical motion is almost certain to be small or downward since upward motion would produce clouds or a more moist atmosphere.

Figures 6 and 7, respectively, depict the 6.5- to 7.0-μm and 20- to 23-μm measurements for the same time as Figure 5. The relatively high 6.5- to 7.0-μm T_{BB} areas generally coincide with the areas of high T_{BB}'s in the 10- to 11-μm channel. However, there are some regions where this does not occur. Whereas the high 10- to 11-μm T_{BB}'s are about the same for the regions where at least low level subsidence is inferred, the 6.5-to 7.0-μm T_{BB}'s are not nearly as high west of Camille as to the northeast and northwest of the cyclone. The strongest upper tropospheric subsidence is inferred northwest of Camille where there is evidence of 200-mbar horizontal speed convergence (Figure 8) over the Southern Plains and New Mexico, and an area of relatively high temperatures at 300 mbar

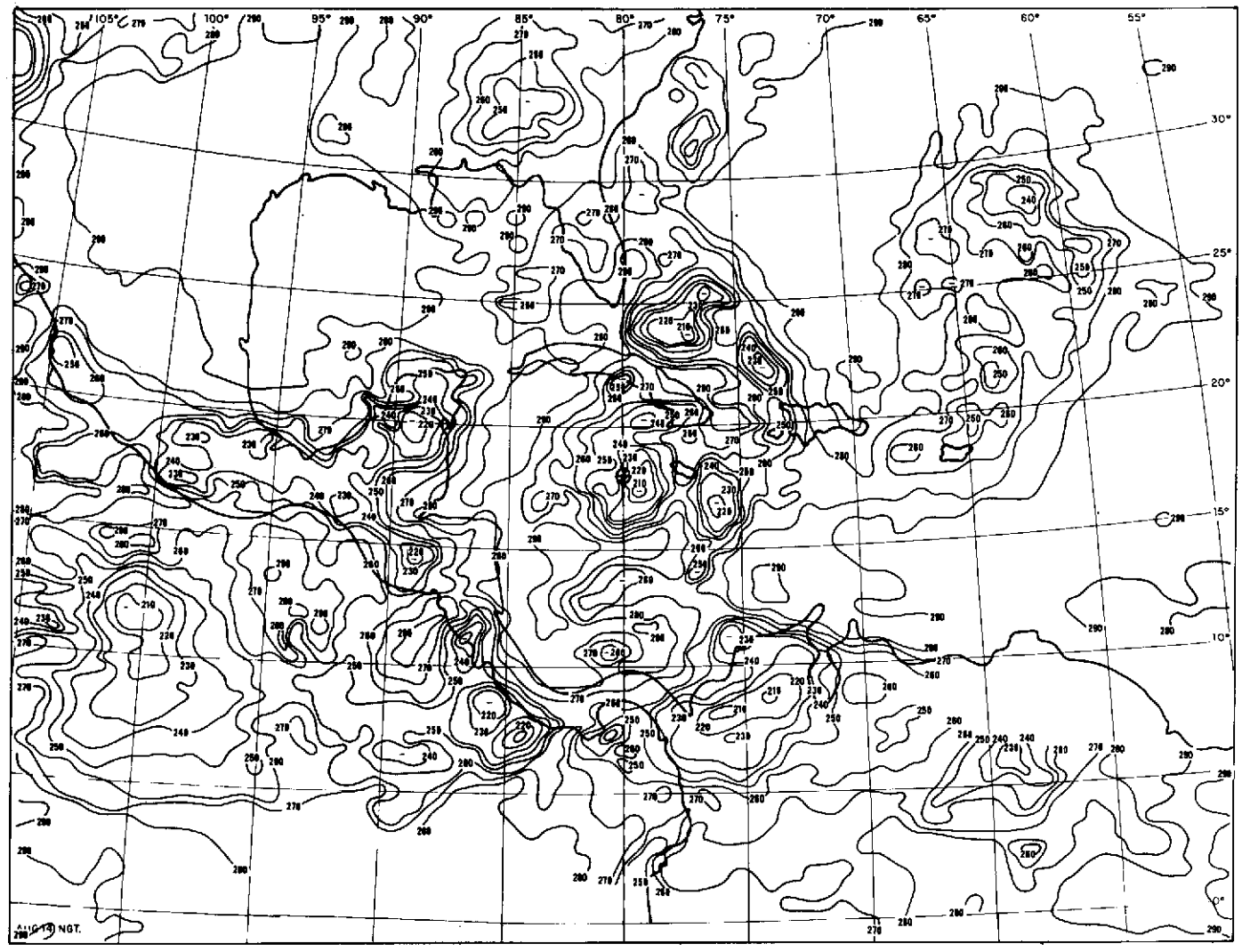

Figure 5. Hurricane Camille at 0300 to 0700 GMT on August 14, 1969, as depicted by 10- to 11-μm T_{BB}'s from the MRIR sensor. The isotherms are given in K and the cyclone center is indicated by the circled cross.

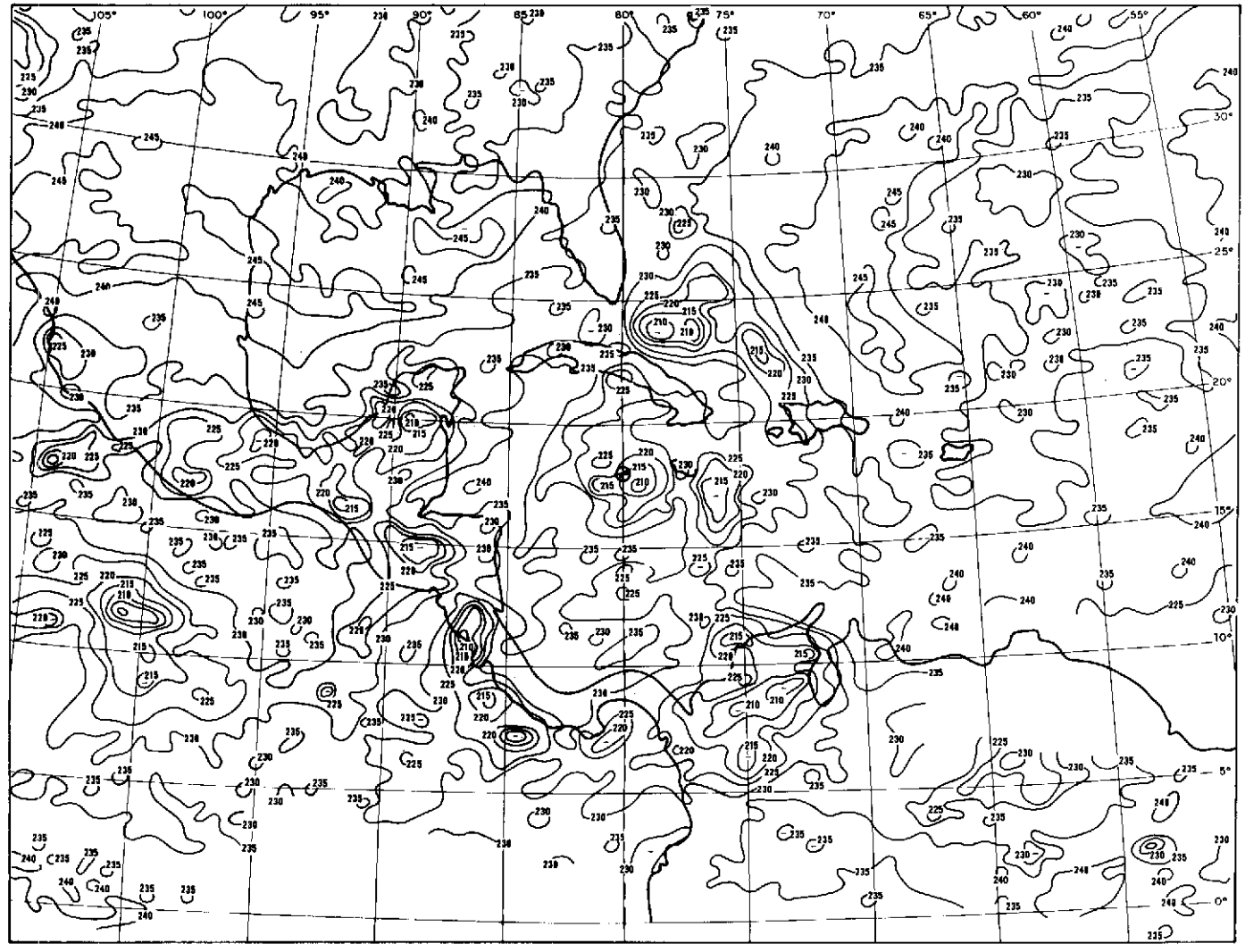

Figure 6. Hurricane Camille at 0300 to 0700 GMT on August 14, 1969, as depicted by 6.5- to 7.0-μm T_{BB}'s from the MRIR sensor. The isotherms are given in K and the cyclone center is indicated by the circled cross.

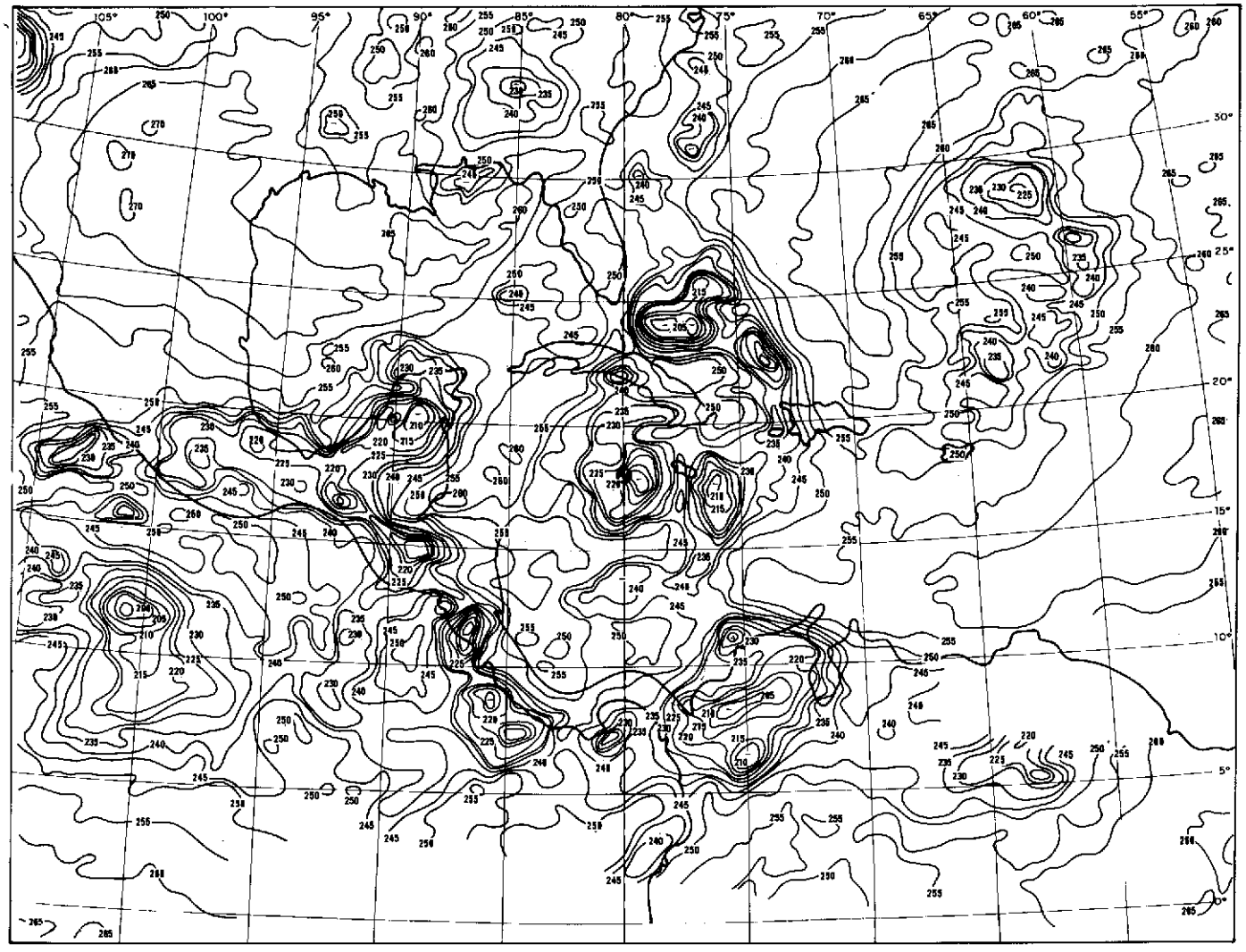

Figure 7. Hurricane Camille at 0300 to 0700 GMT on August 14, 1969, as depicted by 20- to 23-μm T_{BB}'s from the MRIR sensor. The isotherms are given in K and the cyclone center is indicated by the circled cross.

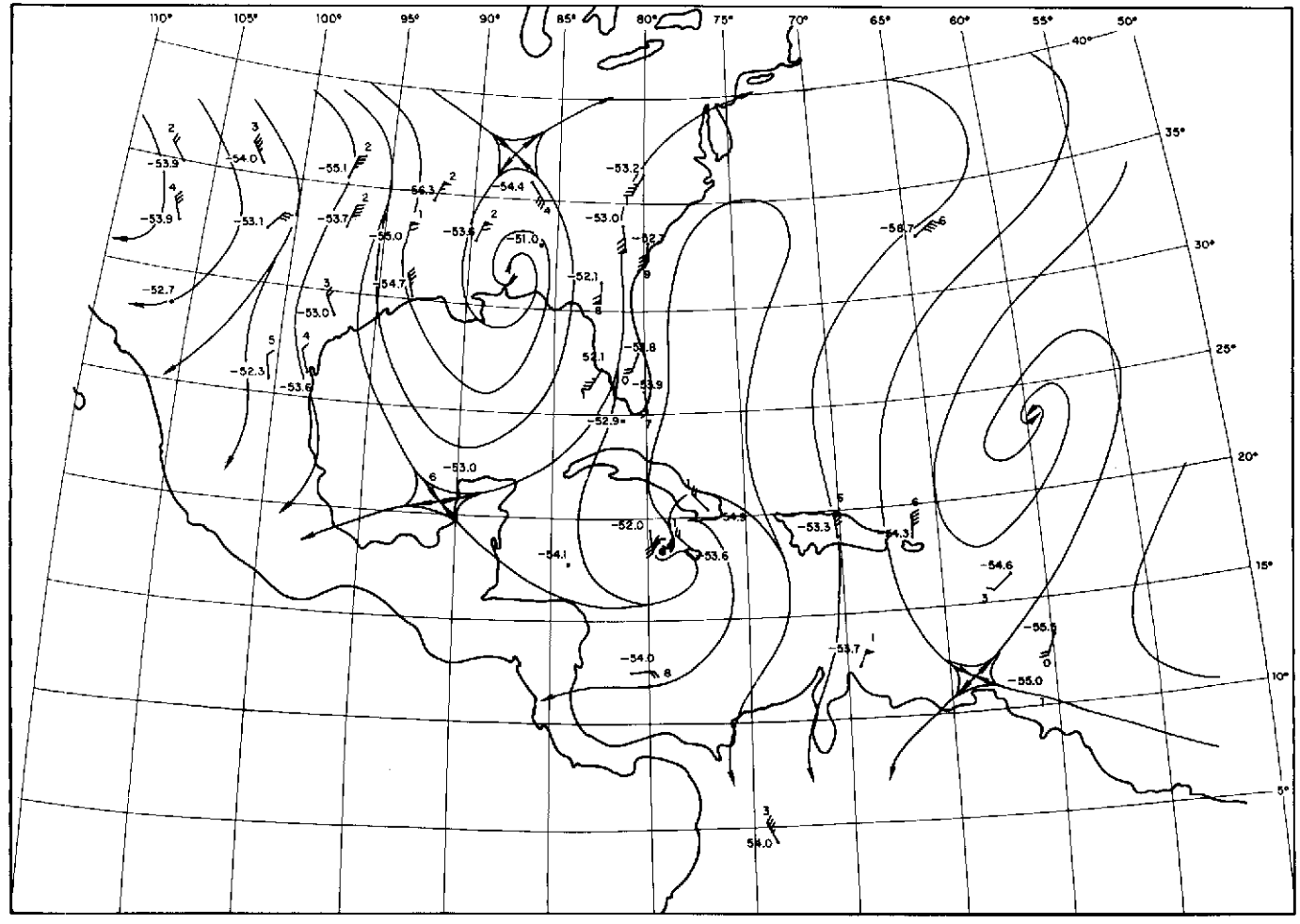

Figure 8. 200-mbar radiosonde data and streamline analysis for 1200 GMT on August 14, 1969.

below the higher level horizontal convergence. Northeast of Camille the inferred subsidence was most likely produced by a ridge line between the strong southerly flow over Florida and the northerly flow at Bermuda. Whereas the 10- to 11-μm measurements indicated a continuous band of high T_{BB} measurements at the northern end of this area, the high 6.5- to 7.0-μm T_{BB}'s shows that the driest air was mostly west and east of the cloud circulation. The relatively high 6.5- to 7.0-μm T_{BB}'s west of the main cloud-shield associated with Camille were not even high enough to be reasonably certain that cirrus clouds were not present. A comparison of high-altitude aircraft cloud photography and Nimbus-3, 6.5- to 7.0-μm T_{BB}'s over the tropics has indicated that when the T_{BB} range was 235 to 237 K the cirrus probability was 40 percent (Reference 7). Thus, the subsidence, if any, west of Camille was probably in response to the low-level inflow and rising motion within the inner portion of the circulation.

From the analysis of the aircraft photography, it was found that 6.5- to 7.0-μm T_{BB}'s of $\leqslant$230 K in the tropics were associated with cirrus clouds. Thus the area of $\leqslant$230-K T_{BB} measurements outlines at least the minimum area of the cirrus shield which covered a much larger region than the areas of deep convection that were noted in Figure 5. The 200-mbar chart for 1200 GMT on August 14 (Figure 8) shows the southerly flow from Jamaica northward to the Carolinas with a break in the data continuity over Cuba. It is important to know if this southerly flow is continuous and if the upper tropospheric air ejected from Camille had begun to move northward in response to what appears to be a favorable pattern for the ventilation of the upper tropospheric air away from the storm. The radiation data cannot determine the continuity of the wind field but the cirrus shield pattern shows a minor break between the storm shield and the cirrus associated with the easterly wave further north. This suggests that a substantial outflow had not begun in that direction. Essentially the same large-scale features are seen in the 20- to 23-μm measurements (Figure 7) as in the 6.5- to 7.0-μm data.

Twelve hours later (1500 to 1900 GMT on August 14) Camille had almost reached tropical storm status. The 10- to 11-μm T_{BB} map (Figure 9) indicates that the cyclone was more organized with an almost circular cloud shield where the deepest convection was in a curved line north and west of the storm center. The area of $\leqslant$ 234 K T_{BB}'s extended over a much larger region than before. However, despite the areal increase in cloud development, the highest cloud tops (lowest T_{BB}'s) reached to about the same levels. Equivalent blackbody temperatures of $\geqslant$ 290 K had persisted on the western semicircle, reflecting the low cloudiness suppression noted earlier (the $\geqslant$300-K measurements northwest of Camille are caused by strong heating of the land during the daytime).

The 6.5- to 7.0-μm (Figure 10) and 20- to 23-μm channels (not shown) indicate that the 12-hr change in the inferred weak subsidence region west of Camille's center had expanded and strengthened slightly. Measurements of 238 to 240 K appeared in contrast to the 235- to 237-K range 12 hours earlier. Based on the aircraft flights, the cirrus probability had dropped to about 15 percent. Figure 10 also shows that the cirrus north of the center was continuous and a little thicker (and/or higher) than before, which suggests that the upper tropospheric ventilation had become more effective. Also, the northern

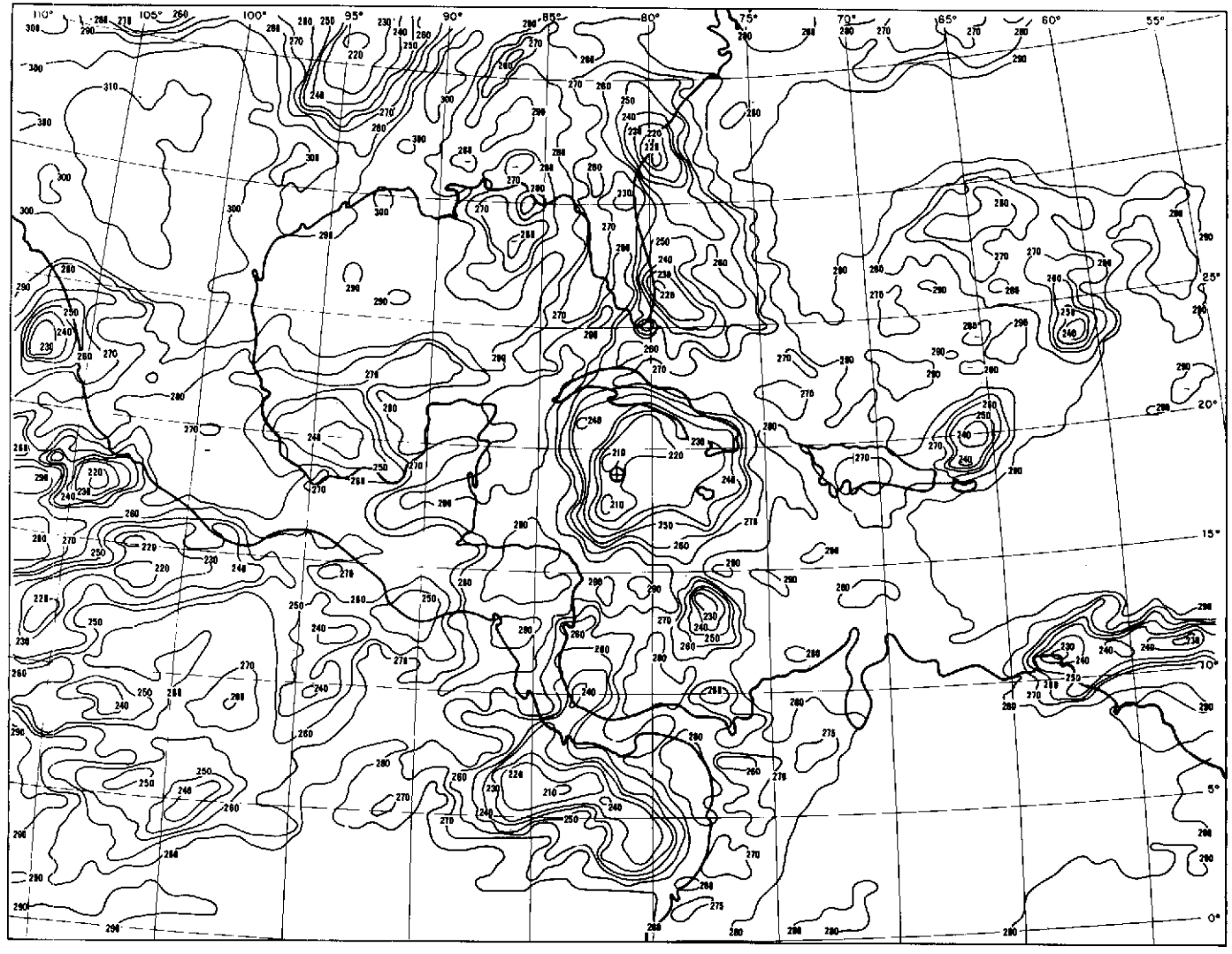

Figure 9. Hurricane Camille at 1500 to 1900 GMT on August 14, 1969, as depicted by 10- to 11-μm T_{BB}'s from the MRIR sensor. The isotherms are given in K and the cyclone center is indicated by the circled cross.

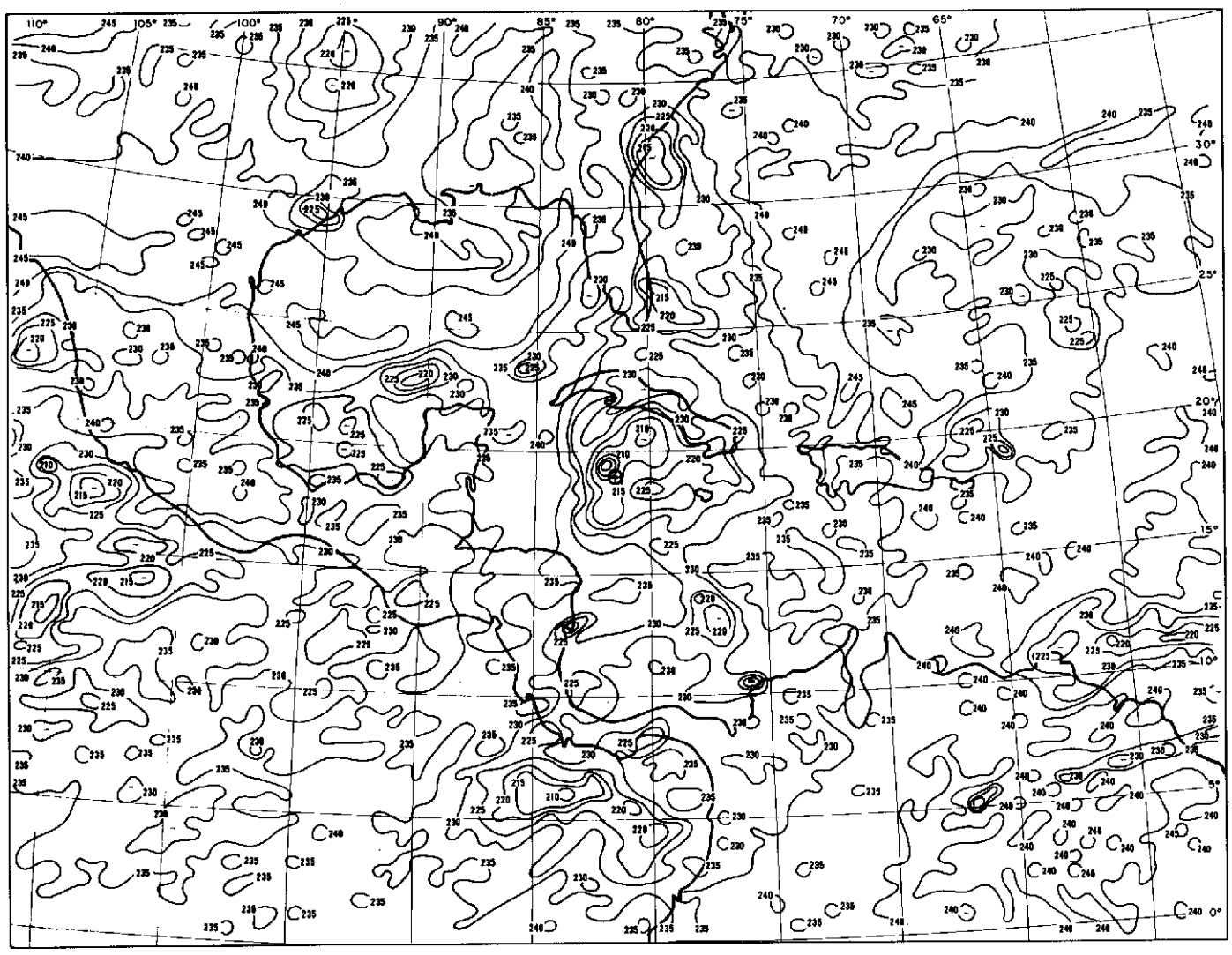

Figure 10. Hurricane Camille at 1500 to 1900 GMT on August 14, 1969, as depicted by 6.5- to 7.0-μm T_{BB}'s from the MRIR sensor. The isotherms are given in K and the cyclone center is indicated by the circled cross.

boundary of the cirrus extends about 15° north of Camille which is approximately 5° further north than 12 hours ago. The large area of inferred subsidence northwest of Camille had split in two and weakened, and the eastern portion became closer to the storm center as a result of a northerly flow on the west side of a strong shear line over the U. S. and the northwestward movement of Camille.

August 15, 1969

The next Nimbus-3 observation of Camille and the surrounding systems was between 0400 and 0800 GMT on August 15. At this time, Camille was a tropical storm rapidly approaching hurricane status about midway through the first deepening phase. Figure 11 depicts the 10- to 11-μm measurements, and it is evident that the symmetrical appearance of the storm had changed to a system where a prominent spiral band extended to the east of the center and the highest clouds were near the center. There is also evidence of two other bands (best shown by the 265-K line) located well southeast of the center. The development of these bands is in apparent response to the organization of a broad southeast current from the surface to 700 mbar which had a large inflow component. The surface chart for 1200 GMT on August 15 (Figure 12) shows two reports of a southeast wind at 15 to 20 kn in the band area. At 850 mbar, the windspeed increased to 30 kn. Thus, with the storm moving northwestward at 8 kn, this boundary-layer air was moving almost directly toward the storm center and was approaching the storm in that indicated area at an average speed of about 15 kn. This air was passing over water with a surface temperature of 303 to 304 K, which is 2 K above the mean sea surface temperature (about two standard deviations) for August in this region (Reference 8). Confluence is indicated in this southeast quadrant up to 700 mbar and most likely resulted in the production of the two bands. The development of these bands with the continuation of an efficient outflow mechanism aloft may be an indication of further deepening of the storm.

The outflow north of the center appears to be operating efficiently as the cirrus is more widespread and either higher or more opaque than 12 hours earlier as seen on the 6.5- to 7.0-μm map (Figure 13). Camille was then in a moist environment, at least in the upper troposphere as there was no evidence of dry air within 5° of the center. The tongue of dry air that was to the northwest is now closer to the storm center, partly due to Camille's motion and partly due to continued advection of dry air toward the southeast. As a result, it is more difficult to detect the subsidence that had probably been produced earlier by Camille, since this apparently had merged with the dry air tongue that had moved southwestward. Slight evidence of the original inferred subsidence pattern remained with the band of relatively high T_{BB}'s in all of the infrared channels southwest of the storm center.

Twelve hours later there was evidence from the reconnaissance aircraft reports that the rate of deepening had slowed or stopped. The 10- to 11-μm channel chart with ATS-3 low-level cloud motions superimposed (Figure 14) shows that Camille had a more circular appearance and that the area of intense cloudiness covered a larger area than 12 hours before. There was an extensive area southeast of the center where the T_{BB}'s were $\leq$ 264 K, which was

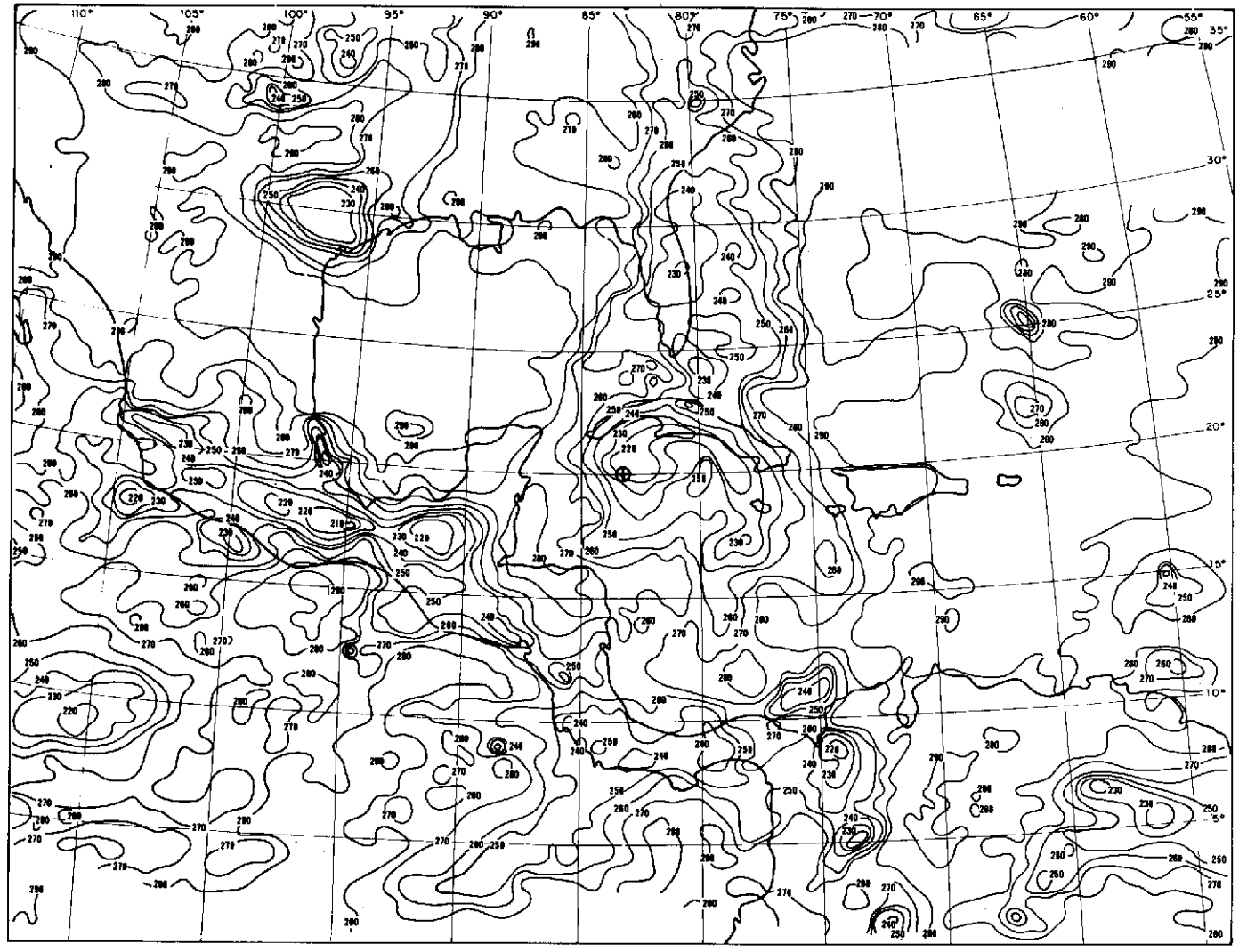

Figure 11. Hurricane Camille at 0400 to 0800 GMT on August 15, 1969, as depicted by 10- to 11-μm T_{BB}'s from the MRIR sensor. The isotherms are given in K and the cyclone center is indicated by the circled cross.

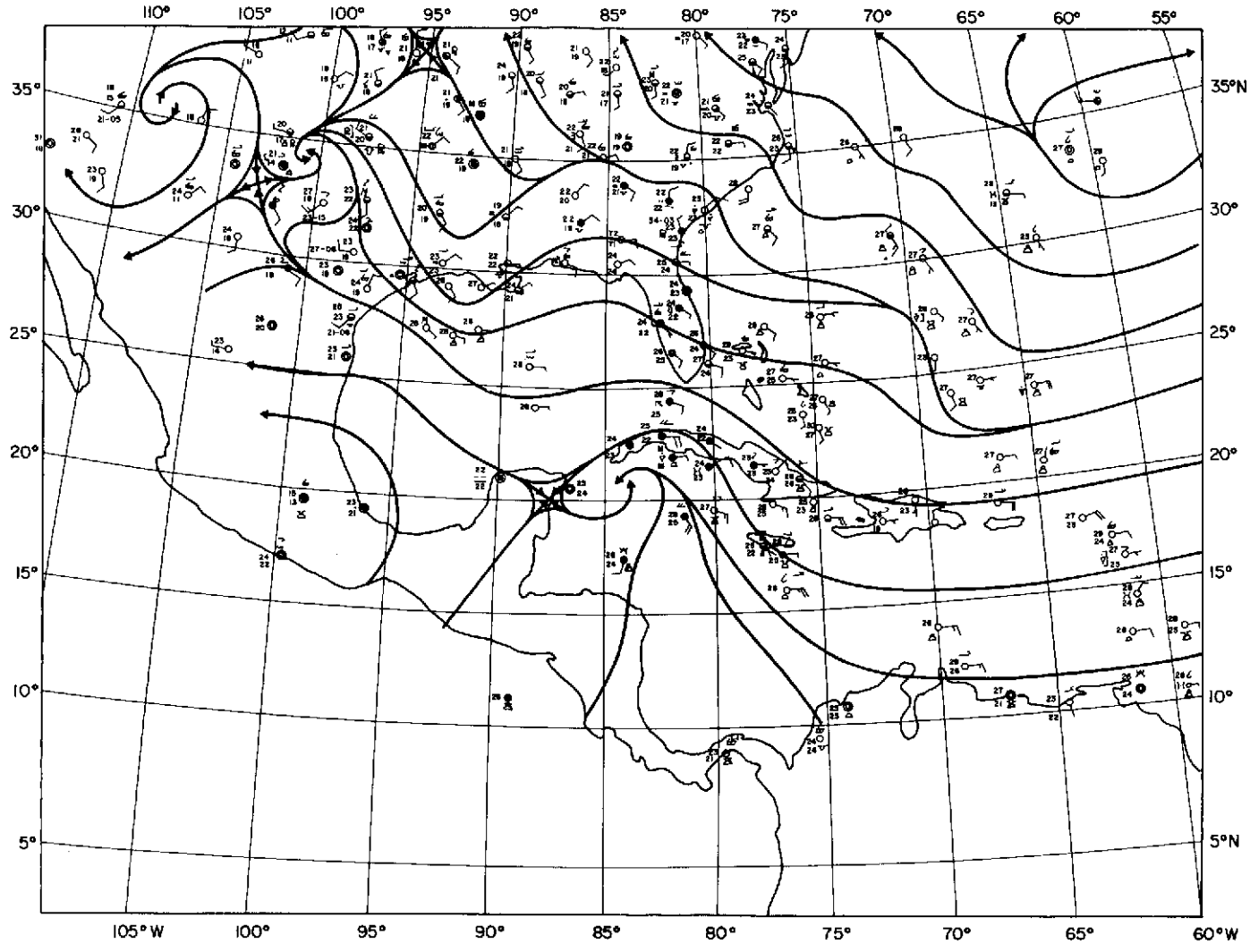

Figure 12. Surface data and streamline analysis for 1200 GMT on August 15, 1969.

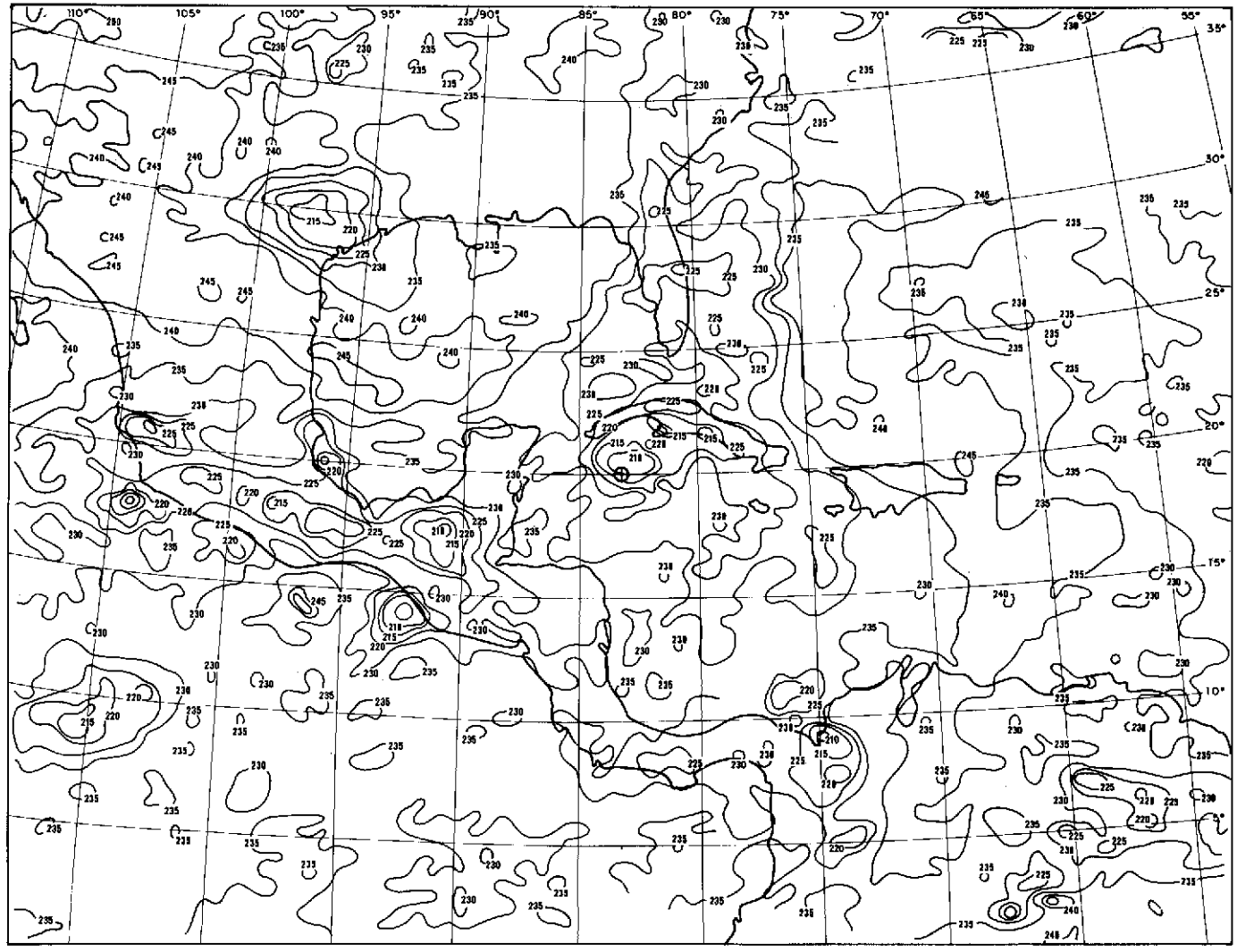

Figure 13. Hurricane Camille at 0400 to 0800 GMT on August 15, 1969, as depicted by 6.5- to 7.0-μm T_{BB}'s from the MRIR sensor. The isotherms are given in K and the cyclone center is indicated by the circled cross.

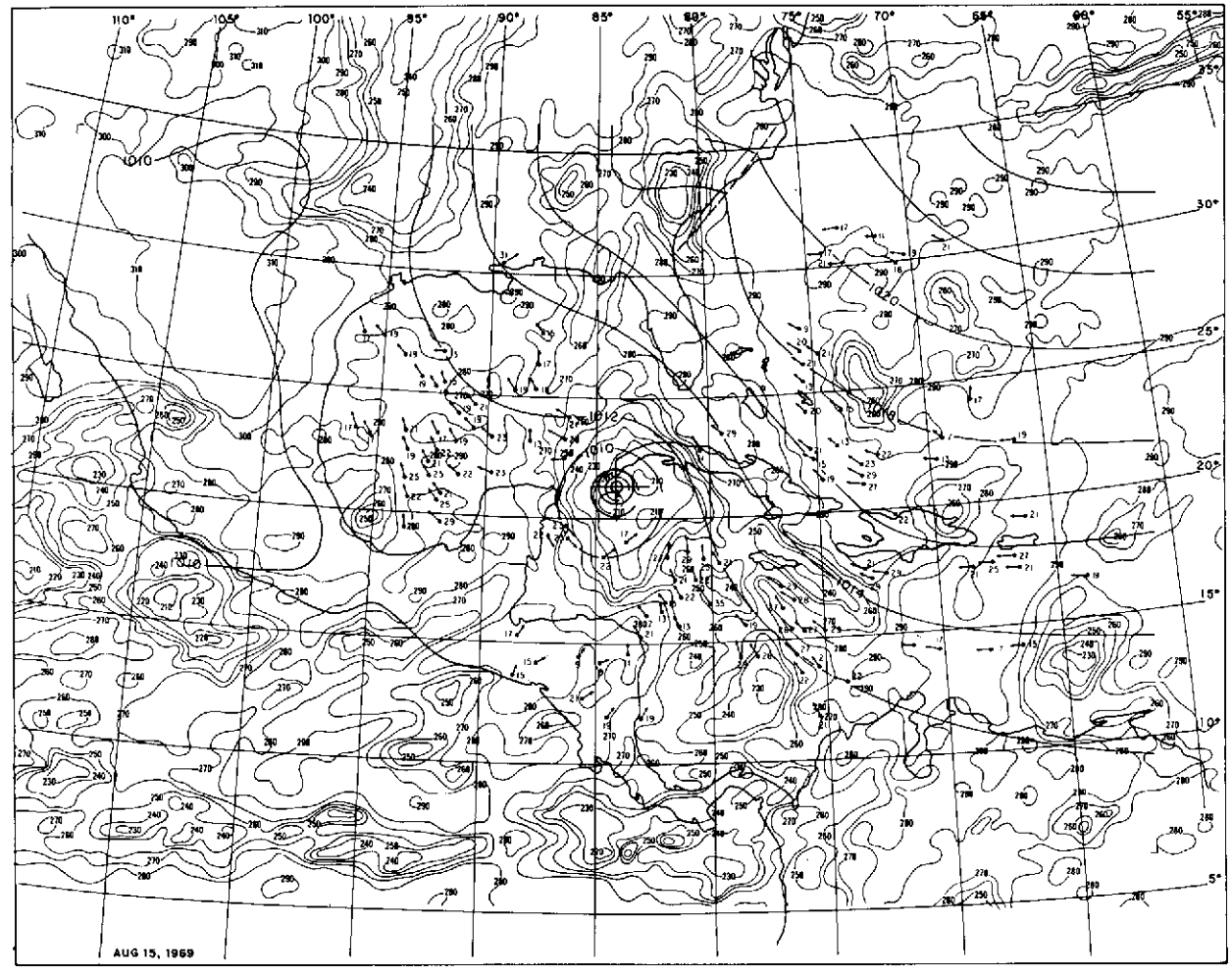

Figure 14. Hurricane Camille at 1400 to 1800 GMT on August 15, 1969, as depicted by 10- to 11-μm T_{BB}'s from the MRIR sensor. The isotherms are given in K and the cyclone center is indicated by the circled cross. Superimposed on the analysis of the radiation data is the surface analysis and cloud motion vectors derived from low clouds tracked from the ATS-3 satellite images. The cloud motion directions are indicated by the arrows and the speeds are in knots.

indicative of the continued cloud development in conjunction with the low-level confluence that was shown by the low cloud motions. The band of cloudiness was continuous from the ITCZ to Camille. The low cloud motions that were located between the two principal developing cloud bands were generally a few knots higher than to the northeast of the bands, even though the pressure gradient from conventional analysis was about the same inside and outside the bands.

The presence of a surface depression along the leading edge of a band would increase the pressure gradient between the band and the environment and thus increase the winds just ahead of the leading edge. Tatehira (Reference 9) has indicated that a depression of about 1 mbar occurred with the passage of the leading edge of an outer spiral band of a typhoon.

The band that is south-southeast of the center of Camille appears to be the most active of the two bands. If this is true, the greatest pressure gradient would be between and parallel to the bands (along the east side of the strongest band). That is where the area of consistently high velocities (26 to 29 kn) are located. The band formation will also increase the low-level convergence and therefore maintain the vigorous cloud growth within the bands.

There is a possibility that the surface pressure is being lowered along the band by tropospheric warming caused by latent heat release. Gentry (Reference 10) has found that the temperatures are lower in hurricane bands at a considerable distance from the eye wall than the immediate surrounding environment due to entrainment. The average width of the precipitating bands in his investigation was around 20 to 40 km. It is not possible to accurately estimate the precipitating width of the strongest band south-southeast of the center of Camille, but the width of extensive cloudiness averages more than 350 km. This suggests that the precipitating width is considerably greater than 20 to 40 km. Under these conditions entrainment would probably have a small effect. Whether the effect is sufficient to produce a warm core band cannot be proven with these data. Simultaneous aircraft flights making temperature measurements would be necessary.

Outflow from the strongest cluster (as measured by the lowest T_{BB}'s along the most active band centered at 13° N, 78° W) was probably augmenting the velocity of two clouds (28 to 29 kn) just to the north of the cluster by about 10 kn. A cloud motion further to the north (19 kn) was most likely more representative of ambient conditions in the band.

The development of the clouds in the confluence zone could be an important factor for a more rapid transport of moist air into the inner circulation of Camille. Conventional data indicate that the winds between the surface and 850 mbar had about the same radial component toward the storm between 0000 GMT on August 15 and 0000 GMT on August 16. The low-level winds were as high as 35 kn transporting moist air at 850 mbar with a large radial component 350 km southeast of the center at 0000 GMT on August 16, preceded by 30-kn and 35-kn winds at similar locations 12 and 24 hours earlier. Thus, with a similar environment for 24 hours the cloud development was able to continue.

A small area of T_{BB}'s $\geq$ 290 K was located west of the storm, which indicated some suppression of low-level cloud development. To the east was a larger area that was most likely associated with upper horizontal convergence produced by the outflow, where the strength and position changed little on the 200 mbar analysis between 1200 GMT on August 15 and 0000 GMT on August 16.

North of the cyclone center, the cirrus shield persisted as seen in the 6.5- to 7.0-μm measurements (Figure 15), indicating that ventilation was still present. The ventilation is clearly shown by the middle and high cloud motions from ATS-3 where a strong southerly current exists at the cloud levels for at least 1100 km. Also, the cloud motions indicate local outflow from one of the clusters in the band southeast of Camille that was assumed to be the most active from the analysis of the 10- to 11-μm measurements. The local outflow that is typical of a vigorous cluster gives further support to the earlier assumption regarding the relative strength of the two bands.

The 200-mbar chart for 0000 GMT on August 16 (Figure 16) indicates that the flow over southern Florida had changed from southerly to westerly. This change was most likely an expansion of the outflow area of Camille. East of the cirrus there is a well-defined ridge line demarcated by 6.5- to 7.0-μm T_{BB}'s as high as 244 K and the cloud motions. The 200-mbar analysis cannot confirm the presence of the line since the high T_{BB}'s were east of Florida. It is likely that some of the cirrus ejected by the outflow dissipated in the dry air associated with the ridge line. West of Camille the relatively high T_{BB} area had weakened and moved little with respect to the center, and the upper horizontal convergence as shown by the cloud motions is coincident with the highest T_{BB}'s.

A chart was prepared combining the measurements from the two water-vapor channels and the reflectance channel to more clearly delineate the regions of most intense cloudiness and the areas where the strongest subsidence could be inferred. The mapped values were generated from the expression $T_1 + T_4 + (100 - R)$, where T_1 and T_4 are the channel 1 and 4 T_{BB}'s respectively, and R is the normalized reflectance. Thus, a dry atmosphere over the ocean would be characterized by relatively high T_{BB}'s and a low reflectance. For example, if T_1 = 245 K, T_4 = 265 K, and R = 10, then the mapped value would be 600. At the other extreme, with deep convection, the same set of measurements could be T_1 = 210 K, T_4 = 210 K, and R = 70, and the mapped value would be 450.

Figure 17 depicts the combined values for the daylight satellite observations on August 15. There are two regions where the values are $\geq$ 580 and these are about where the two areas of maximum T_{BB}'s were seen in Figure 15. Values of $\geq$ 600 occur only over a very limited area in the western region and in the center of the ridge line in the eastern region. This chart indicates that the air was probably drier throughout the tropospheric column in the eastern region. This same result could have been deduced from the examination of the data from each of the three channels, but the new chart presents the information in a more convenient form. Near the storm center values of $\leq$ 440 indicate the two portions within the cloud shield where the most intense cloudiness was located. These values are comparable to those observed in the most intense portion of the ITCZ on the same day.

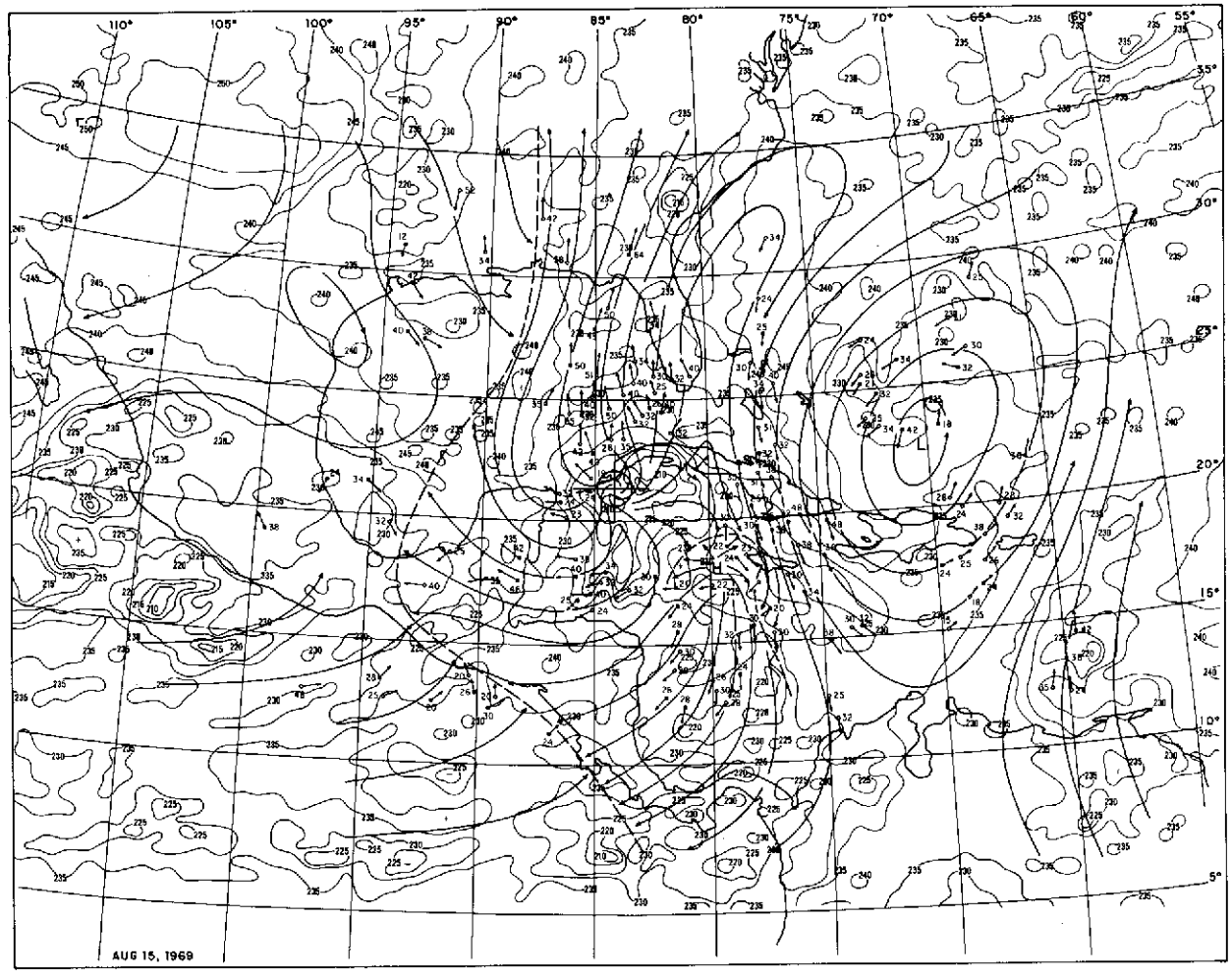

Figure 15. Hurricane Camille at 1400 to 1800 GMT on August 15, 1969, as depicted by 6.5- to 7.0-μm T_{BB}'s from the MRIR sensor. The isotherms are given in K and the cyclone center is indicated by the circled cross. Superimposed on the analysis of the radiation data are cloud motion vectors derived from high and middle clouds tracked from ATS-3 satellite images and the streamline analysis based on the cloud motions and 200-mbar rawins. The cloud motion directions and speeds are indicated in the same manner as in Figure 14.

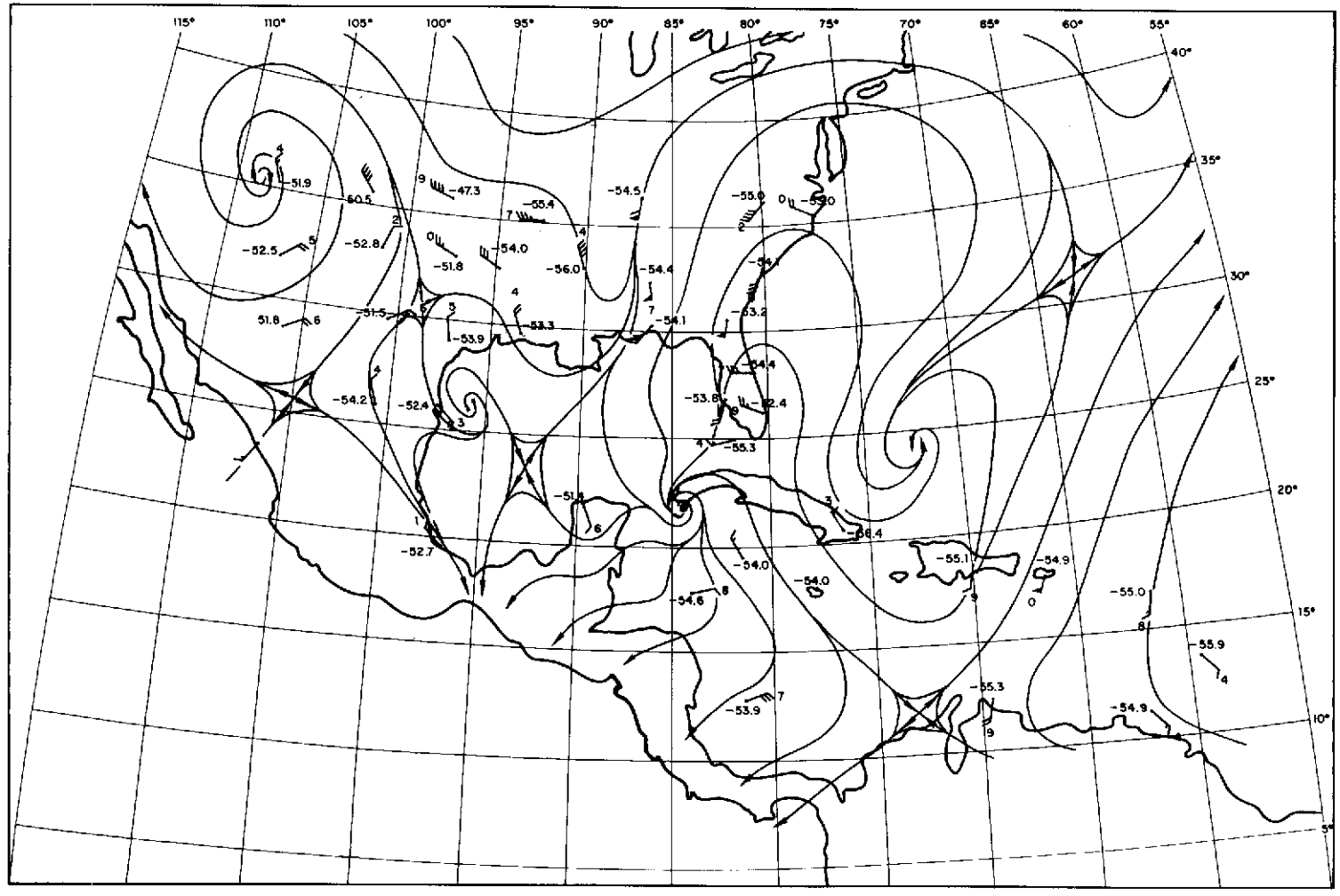

Figure 16. 200-mbar radiosonde data and streamline analyses for 0000 GMT on August 16, 1969.

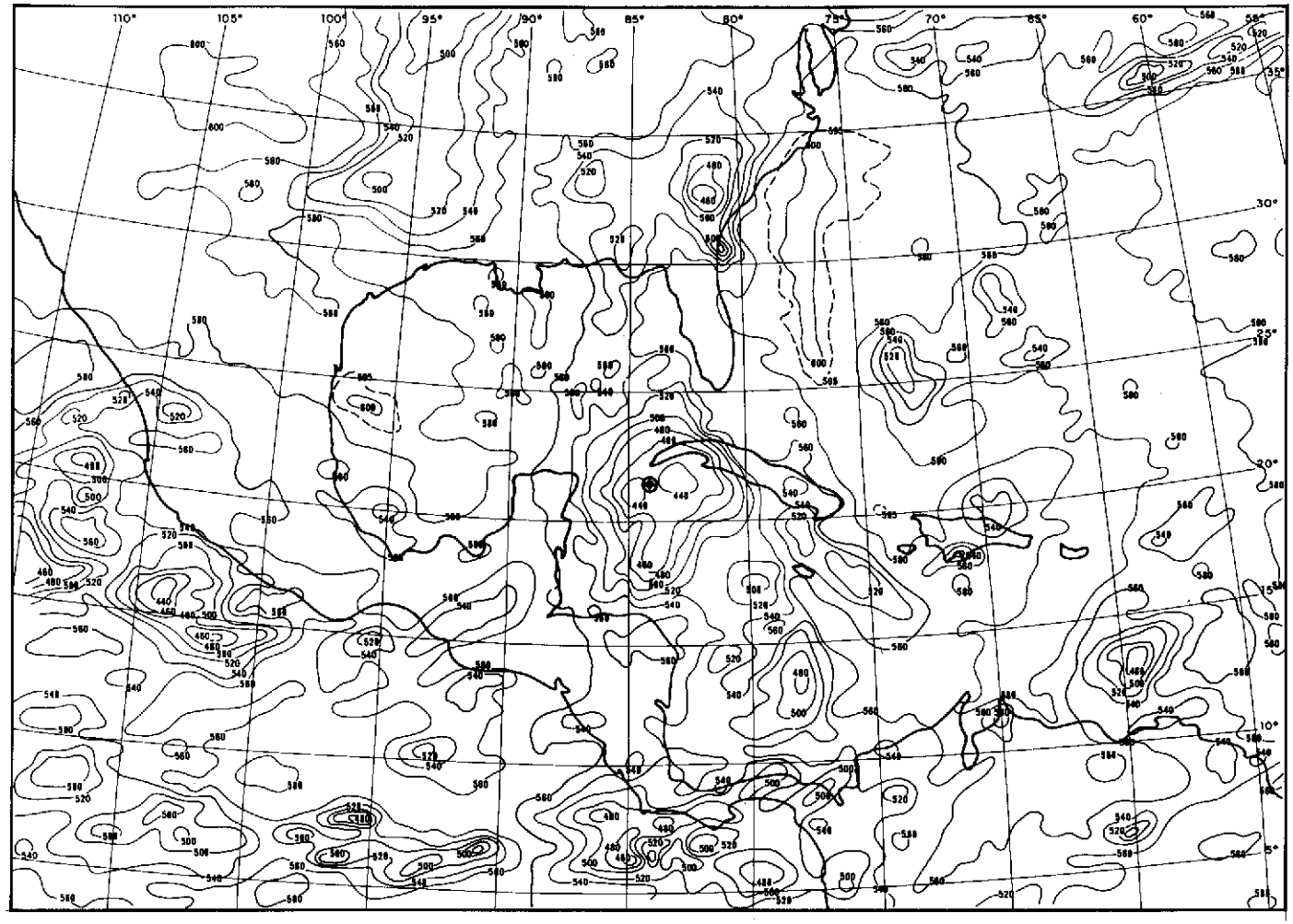

Figure 17. Hurricane Camille at 1400 to 1800 GMT on August 15, 1969, as depicted by the combination of the T_{BB} measurements (in K) from the two water vapor channels and the normalized reflectance measurements from the reflectance channel (spectral albedo in percent) of the MRIR sensor. The cyclone center is shown by the circled cross.

August 16, 1969

Twelve hours later, Camille had probably begun the most dynamic deepening phase of its life cycle. The changes in the structure of Camille as seen in satellite observations also reach a climax. The 10- to 11-μm T_{BB}'s (Figure 18) show that the size of the active cloudiness, as defined by the 235-K isotherm, had been reduced by about a factor of three from the last satellite observation. Therefore, during the early portion of rapid deepening, the cloud canopy contracted sharply. The cloud bands in the converging moist air southeast of the center were still strong and extended 1100 km from the center. The outer limit of the cloud bands was almost exactly the distance from Camille's center where the surface streamlines began to converge at 1200 GMT on August 16 (Figure 19). There were no rawinsonde measurements close to the center but the surface reports show the continued inflow where the wind speeds were 20 to 30 kn. West of the center, the area covered by $T_{BB} \geqslant 290$ K had expanded considerably in 12 hours. This large expansion represents a substantial increase in the region where the cloudiness was being suppressed. This would indicate that the subsidence surrounding Camille over a large area was beginning to affect the cloudiness in response to the increased vigor of the inner circulation.

The 6.5- to 7.0-μm and 20- to 23-μm measurements (Figures 20 and 21) also indicate the subsidence increase west and northwest of the center at higher levels. Twelve hours earlier there had been a weakening band of high T_{BB}'s oriented northwest-southeast that was most likely advected from north of the storm. The high T_{BB}'s at this time encircle the center in the western semicircle, which suggests that they were produced by the hurricane. They cover approximately the same area as that covered by the $\geqslant$ 290-K isotherm in Figure 18. It is interesting that the time lag between the increased vertical motion in the inner portion of Camille and the subsidence appeared to be small. The cyclone center had moved off the northern Cuban coast for only about 4 hours. A more exact assessment of the lag would require geosynchronous satellite measurements.

By 1500 to 1900 GMT on August 16, Camille had become a very severe hurricane. At 1800 GMT a U.S. Air Force reconnaissance aircraft measured a central pressure of 908 mbar. Therefore, Camille deepened about 60 mbar in 24 hours. The 10- to 11-μm measurements (Figure 22) show that the intense portion of the Camille cloud canopy ($T_{BB} \leqslant 235$ K) had expanded by about a factor of four in 12 hours. There were two areas of great activity, one near the center with T_{BB}'s between 200 and 204 K (the lowest recorded during the entire life cycle) and another of 205 to 209 K imbedded in the broad band southeast of the center. The low T_{BB} measurements near the eye were almost perfectly centered, thus suggesting an intense circular wall cloud. This is verified by the concurrent high resolution (3 km) image dissector camera system (IDCS) image (Figure 23) in which the eye is clearly seen and the wall cloud is like an inner ring surrounded by the rest of the cloud system that is separated by a ring that had a lower brightness than the clouds forming the rest of the canopy or the wall cloud. These features suggest that the cloud tops within the wall cloud ring had reached a higher level than the surrounding clouds and that the air was descending immediately once it moved outside of the wall

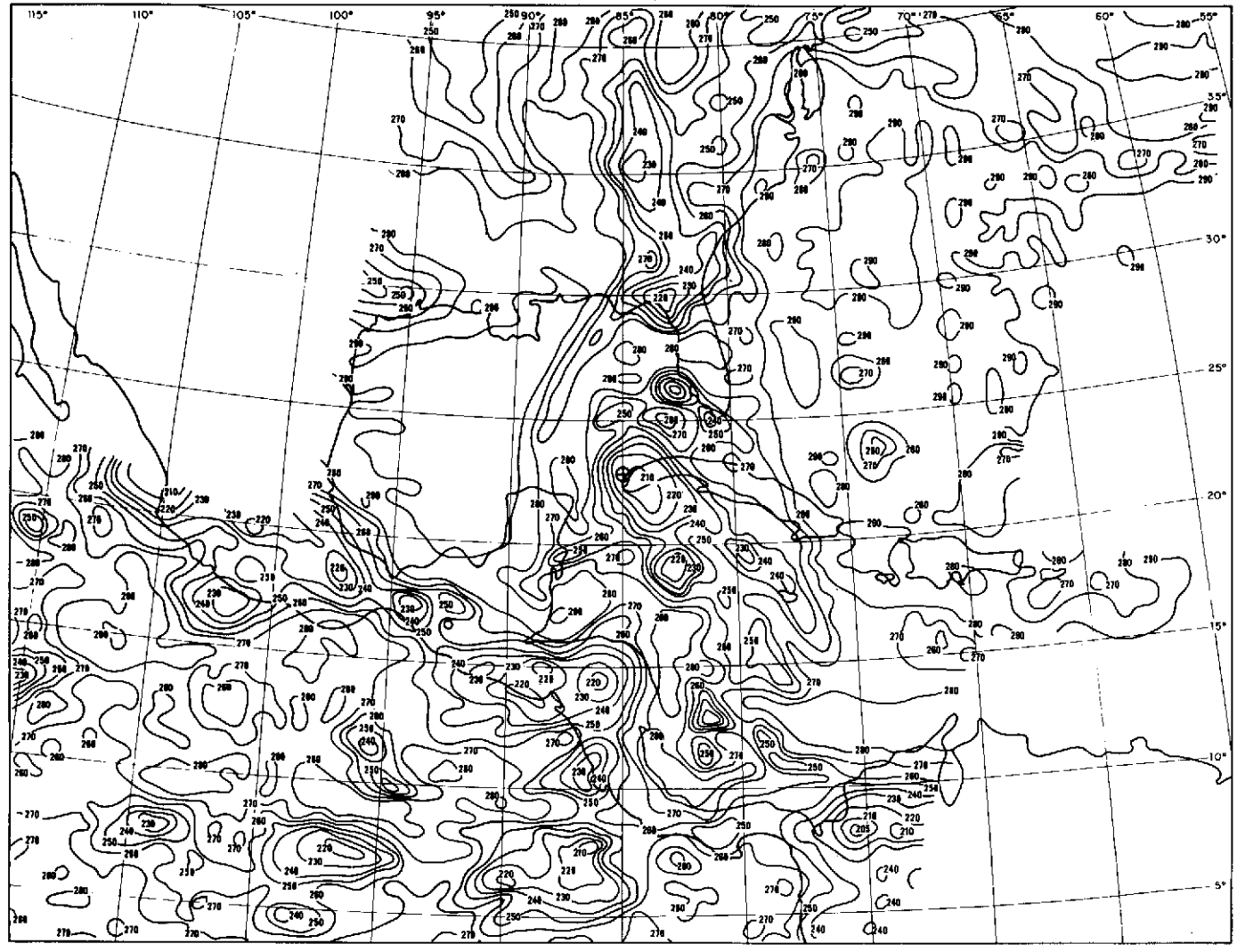

Figure 18. Hurricane Camille at 0300 to 0700 GMT on August 16, 1969, as depicted by 10- to 11-μm T_{BB}'s from the MRIR sensor. The isotherms are given in K and the cyclone center is indicated by the circled cross.

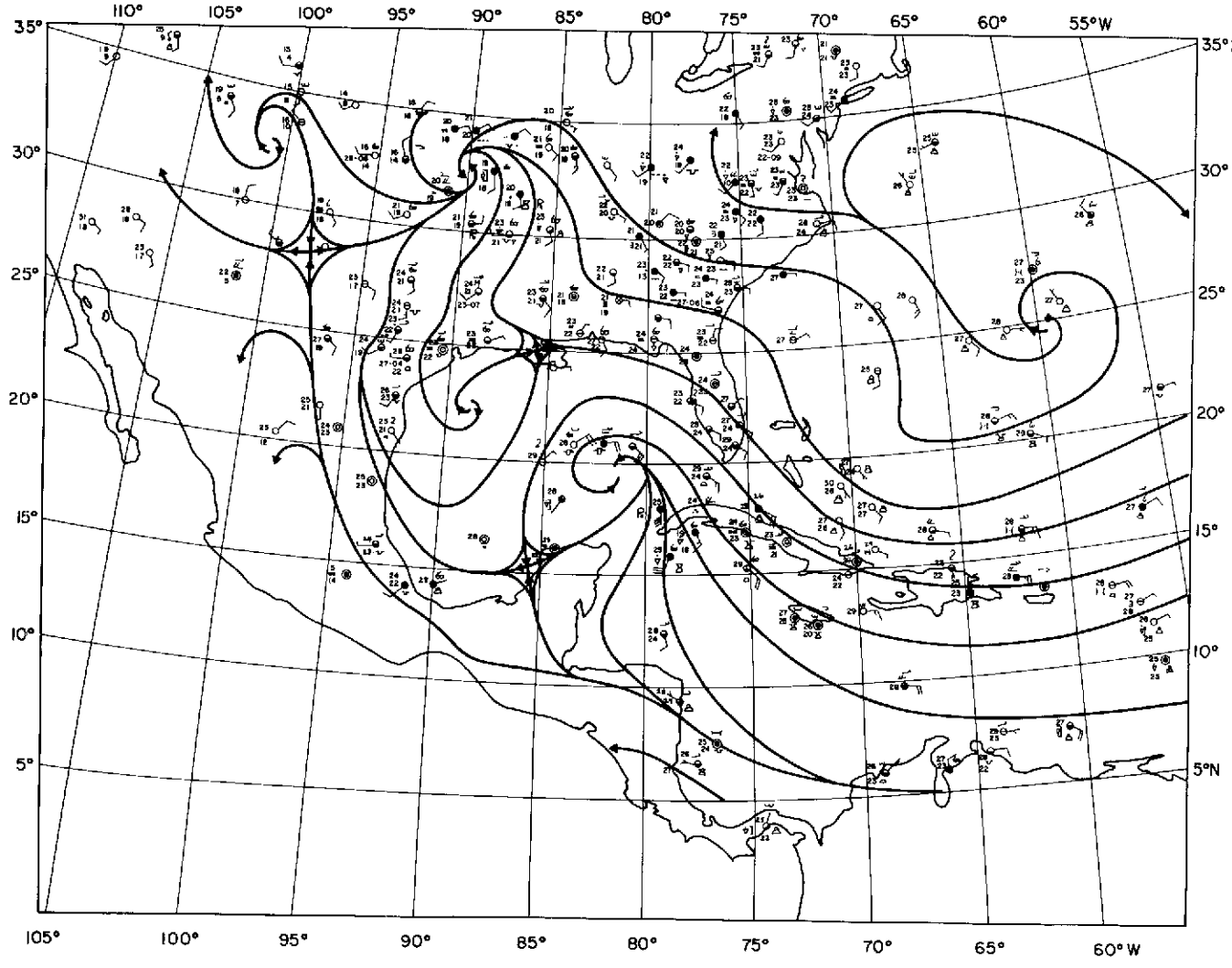

Figure 19. Surface data and streamline analysis for 1200 GMT on August 16, 1969.

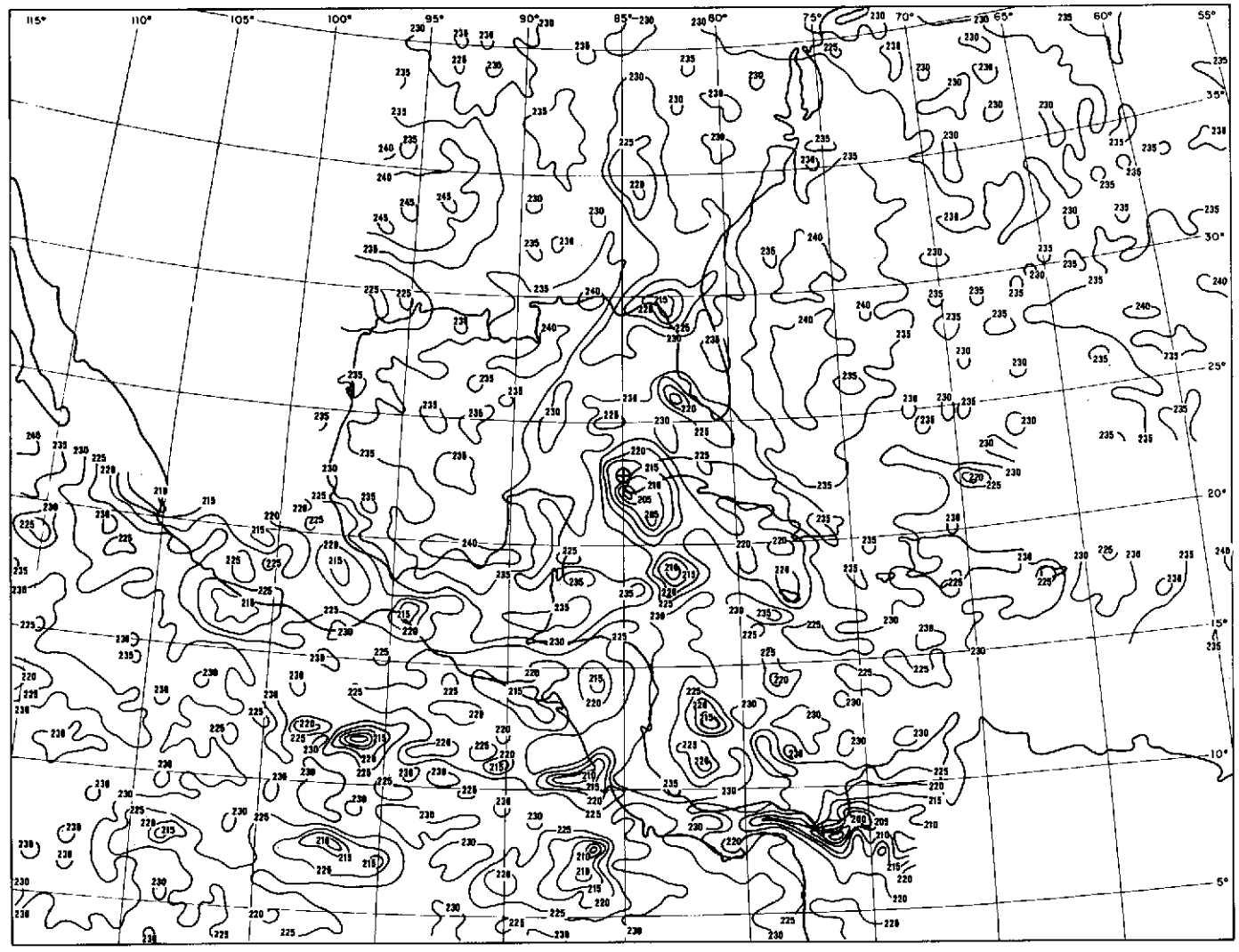

Figure 20. Hurricane Camille at 0300 to 0700 GMT on August 16, 1969, as depicted by 6.5- to 7.0-μm T_{BB}'s from the MRIR sensor. The isotherms are given in K and the cyclone center is indicated by the circled cross.

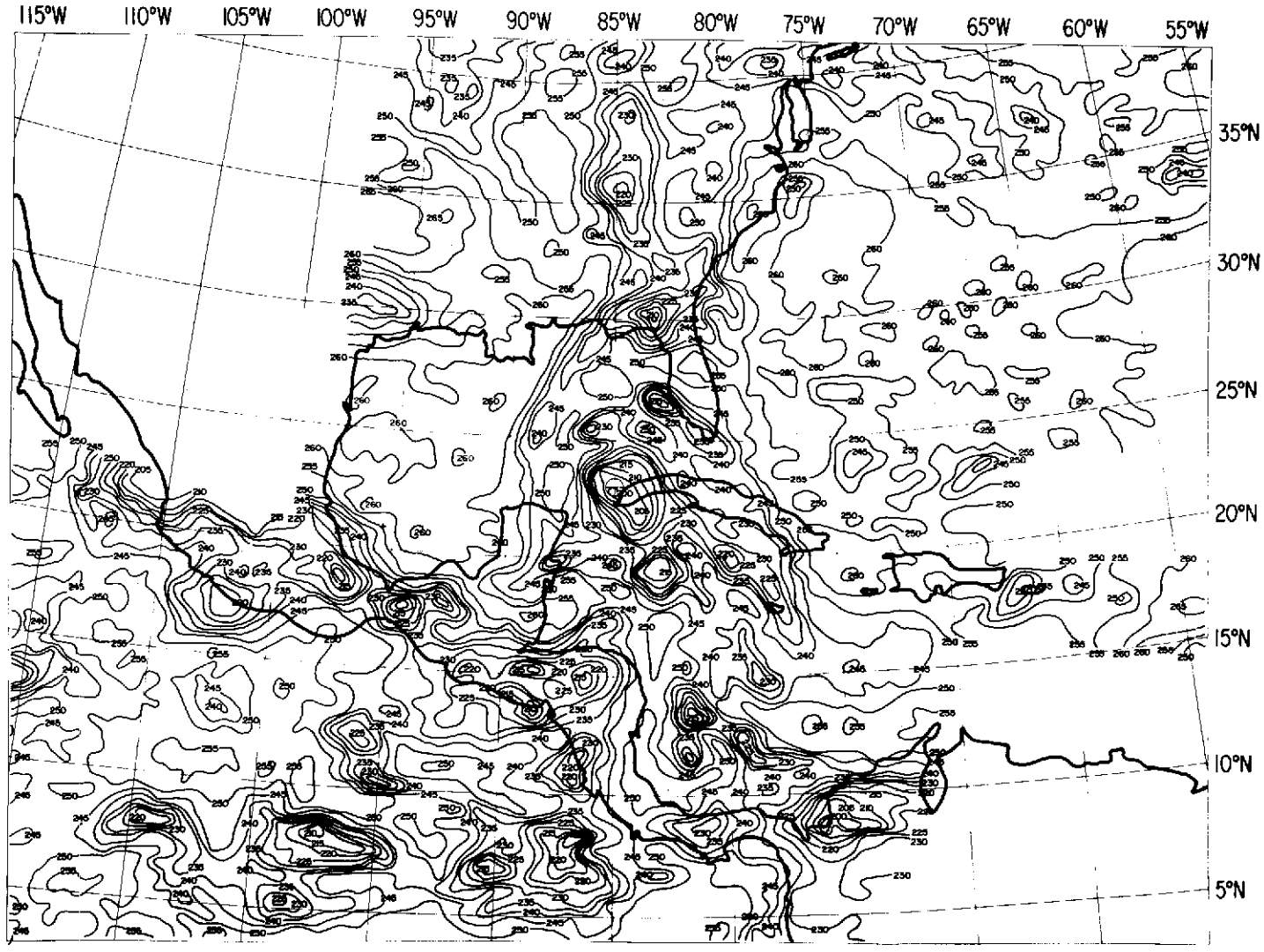

Figure 21. Hurricane Camille at 0300 to 0700 GMT on August 16, 1969, as depicted by 20- to 23-μm T_{BB}'s from the MRIR sensor. The isotherms are given in K and the cyclone center is indicated by the circled cross.

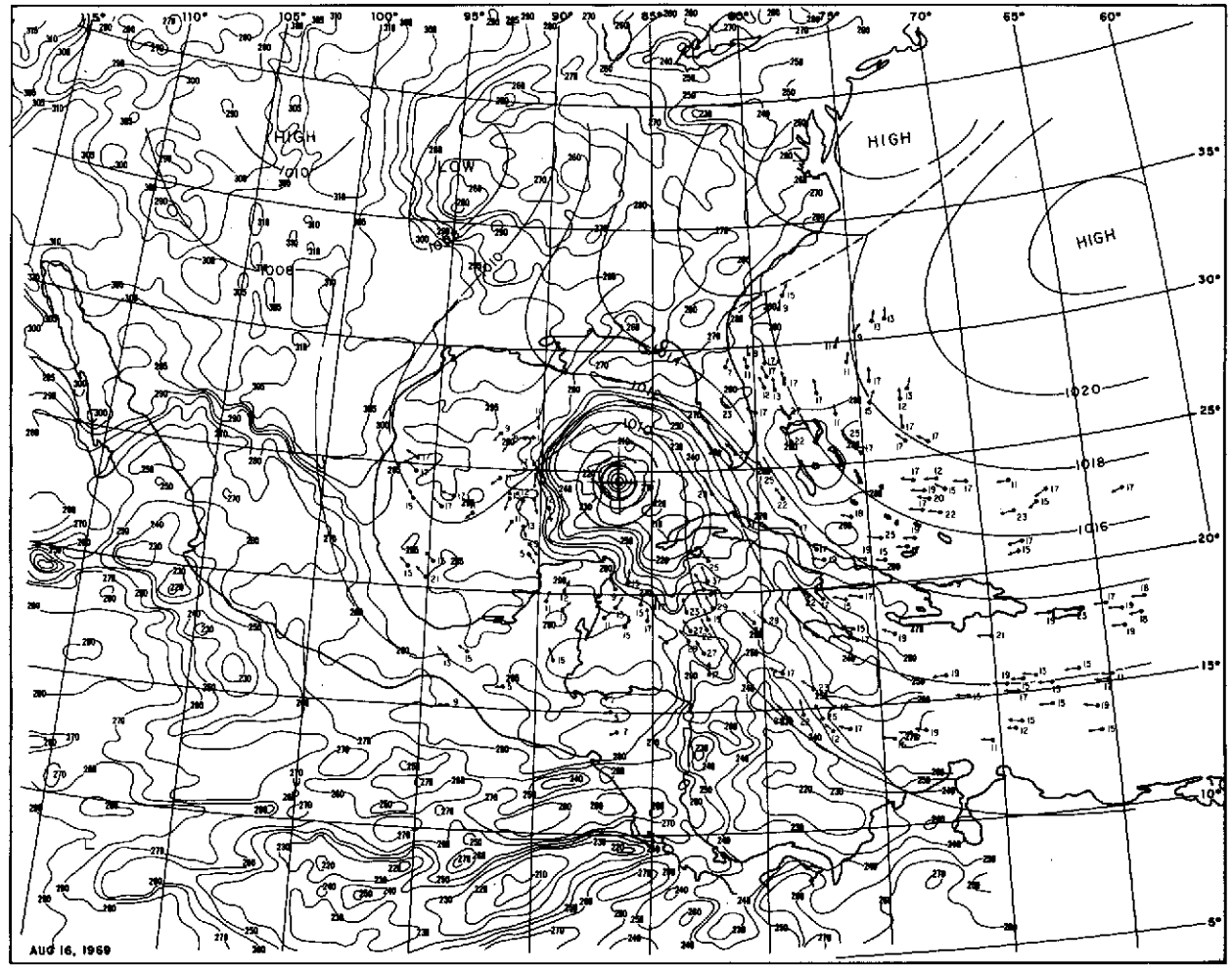

Figure 22. Hurricane Camille at 1500 to 1900 GMT on August 16, 1969, as depicted by 10- to 11-μm T_{BB}'s from the MRIR sensor. The isotherms are given in K and the cyclone center is indicated by the circled cross. Superimposed on the analysis of the radiation data is the surface analysis and cloud motion vectors derived from low clouds tracked from the ATS-3 satellite images. The cloud motion directions are indicated by the arrows and the speeds are in knots.

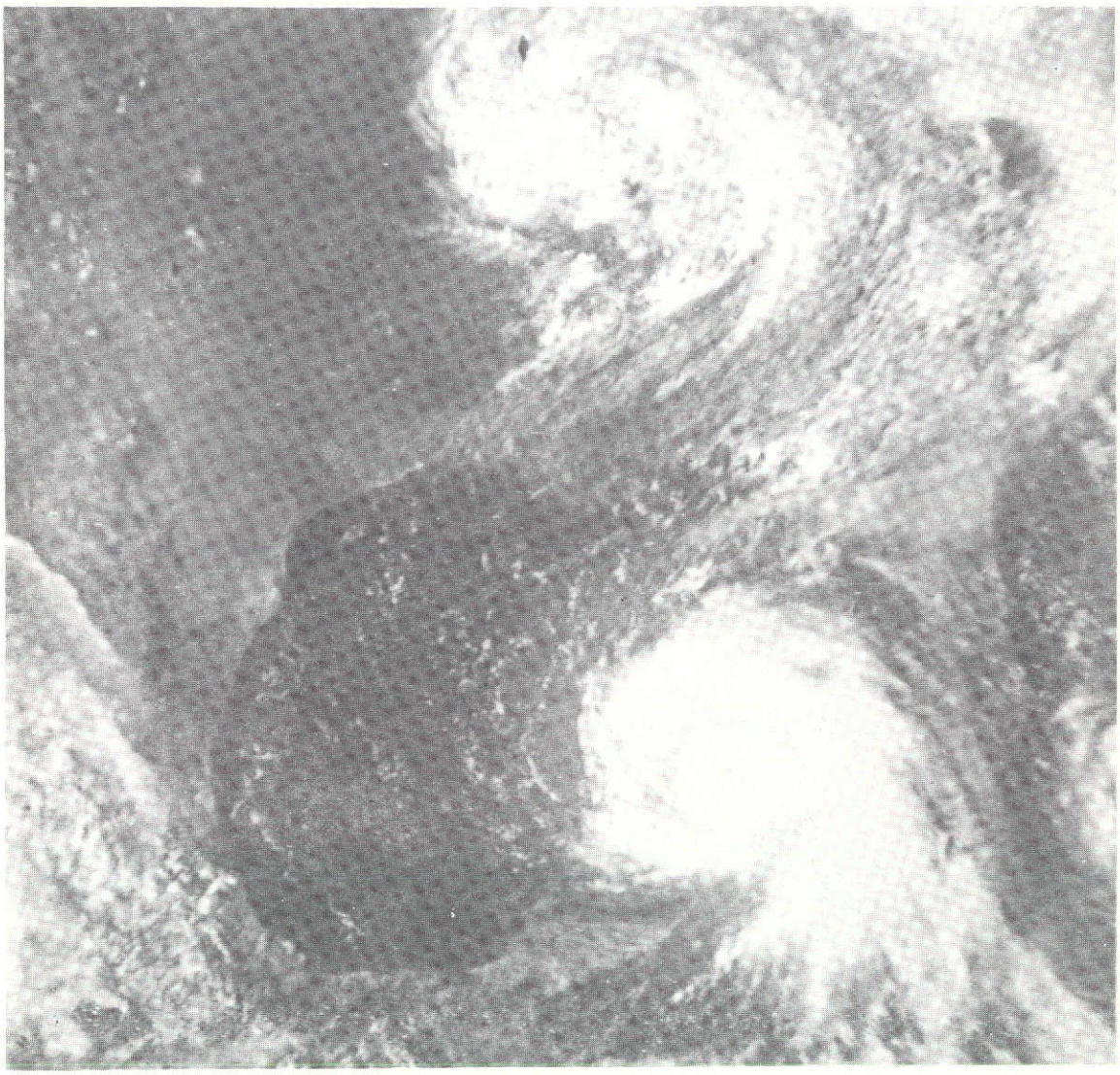

Figure 23. Hurricane Camille at 1900 GMT on August 16, 1969, as seen by the Nimbus-3 Image Dissector Camera System (IDCS).

cloud. The subsidence would dissipate or reduce the opacity of the cirrus and produce the lower brightness ring that separates the wall cloud from the rest of the cloud system.

Southeast of the center, the broad cloud band system was continuous from the ITCZ into Camille's circulation, and the low T_{BB}'s seen in Figure 22 indicate that a substantial percentage of the area contained middle and high cloudiness. The low-level cloud motions shown in Figure 22 continue to exhibit the general confluence in the low-level wind field, and the cloud speeds toward the cyclone are much higher than the northwest motion of the storm. West of the center the area of T_{BB}'s $\geqslant$ 290 K had continued to expand and measurements of $\geqslant$ 295 K covered approximately 40 percent of the area where T_{BB}'s

$\geqslant$ 290 K occurred over the Gulf of Mexico. Thus, the suppression of cloudiness (probably low-level) had become more widespread and had intensified in some of the areas to the point where all cloudiness had probably disappeared. After correction for the atmosphere, a 295 K T_{BB} was within 2 K of the sea surface temperature. The cloud motions showed evidence of low-level divergence over portions of the area where $T_{BB} \geqslant 290$ K. Also, the 0.2- to 4.0-μm reflectance (Figure 24) of $\leqslant$ 10 percent covered nearly the entire Gulf west of the Yucatan Peninsula.

The water vapor channels exhibited some remarkable changes (Figures 25 and 26). In the entire western semicircle over a radial width of about 5°, higher T_{BB}'s were found with the maximum measurements of 245 K in the 6.5- to 7.0-μm channel northwest of the center, and 268 K in the 20- to 23-μm channel further away and west of the eye. Massive subsidence can be inferred as the increased circulation within Camille became reflected in the large ejection of air to the periphery. This is particularly impressive when the evidence from the conventional data indicates that the 200-mbar flow east of the storm also increased between 0000 GMT and 1200 GMT on August 16 and did not diminish in the following 12 hours. The region of maximum upper convergence appears to be along a line 5° northwest of the center where the 6.5- to 7.0-μm T_{BB}'s were 245 K. Air was apparently flowing northwestward to converge with the eastward moving air around the base of the trough over the central United States. A combination of the 200-mbar rawinsonde reports for 1200 GMT and the high and middle cloud motions from ATS supports that interpretation of the radiation map (Figure 25). The analyzed line of upper horizontal convergence was within 100 km of the area of 245 K T_{BB}'s northwest of the cyclone center. Because most of the emission in the 6.5- to 7.0-μm channel came from the 300- to 500-mbar layer, which was just below the region of probable maximum horizontal convergence at about 200 mbar, the subsiding air in this layer was most likely not far from the position where the air initially began its descent. The location and shape of the maximum 20- to 23-μm T_{BB}'s suggests that the air did not descend vertically. The maximum descent in the 400- to 700-mbar layer is inferred to be further west and over a larger region. With the lack of conventional measurements it was not possible to correlate the 12- or 24-hr, 6.5- to 7.0-μm and 20- to 23-μm T_{BB} changes with computed vertical motions. However, these T_{BB} changes should be related to the relative difference between the vertical motion in the two layers. Over the area 6 to 8° W of the center, where clouds were probably absent for the 24-hr interval, the ΔT_{BB}'s in the 6.5- to 7.0-μm and 20- to 23-μm channels were about 6° and 10°, respectively. Thus, an estimate of the ratio of the subsidence strength would be 10/6, with the greatest sinking in the 400- to 700-mbar layer. Since the maximum vertical motion usually occurs at the level of nondivergence and this level is about 600 mbar, the result was not surprising.

The three-channel combination chart is shown in Figure 27. West of Camille the large-scale subsidence had produced widespread values that were at or slightly below 600, in contrast to a small area 24 hours earlier. A value of 418 near the center was the minimum for Camille during its life cycle and was close to the minimum observed for any cloud mass anywhere on the charts during the Camille period.

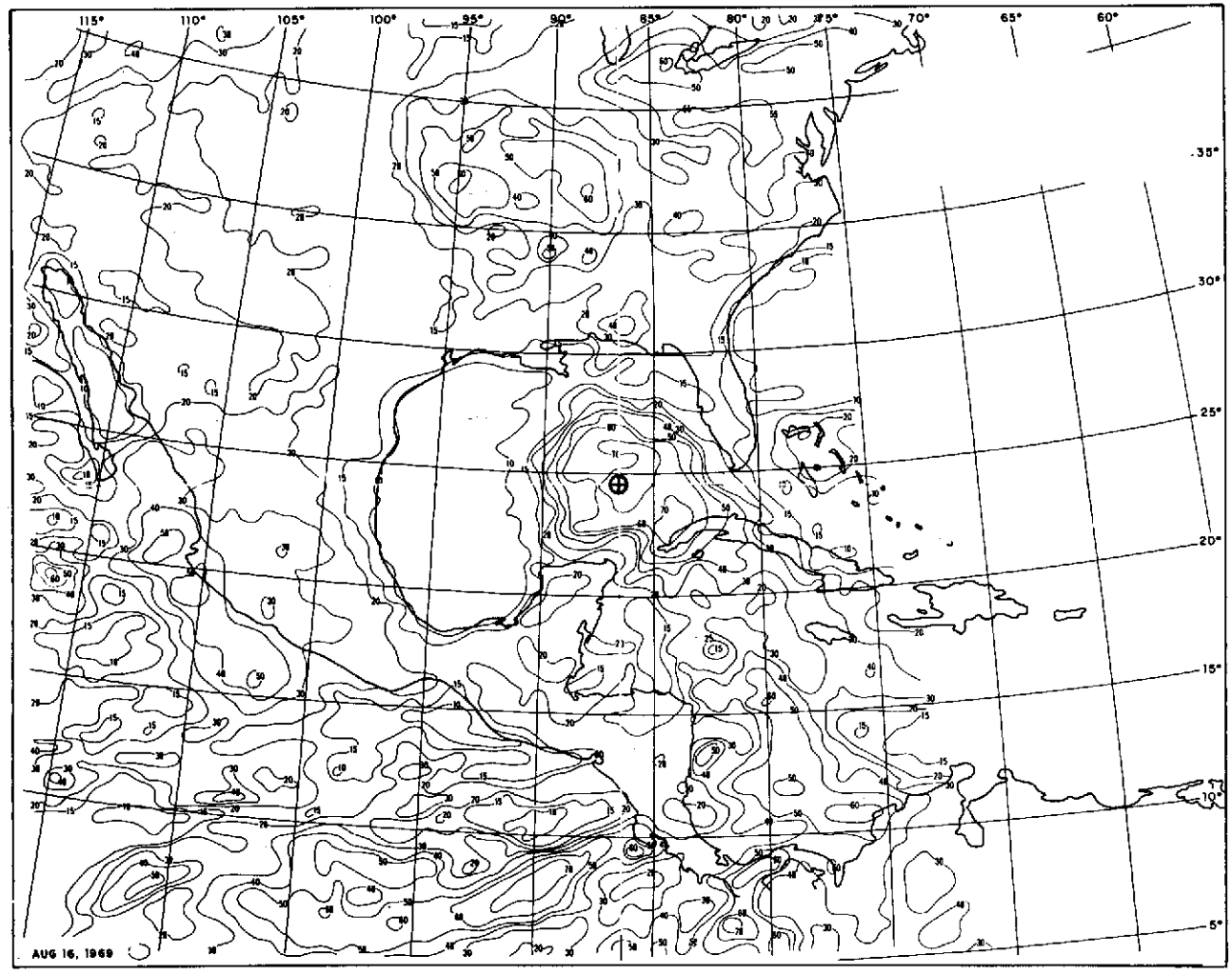

Figure 24. Hurricane Camille at 1500 to 1900 GMT on August 16, 1969, as depicted by 0.2- to 4.0-μm normalized reflectance measurements from the MRIR sensor. The isolines are spectral albedo in percent and the cyclone center is indicated by the circled cross.

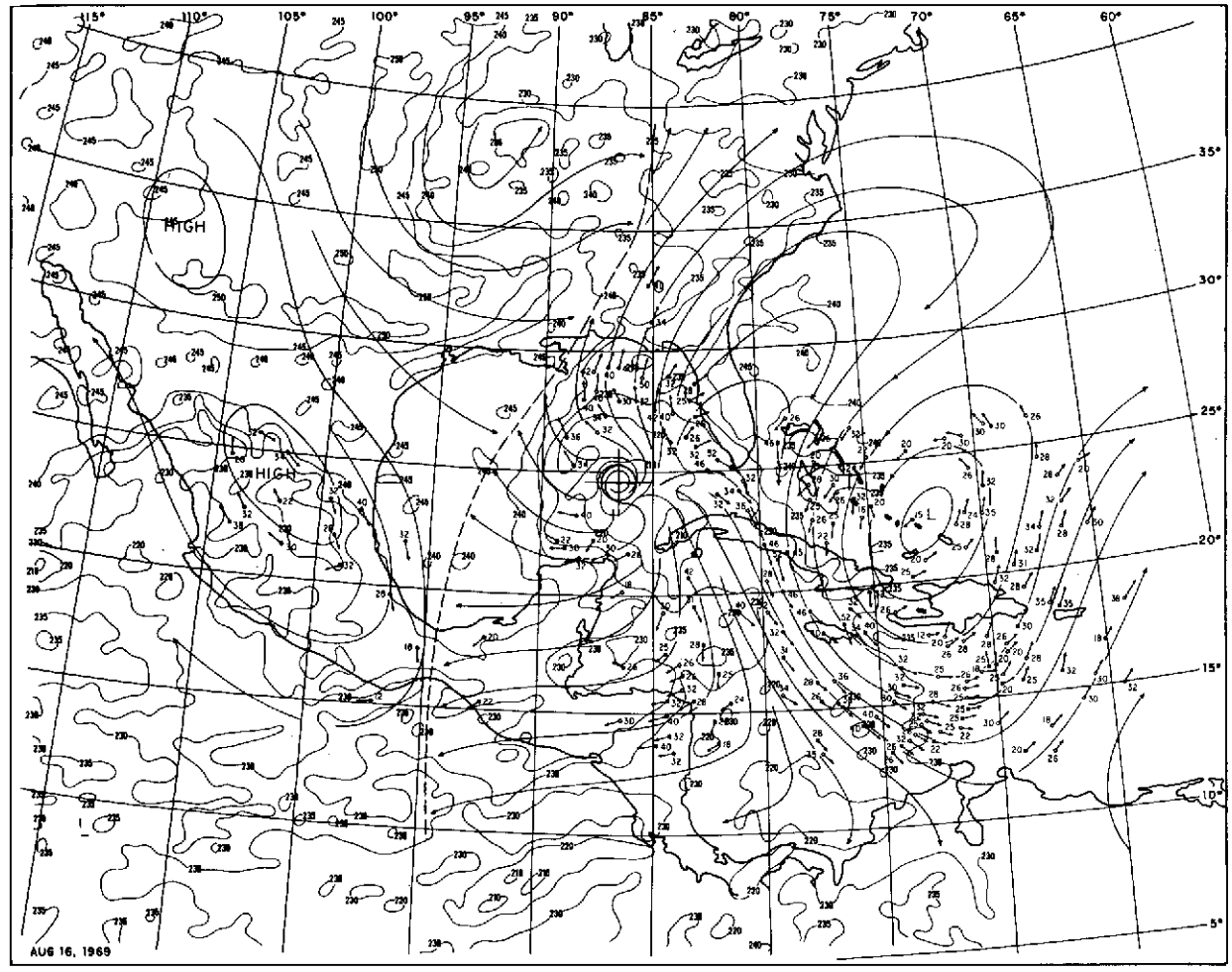

Figure 25. Hurricane Camille at 1500 to 1900 GMT on August 16, 1969, as depicted by 6.5- to 7.0-μm T_{BB}'s from the MRIR sensor. The isotherms are given in K and the cyclone center is indicated by the circled cross. Superimposed on the analysis of the radiation data are cloud motion vectors derived from high and middle clouds tracked from ATS-3 satellite images and the streamline analysis based on the cloud motions and 200-mbar rawins. The cloud motion directions and speeds are indicated in the same manner as in Figure 14.

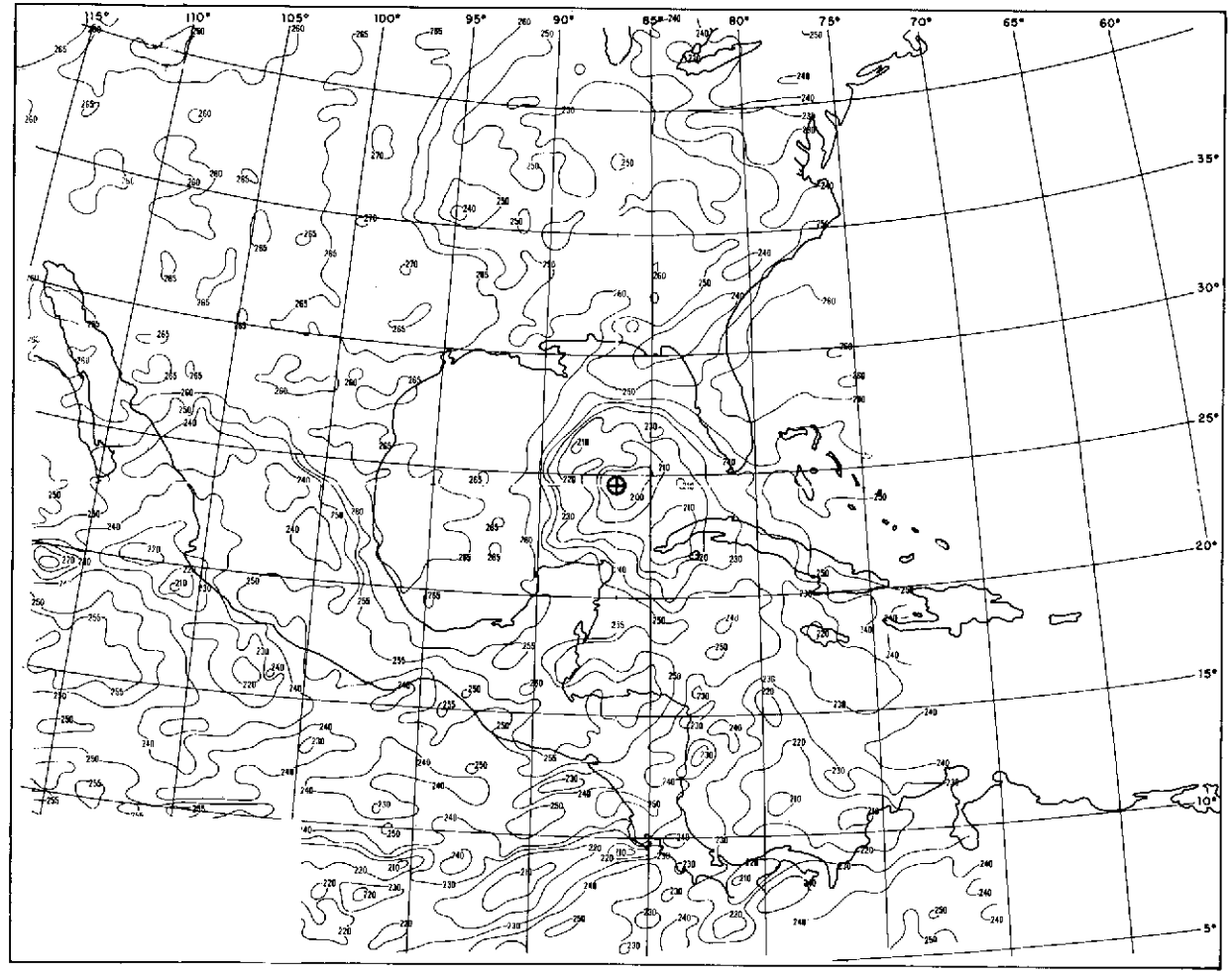

Figure 26. Hurricane Camille at 1500 to 1900 GMT on August 16, 1969, as depicted by 20- to 23-μm T_{BB}'s from the MRIR sensor. The isotherms are given in K and the cyclone center is indicated by the circled cross.

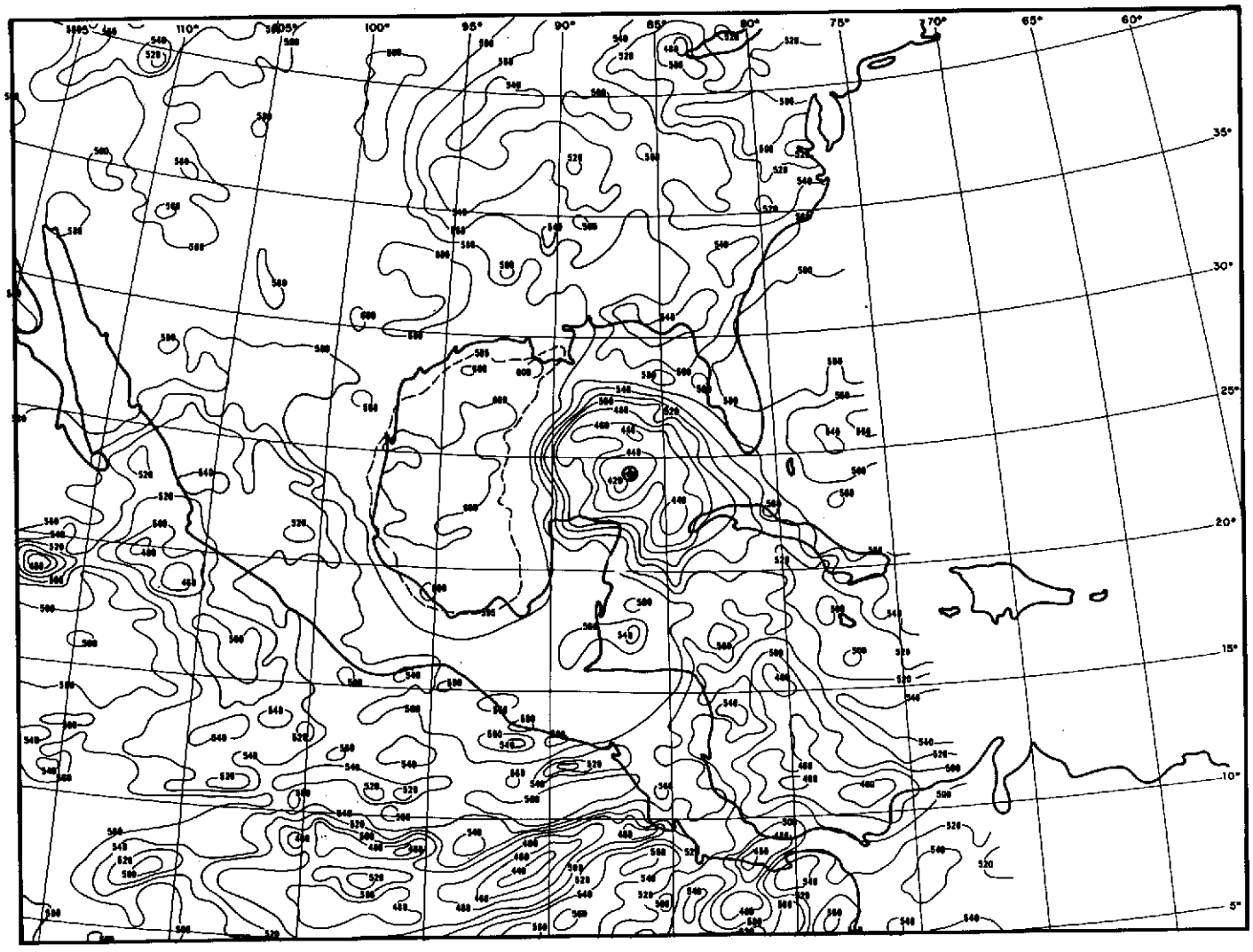

Figure 27. Hurricane Camille at 1500 to 1900 GMT on August 16, 1969, as depicted by the combination of the T_{BB} measurements from the two water vapor channels and the normalized reflectance measurements from the reflectance channel (spectral albedo in percent) of the MRIR sensor.

August 17, 1969

Thirteen hours later (0400 to 0800 GMT) Camille gave the appearance in the satellite data of a storm that had weakened. There were no reconnaissance eye penetrations near the satellite observation time, but the aircraft monitoring the storm on radar and making wind estimates outside the most active region reported that the cyclone appeared to maintain its peak strength. The low 10- to 11-μm T_{BB}'s (Figure 28) near the center covered a sharply reduced area from 12 hours before. Southeast of the center there was still evidence of a low-level moisture inflow where the T_{BB}'s associated with the broad cloud bands were generally not as low as 12 hours earlier.

The 6.5- to 7.0-μm measurements (Figure 29) show that a new surge of cirrus had apparently moved northeastward in response to southwesterly flow over western Florida, Alabama, and Mississippi. The area of dry air west of the center had become smaller and the T_{BB}'s were not as high as 12 hours before in both the 6.5- to 7.0-μm and 20- to 23-μm measurements (Figure 30), which indicated that there had been similar reduction in the size of the relatively clear area. Thus, the subsidence had most likely weakened.

It is unfortunate that there were no reconnaissance aircraft measurements of central pressure taken at the time of the satellite observations early on August 17. The strong surge in the conversion from potential to kinetic energy that accompanied the rapid deepening could have surpassed an equilibrium state during the day on August 16. Then, 12 hours later in response to the equilibrium overshoot, the reverse was observed where the circulation was below the equilibrium state. The details of any possible oscillations in energy level could be specified more definitively with frequent measurements in the same spectral intervals from a geosynchronous satellite.

In the last Nimbus satellite view of Camille before it crossed the U.S. coastline (1500 to 1800 GMT on August 17), the 10- to 11-μm T_{BB}'s (Figure 31) indicated that the cyclone cloud shield had again expanded both horizontally and vertically, but not to the extent that it had near midday on August 16. Perhaps equilibrium had now been reached. Also, the cloud bands southeast of the center had become narrower than before. This suggests that the rapid inflow of high moisture content air from that quadrant was diminishing. Camille had now increased its forward movement to 11 to 12 kn in the same direction as the flow in the southeast quadrant. Thus, even with the same windspeeds, the net inflow would be smaller. There appeared to be a cloud band almost due south of the center that was separated from the other cloudiness. Streamline analyses show that the maximum surface and 850-mbar convergence was the greatest in this region. Since the distance between the ITCZ and Camille was increasing, the entrainment of drier air was becoming a greater possibility, further reducing the chances that the influx of moisture from that source could be continued at the previous rate.

Despite these circumstances, Camille was still a severe hurricane (minimum central pressure of 905 mbar). A probable major contributing factor was that the sea surface temperatures surrounding the storm were 2 to 3 standard deviations above normal (304 to 305 K).

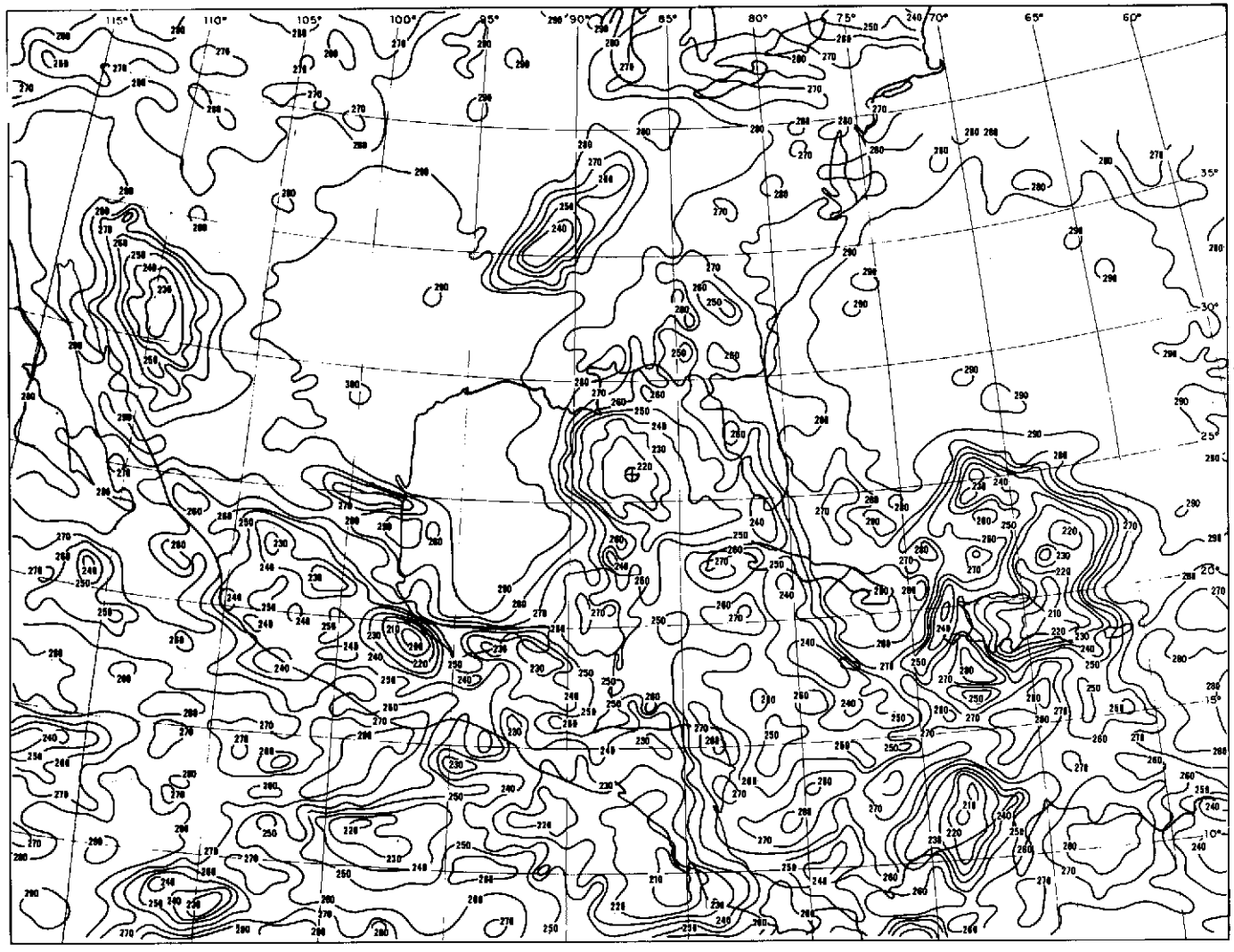

Figure 28. Hurricane Camille at 0400 to 0800 GMT on August 17, 1969, as depicted by 10- to 11-μm T_{BB}'s from the MRIR sensor. The isotherms are given in K and the cyclone center is indicated by the circled cross.

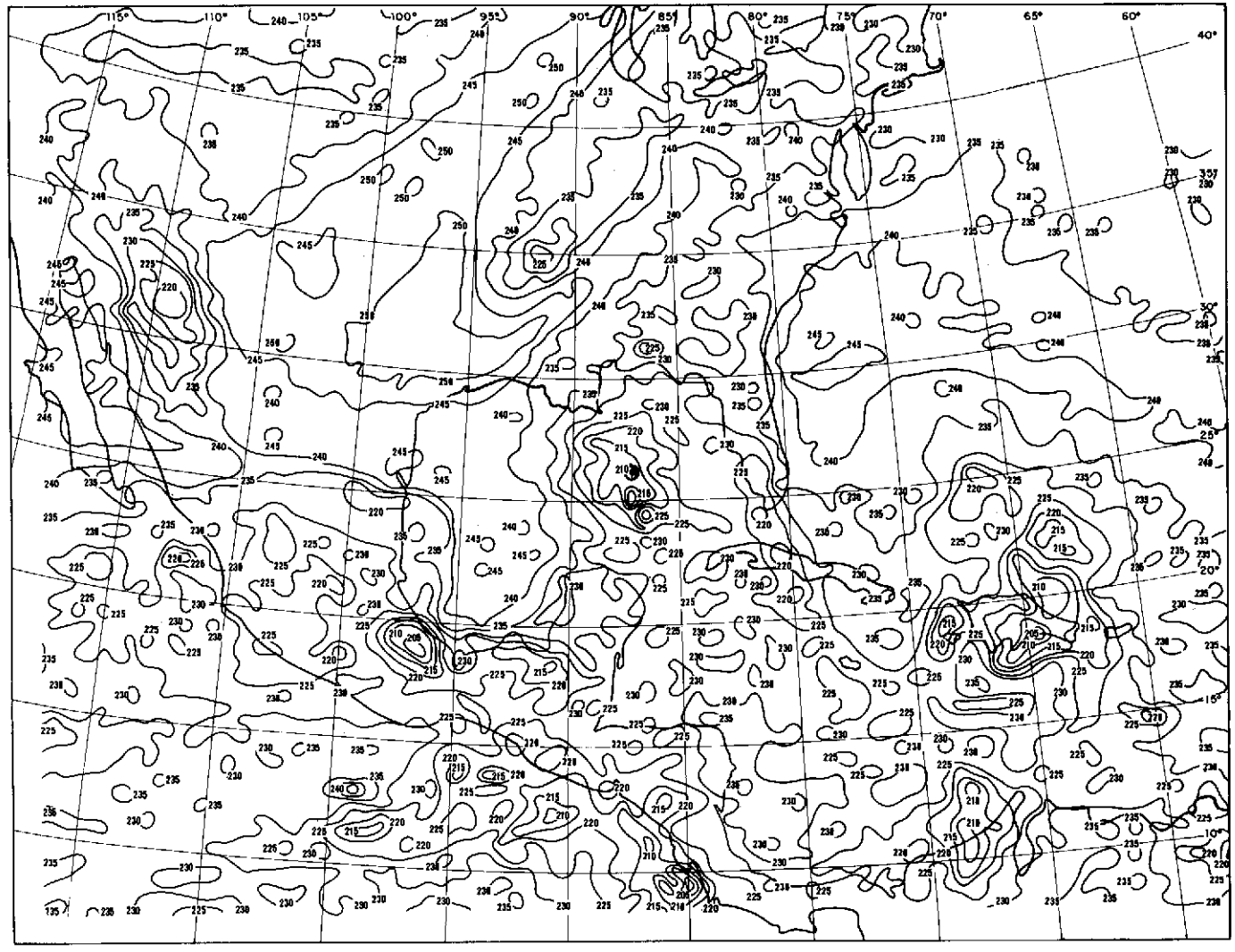

Figure 29. Hurricane Camille at 0400 to 0800 GMT on August 17, 1969, as depicted by 6.5- to 7.0-μm T_{BB}'s from the MRIR sensor. The isotherms are given in K and the cyclone center is indicated by the circled cross.

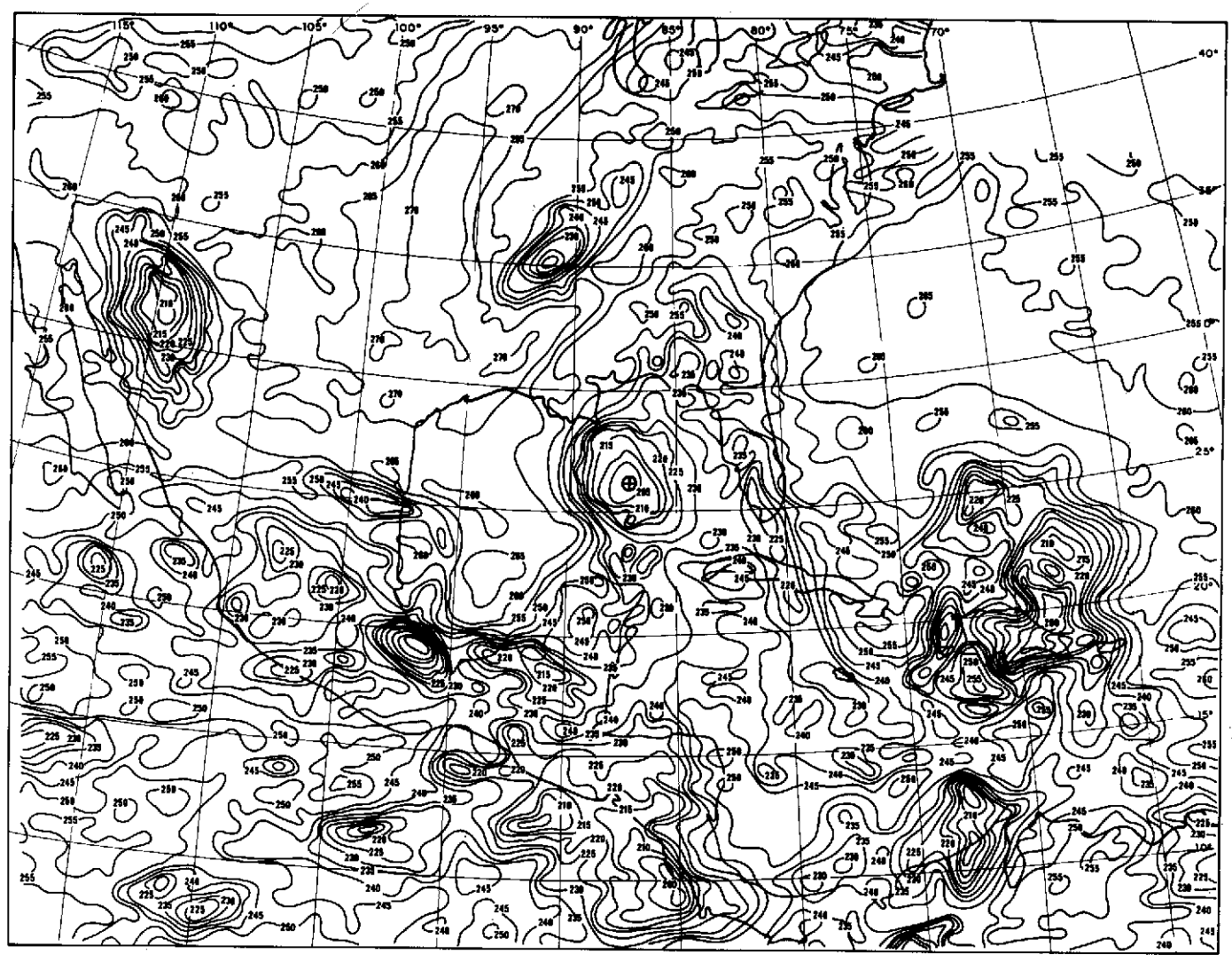

Figure 30. Hurricane Camille at 0400 to 0800 GMT on August 17, 1969, as depicted by 20- to 23-μm T_{BB}'s from the MRIR sensor. The isotherms are given in K and the cyclone center is indicated by the circled cross.

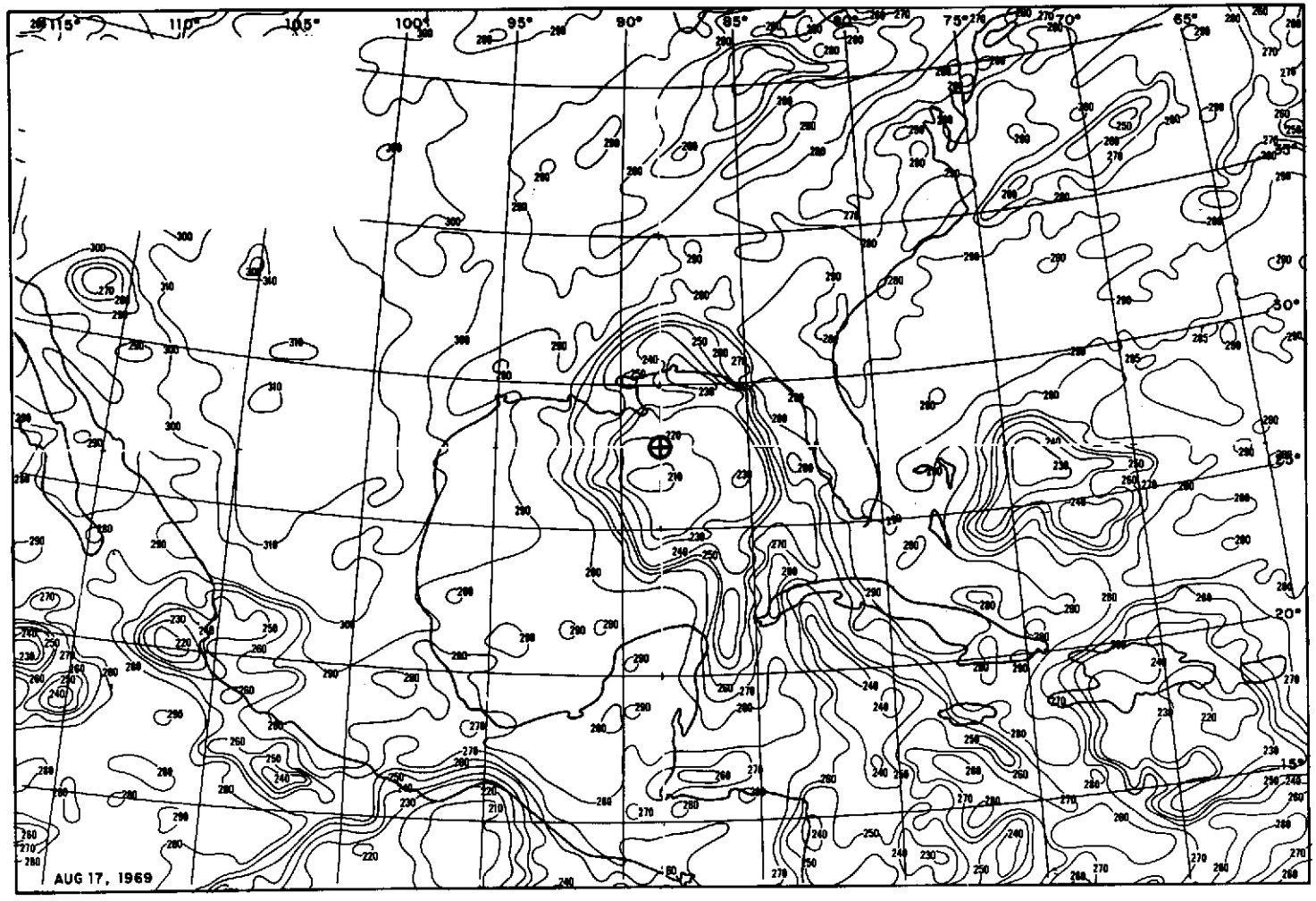

Figure 31. Hurricane Camille at 1500 to 1800 GMT on August 17, 1969, as depicted by 10- to 11-μm T_{BB}'s from the MRIR sensor. The isotherms are given in K and cyclone center is indicated by the circled cross.

The 6.5- to 7.0-μm measurements (Figure 32) indicate that dry air produced by the trough to the north of Camille had moved southward to the northwestern Gulf of Mexico, Southern Texas, and Northeastern Mexico. Since the advected dry air was close to Camille, it was not possible to assess the contribution of any possible subsidence caused by Camille to explain the processes that caused the dry atmosphere. However, some subsidence still should have been present because the line of upper horizontal convergence had persisted west of the center as determined from the 200-mbar rawinsondes and the high and middle cloud motions.

August 18, 1969

At about 0430 GMT, Camille crossed the Mississippi coast with maximum wind speeds estimated from damage surveys at 175 kn, and was observed by Nimbus-3 1 hour later. There had been a sizeable 12-hr decrease in the intense portion of the cloud area as seen in the 10- to 11-μm measurements (Figure 33), although the maximum cloud-top heights reached are about the same level near the eye. The separation distance between the cyclone and the ITCZ had continued to increase, and the cloud patterns suggest that the main movement of the moist air tongue was passing to the east of Camille with a cloud band south of the center that was weaker than 12 hours before. The surface air southeast of the center was still flowing almost directly towards the center, but at 850 mbar the flow had a smaller component to the west and this air was being carried east of the main portion of Camille. The principal change in the 6.5- to 7.0-μm measurements (Figure 34) had been that the T_{BB}'s were lower in the dry air advected southwest of the center. At the same time, the 6.5- to 7.0-μm T_{BB}'s associated with the dry air northwest of Camille had remained about the same. The middle and high cloud motions on August 17 and the 0000 GMT 200-mbar chart indicated that upper tropospheric horizontal convergence appeared to be increasing in this area as the southwest flow along the outer boundary of the outflow moved northward into an area of northwest flow.

Over the United States

Interaction with the Westerlies

Camille rapidly weakened as it moved inland. By 1200 GMT the storm had reached Jackson, Mississippi, with maximum wind gusts of about minimum hurricane force. Nimbus-3 observed the cyclone near midday when Camille was at tropical storm strength. Figures 35 through 38 show the 10- to 11-μm, 0.2- to 4.0-μm, 6.5- to 7.0-μm, and 20- to 23-μm channel measurements, respectively. There had been a sharp decrease in the maximum cloud-top levels (Figure 35). The minimum 10- to 11-μm T_{BB} is 225 K, and assuming that the clouds were opaque and filled the field of view of the radiometer, this temperature is located at 200 mbar on the 1200 GMT, Jackson, Mississippi, sounding. Twelve hours earlier the minimum cloud top T_{BB}'s were 205 to 209 K, which is near 150 mbar on both the 0000 GMT, August 18 soundings at Jackson and Shreveport, Louisiana. The 2-km drop

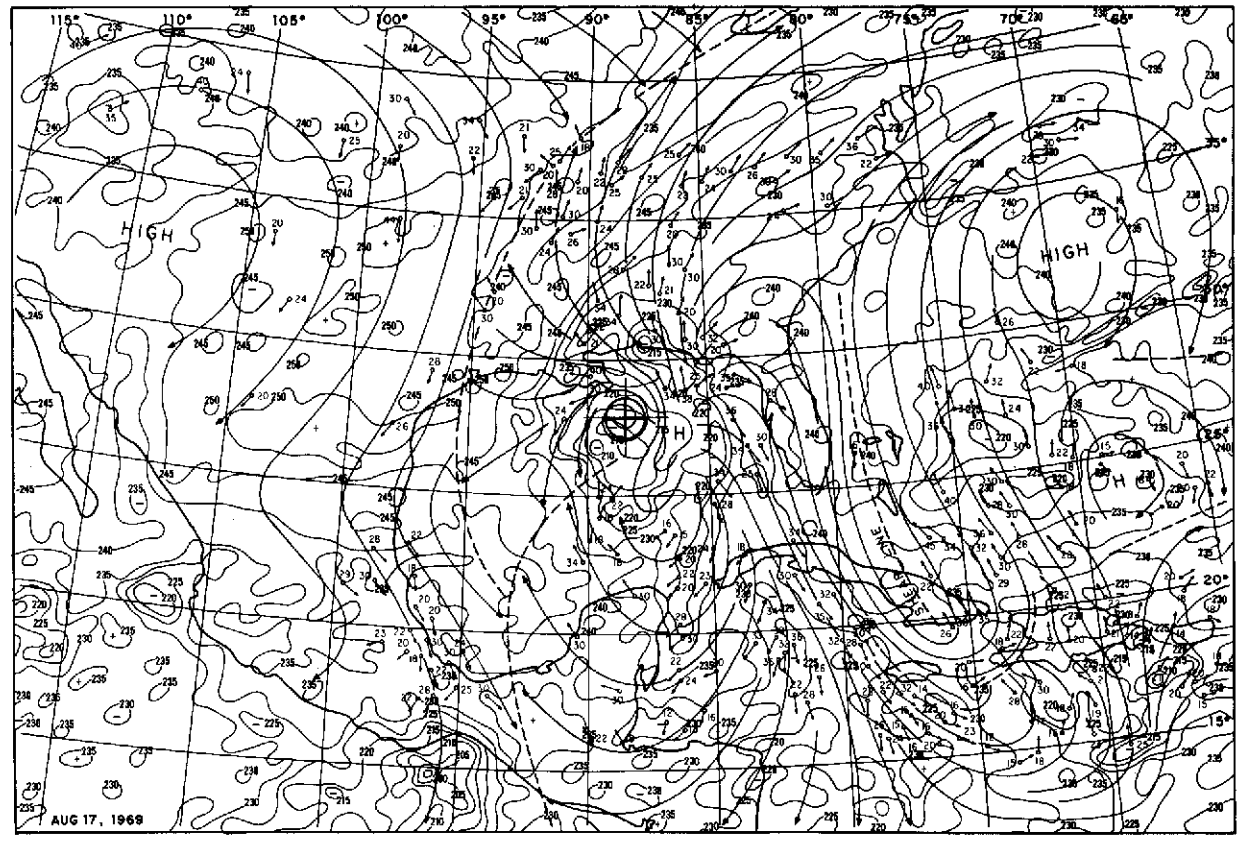

Figure 32. Hurricane Camille at 1500 to 1800 GMT on August 17, 1969, as depicted by 6.5- to 7.0-μm T_{BB}'s from the MRIR sensor. The isotherms are given in K and the cyclone center is indicated by the circled cross. Superimposed on the analysis of the radiation data are cloud motion vectors derived from high and middle clouds tracked from ATS-3 satellite images and the streamline analysis based on the cloud motions and 200-mbar rawins. The cloud motion directions and speeds are indicated in the same manner as in Figure 14.

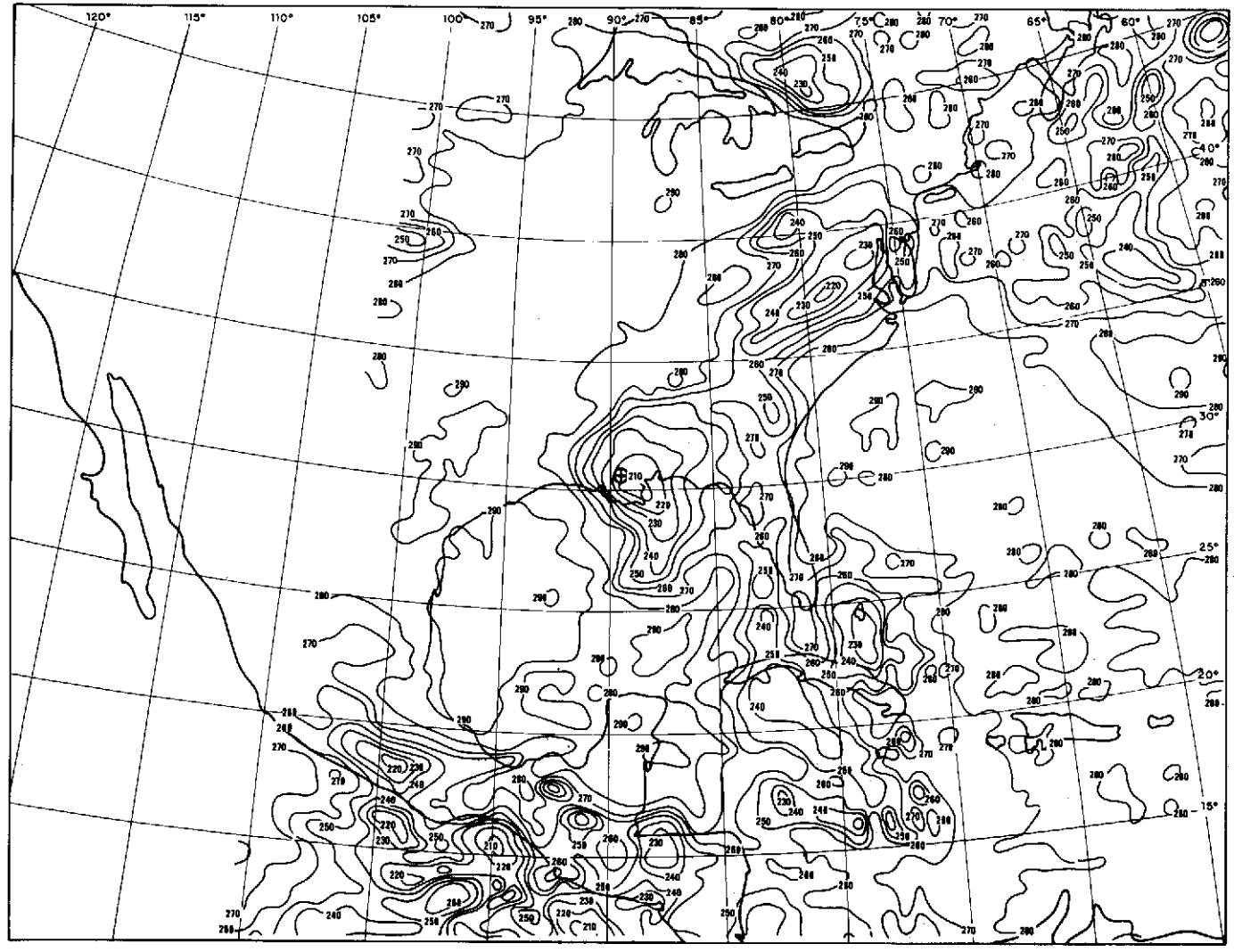

Figure 33. Hurricane Camille at 0400 to 0600 GMT on August 18, 1969, as depicted by 10- to 11-μm T_{BB}'s from the MRIR sensor. The isotherms are given in K and the cyclone center is indicated by the circled cross.

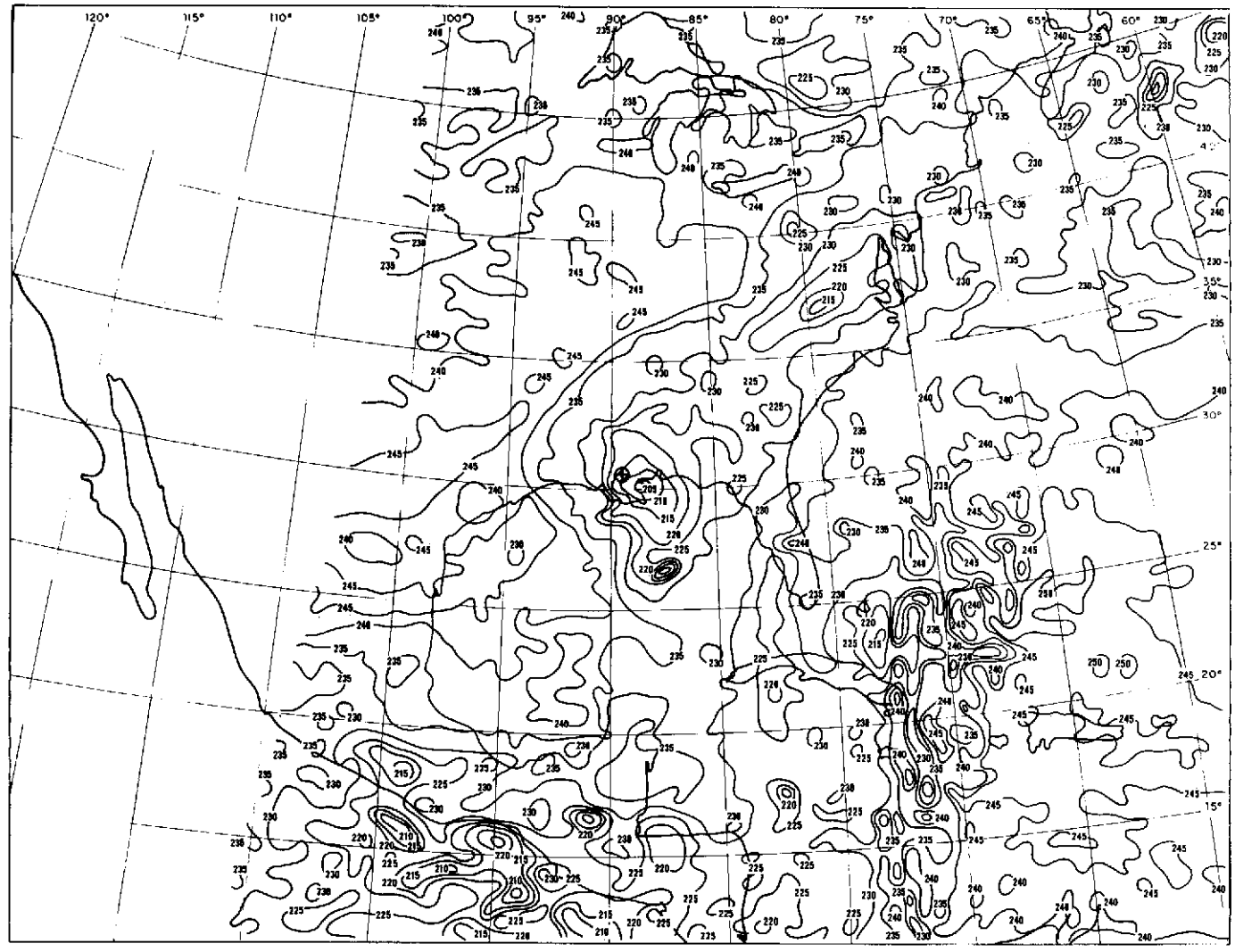

Figure 34. Hurricane Camille at 0400 to 0600 GMT on August 18, 1969, as depicted by 6.5- to 7.0-μm T_{BB}'s from the MRIR sensor. The isotherms are given in K and cyclone center is indicated by the circled cross.

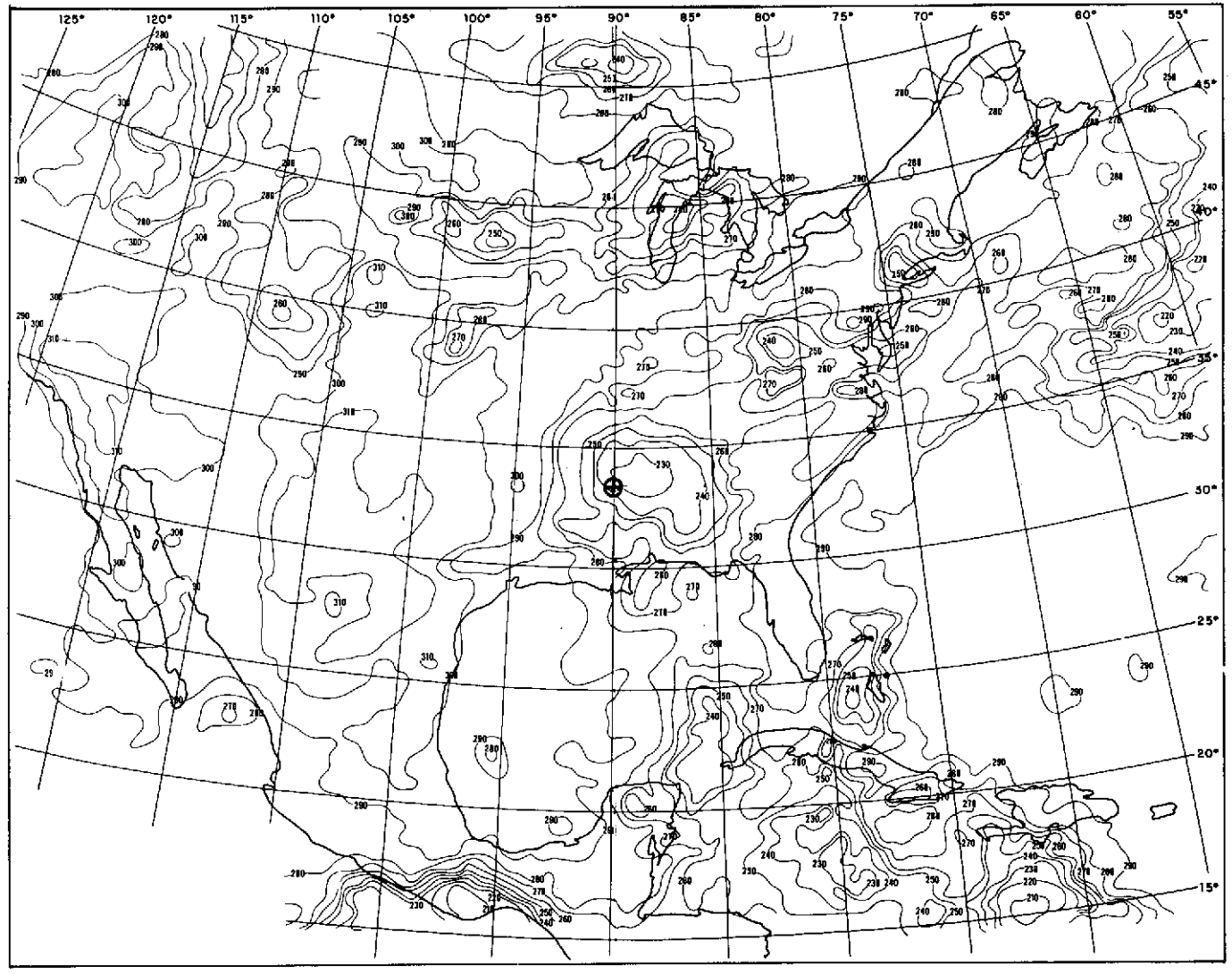

Figure 35. Tropical storm Camille at 1600 to 1900 GMT on August 18, 1969, as depicted by 10- to 11-μm T_{BB}'s from the MRIR sensor. The isotherms are given in K and the cyclone center is indicated by the circled cross.

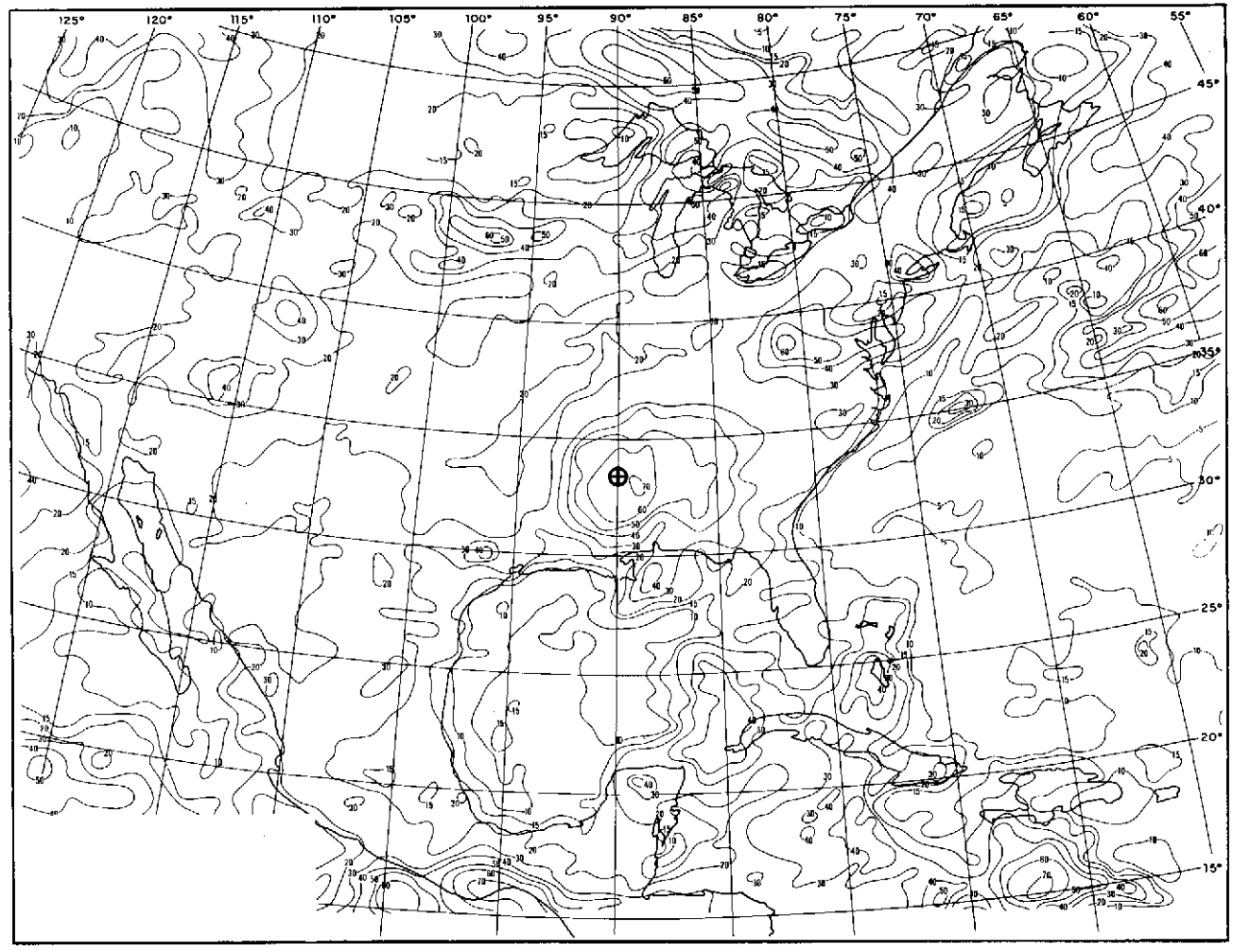

Figure 36. Tropical storm Camille at 1600 to 1900 GMT on August 18, 1969, as depicted by 0.2- to 4.0-μm normalized reflectance measured from the MRIR sensor. The isolines are spectral albedo in percent and the cyclone center is indicated by the circled cross.

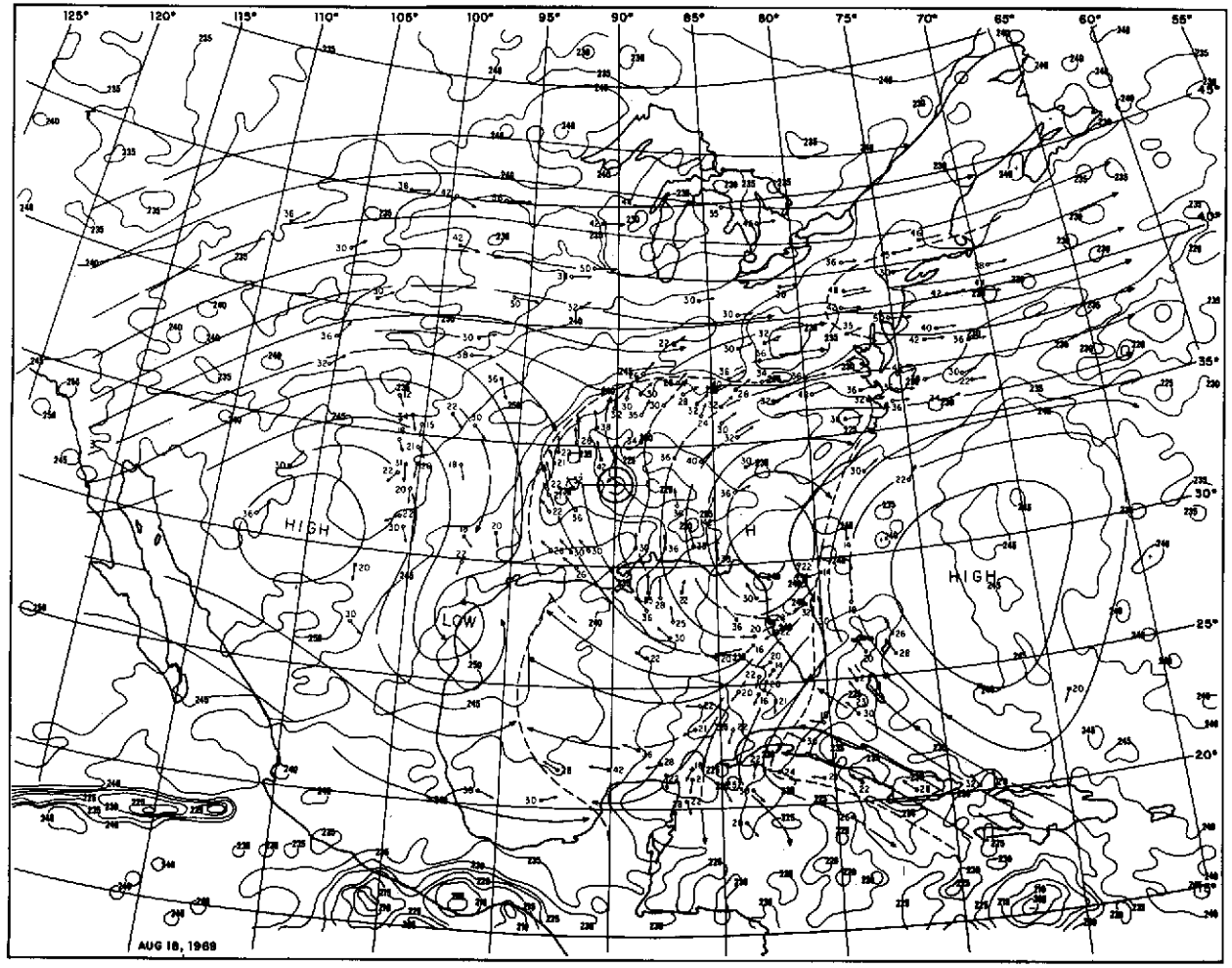

Figure 37. Tropical storm Camille at 1600 to 1900 GMT on August 18, 1969, as depicted by 6.5- to 7.0-μm T_{BB}'s from the MRIR sensor. The isotherms are given in K and the cyclone center is indicated by the circled cross. Superimposed on the analysis of the radiation data are cloud motion vectors derived from high and middle clouds tracked from ATS-3 satellite images and the streamline analysis based on the cloud motions and 200-mbar rawins. The cloud motion directions and speeds are indicated in the same manner as in Figure 14.

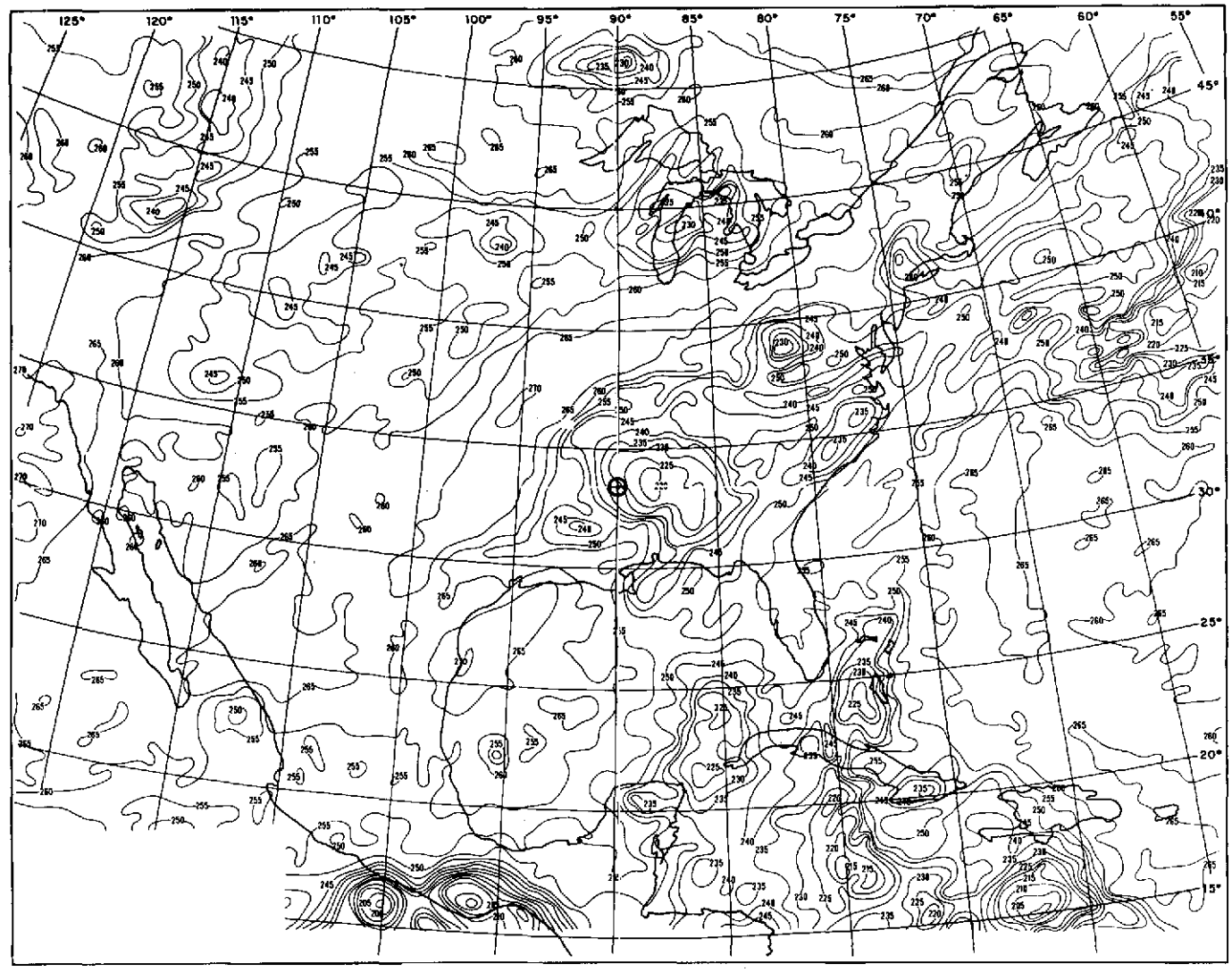

Figure 38. Tropical storm Camille at 1600 to 1900 GMT on August 18, 1969, as depicted by 20- to 23-μm T_{BB}'s from the MRIR sensor. The isotherms are given in K and the cyclone center is indicated by the circled cross.

in maximum cloud-top height was most likely due to the diminished vigor of the upward vertical motion in the most intense activity near the center.

Normalized reflectances as high as 70 percent were found near the center (Figure 36), where the highest reflectances were associated with low 10- to 11-μm T_{BB}'s. The reflectances that were near 60 percent were accompanied by a wide range of T_{BB}'s, some as high as 260 K. This suggests that there may be a relationship between reflectance and the range of concurrent 10- to 11-μm T_{BB}'s when the reflectance is high. The results of a small study investigating this possible relationship are shown in the Appendix.

Perhaps the most interesting satellite observations made of Camille during this phase of its lifecycle were taken by the two water vapor channels (Figures 37 and 38). Surrounding the center to the north and west was a band of high T_{BB}'s which were higher than 12 hours before. This was surprising since the cyclone had weakened so much, and therefore, it should follow that any storm-produced subsidence would diminish. Upper horizontal convergence between the outflow and the westerlies over the lower Mississippi Valley that was first noted from the cloud motions and 200-mbar measurements on August 17 (Figure 37) had become more extensive and intense. The cloud motions on August 18 best illustrated the horizontal convergence zone, with the clouds within the outflow moving from the south and the clouds moving from the northwest in toward Camille in the area northwest of the outflow.

To obtain a better understanding of this area of high T_{BB}'s, both the 1200 GMT, August 18 and 0000 GMT, August 19 constant pressure charts were analyzed every 50 mbar from the surface to 100 mbar and at the 70-, 50-, 30-, and 20-mbar levels to examine the synoptic features. The pressure charts were examined individually and by making a time-lapse movie for each time, vertical continuity could be observed. Selected constant-pressure charts will be shown that highlight the results of viewing the movies.

A quasi-geostrophic adiabatic 10-level diagnostic model was employed for the same period to examine the middle- and upper-tropospheric dynamics and the water vapor budget. The model computes vertical velocity from the quasi-geostrophic adiabatic omega equation for a midlatitude synoptic scale atmosphere at ten levels (1000 mbar to 100 mbar at 100-mbar increments), with a lateral grid spacing of 169 km (Reference 11). The model was later modified to compute the local change of water vapor in an adiabatic atmosphere (Reference 12). Since the model will only handle adiabatic processes, results from the model are most realistic outside the tropical cyclone.

Figure 39 depicts the ground-observed present weather and cloud cover and types at 1800 GMT (less than 1 hour after the satellite overflight), superimposed on the 6.5- to 7.0-μm T_{BB}'s. The cloud information assists in the interpretation of the 6.5- to 7.0-μm measurements where the regions of clouds can be identified that could contribute along with the water vapor to the sensed radiance. Clouds beneath the cirrus level had a negligible effect. The areas covered at least in part by cirrus clouds are shown within the dashed lines in Figure 39. In general, cirrus clouds were not present when $T_{BB} \geqslant 240$ K. Where the

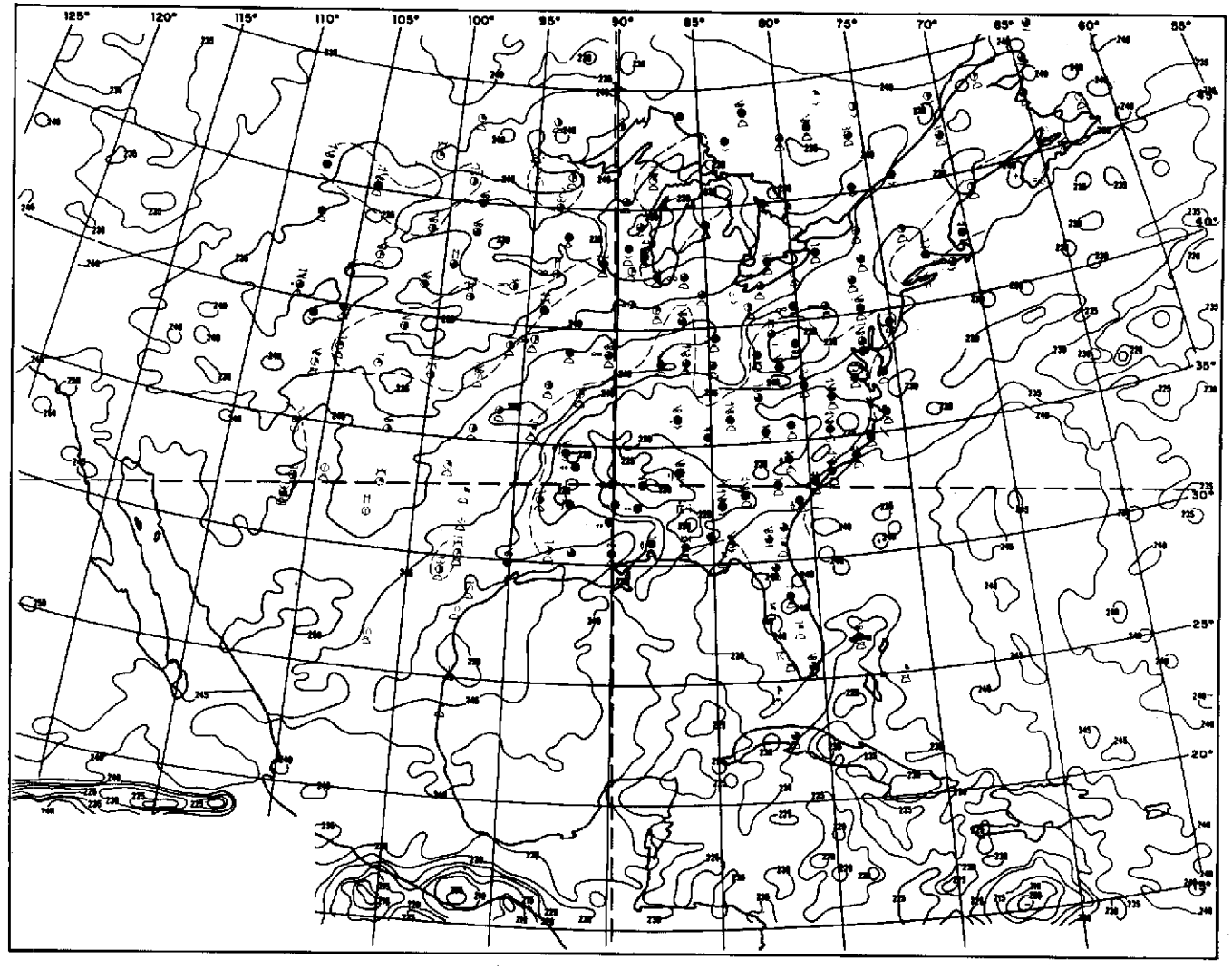

Figure 39. Tropical storm Camille at 1600 to 1900 GMT on August 18, 1969, as depicted by 6.5- to 7.0-μm T_{BB}'s from the MRIR sensor superimposed upon the ground-observed cloud cover and type and present weather. The isotherms are given in K. Areas covered by some cirrus cloud cover are shown within the thin dashed line.

T_{BB}'s of ≥ 240 K and cirrus coincide, the occurrence could be explained by satellite gridding errors, areas of cirrus much smaller than the radiometer field of view, or cirrus near the local horizon of the observer. Only low and middle clouds occurred in the area of maximum T_{BB}'s northwest of the center. Cirrus were almost always present when the T_{BB}'s were ≤ 235 K. Thus, the only T_{BB} range where considerable interpretation ambiguity existed was 235 to 239 K.

Figure 40 is the superposition of the August 18, 1200 GMT, 300-mbar chart on the 6.5- to 7.0-μm measurements that were taken 5 hours later. Immediately to the northwest of the

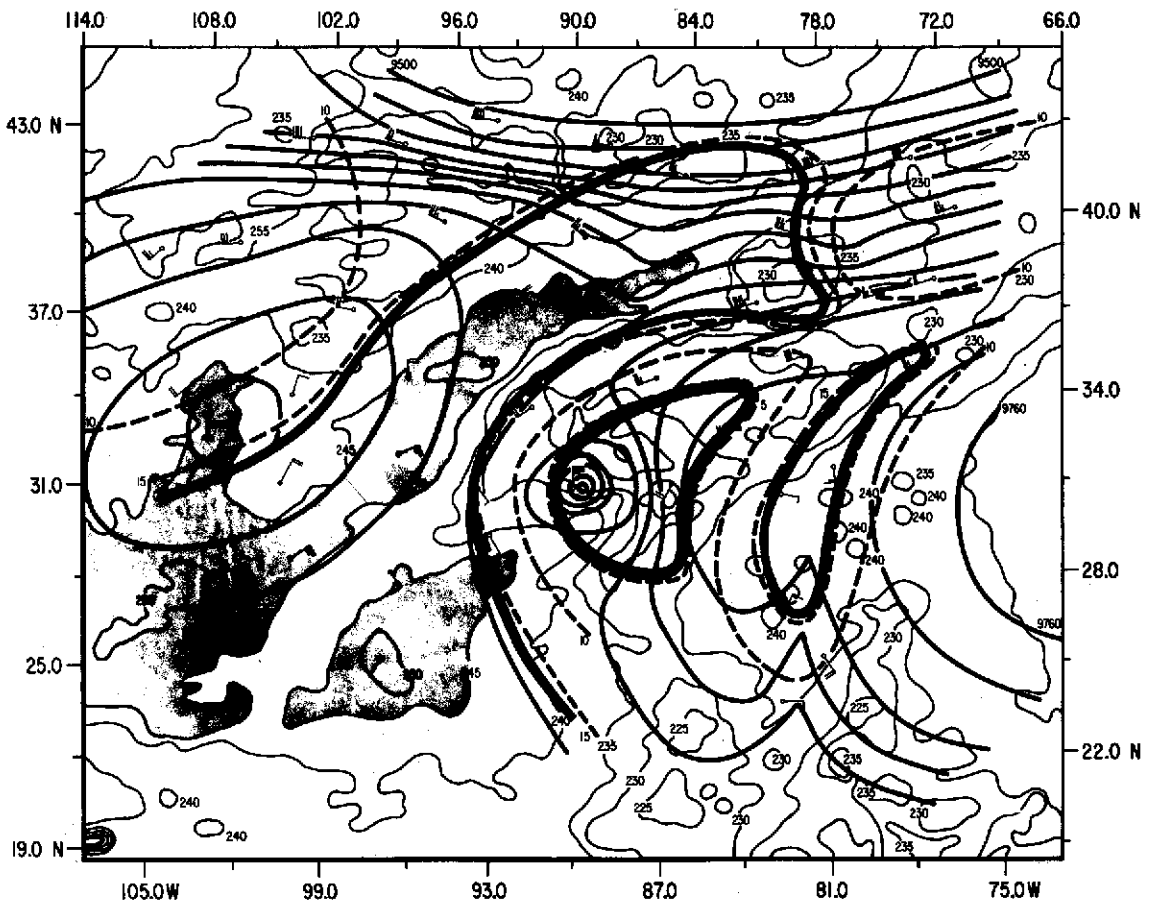

Figure 40. Superposition of the 300-mbar geopotential heights, dewpoint depressions, and winds at 1200 GMT on August 18, 1969, upon the 6.5- to 7.0-μm T_{BB}'s from the MRIR sensor at 1600 to 1900 GMT. The 6.5- to 7.0-μm (thin solid lines) and dewpoint depression (dashed lines) isotherms are given in K and the geopotential heights are in meters. The areas where the dewpoint depressions are ≤ 5 or ≥ 15 are accentuated with a stippled border. Additional stippling depicts the regions where the 6.5- to 7.0-μm T_{BB}'s are ≥ 245 K.

cyclone is the southwest flow that is part of the outflow. In the dry air further to the northwest the environmental current is from the northwest. The northwest flow has a vertical extent from 450 mbar to 150 mbar and the maximum angle with the outflow

was at 300 mbar. When the northwest flow reaches the edge of the outflow the air must go over or around the storm. Since the outflow extends to, or near, the tropopause, the majority of the air must have flowed around the cyclone. Therefore, the outflow from Camille was acting as a barrier to the ambient winds.

The barrier effect was at its maximum north-northwest of the center where the outflow and the ambient flow were almost perpendicular. Since the 6.5- to 7.0-μm T_{BB}'s were high and had risen north and west of the center in the past 12 hours, the interaction was most likely producing subsidence. Some of the dry air was carried east-northeastward from the point of maximum upper horizontal convergence, but the majority of the air was transported toward the southwest. The dewpoint depression ($T - T_d$) from radiosonde measurements was $\geqslant 15$ K over a broad region that included the high T_{BB}'s north and west of the center. Cirrus overriding the dry air, inaccuracies in the radiosonde humidity element at cold temperatures, and the 5-hr time difference between the conventional and satellite observations are probably the main reasons why there were some T_{BB}'s of $\leqslant 230$ K within the area where $T - T_d \geqslant 15$ K. Where the upper horizontal convergence occurred between the outflow and the environment, the time-lapse analysis of the moisture and wind field indicated that the dry air was penetrating beneath the outflow layer in the middle and upper troposphere.

To obtain further insight into the causes producing the increasingly warm equivalent T_{BB}'s in the 6.5- to 7.0-μm MRIR water vapor channel west and northwest of Camille, two procedures were followed. The first was to examine the upper tropospheric dynamics, and the second was to determine how these dynamics affected the upper tropospheric water vapor.

Figure 41 depicts the 350-mbar vertical motion patterns superimposed upon the 300-mbar geopotential height and radiosonde wind observations. There are two areas of interest. The first is located behind the weakening trough north of Camille. Subsidence of $\geqslant 1$ μbar/s had been induced mainly by differential advection of negative vorticity. Cross section A in Figure 42, which is located west-east vertically through the base of the trough (designated by line A in Figure 41), delineates the vertical extent of this subsidence between longitudes 85° to 95° W. It can be seen that the greatest subsidence was in the upper troposphere. The second area of interest is the obstruction effect previously mentioned in the synoptic discussion. Here subsidence of $\geqslant 0.5$ μbar/s is observed and is attributed to both the Laplacian of horizontal cold air advection and to differential advection of negative vorticity. Since the boundary between the outflow and the ambient flow was much smaller than the spatial resolution of the grid mesh in the model, it is possible that higher vertical velocities could be concentrated along the boundary than were calculated by the model. In quantitatively investigating the horizontal convergence within this area, it was found from vertical mass influx computations at all 10 levels for 1200 GMT, August 18, 1969, that the level of maximum horizontal convergence was above the 350-mbar level with horizontal divergence below. Thus, as was suggested in the synoptic discussion, Camille's upper tropospheric outflow was converging with the westerlies with

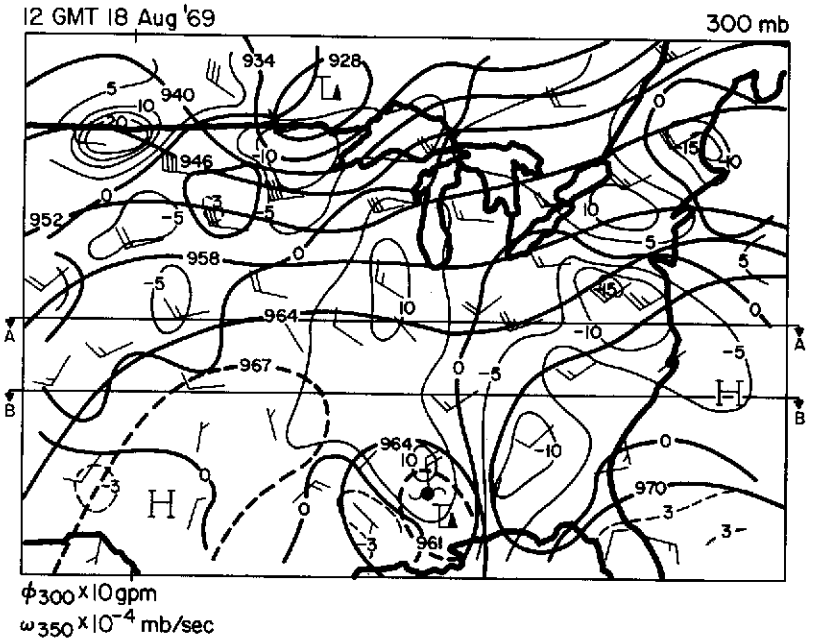

Figure 41. 300-mbar geopotential heights and winds and 350-mbar vertical motions for 1200 GMT on August 18, 1969. Lines A and B denote cross sections A and B which are shown in later diagrams.

subsidence below. Figure 43 depicts the 300-mbar horizontal divergence field superimposed upon the 300-mbar geopotential height and radiosonde wind observations. An area of horizontal convergence of $\leq -5 \times 10^{-6}$ s^{-1} is seen northwest of Camille. As seen in cross section B in Figure 44 which is located west-east vertically through the obstruction effect area (designated by line B in Figure 41), the subsidence again extends throughout the troposphere between longitudes 88° to 98° W, but with weaker magnitudes in the upper troposphere as compared with the upper troposphere subsidence behind the trough as seen in cross section A.

To best illustrate how the two areas of dynamical interest support the tongue of warm T_{BB}'s measured northwest of Camille at 1800 GMT on August 18, three-dimensional trajectories were computed at 3-hr intervals between 1200 GMT on August 18 to 0000 GMT on August 19 at the 350-mbar level. Figure 45 depicts four such trajectories superimposed upon the field of 6.5- to 7.0-μm T_{BB}'s for 1800 GMT on August 18. Trajectories 1 and 2 best outline the upper tropospheric flow from the base of the trough southwestward into the obstruction effect area. It is seen that the parcels were first under the influence of subsidence behind the trough, but as they moved out of the trough and into the area of the obstruction effect, the parcels were forced to continue to subside. Further downstream, southwest of this obstruction effect as outlined by trajectory 4, the air parcel continued to subside during the first 6 hours as it moved southwestward, but at a much slower rate. This subsidence was completely induced by the

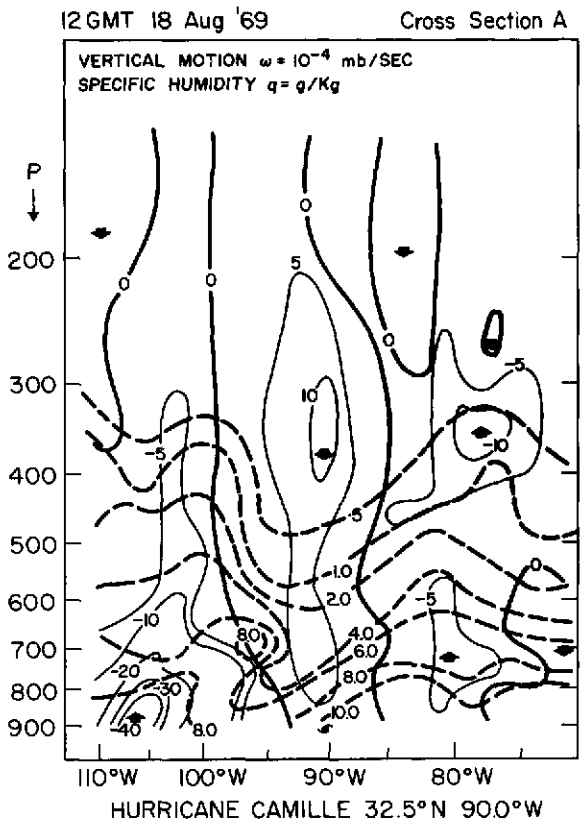

Figure 42. Cross section A, depicting vertical motions (solid lines) and specific humidity (dashed lines) for 1200 GMT, August 18, 1969.

Laplacian of the horizontal advection of colder air from the northeast. After 6 hours the parcel moved into an area of slight ascending motion. Trajectory 3 illustrates an air parcel moving through the base of the trough. During the first 9 hours the parcel experienced subsidence induced mainly by differential negative vorticity advection from behind the trough. However, once the parcel moved out in front of the trough it moved into an area of ascending motion. Thus the trajectories suggest that there were two tongues of subsidence that were associated with the tongue of warm T_{BB}'s: one moving cyclonically northeastward through the base of the trough and the other moving anticyclonically southwestward out of the trough and into the area of enhanced subsidence below the obstruction effect area.

To obtain a better comprehension of what the 6.5- to 7.0-μm water vapor channel measurements indicated, an examination of the effects of the upper troposphere dynamics upon water vapor amounts at this same level was made. In determining the water vapor budget the local change of specific humidity for an adiabatic atmosphere was calculated. Assuming

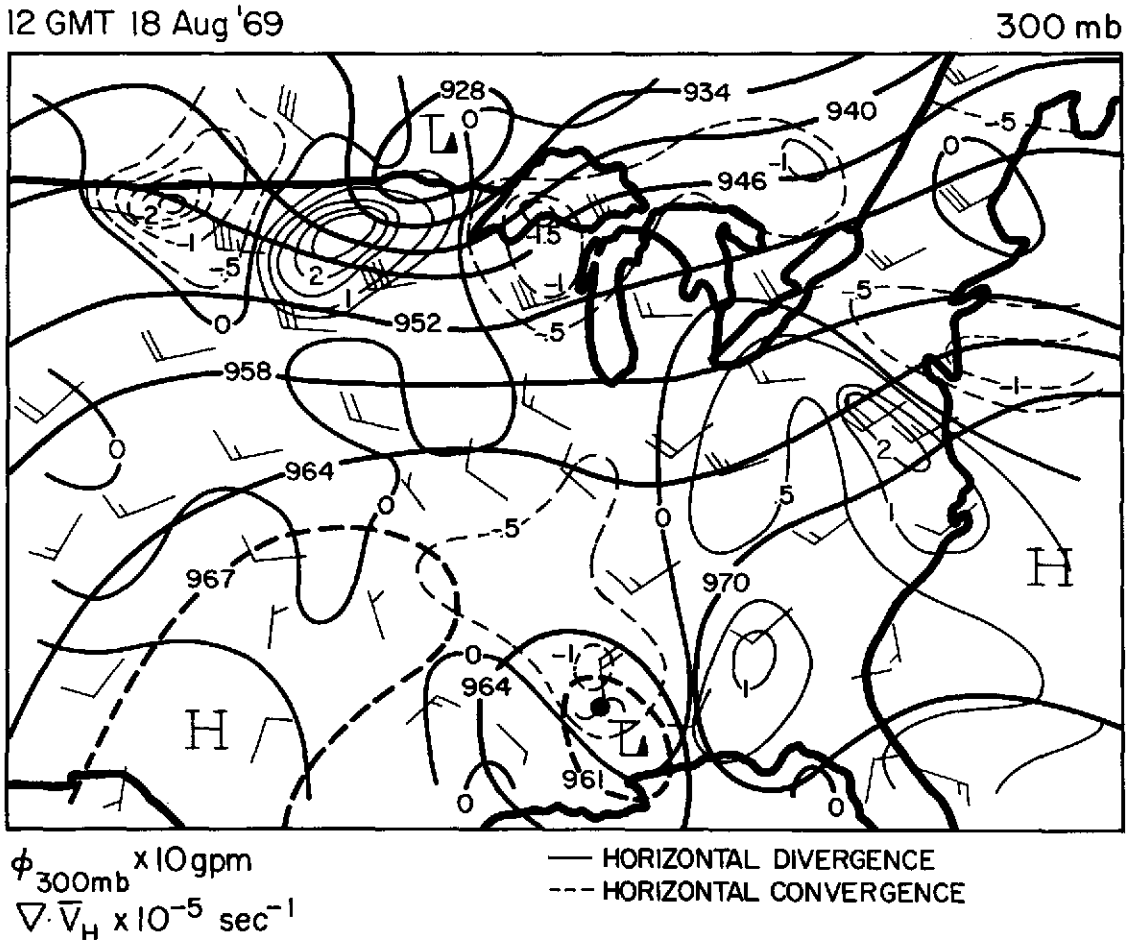

Figure 43. 300-mbar geopotential heights (in decameters), winds, and horizontal divergence analysis (thinner lines) for 1200 GMT on August 18, 1969.

that precipitation was not occurring in the subsidence areas and that there was little or no evaporation, the following expression for the water vapor budget is obtained:

$$P - E = 0 = -\frac{\partial q}{\partial t} - \nabla \cdot q\overline{V} - \frac{\partial (qw)}{\partial p} \qquad (1)$$

or

$$\frac{\partial q}{\partial t} = -\overline{V} \cdot \nabla q + q\frac{\partial w}{\partial p} - \frac{\partial (qw)}{\partial p} \qquad (2)$$

where

$\partial q/\partial t$ = local change of specific humidity

$-V \cdot \nabla q$ = horizontal advection of specific humidity

$q \frac{\partial w}{\partial p}$, $-\frac{\partial (qw)}{\partial p}$ = vertical advection of specific humidity

P = precipitation

E = evaporation

All three terms on the right side of Equation 2 were computed from data from 1200 GMT on August 18, 1969, for the interior grid points from 800 mbar to 300 mbar and were then algebraically added to obtain the local change of specific humidity. Figures 46 and 47

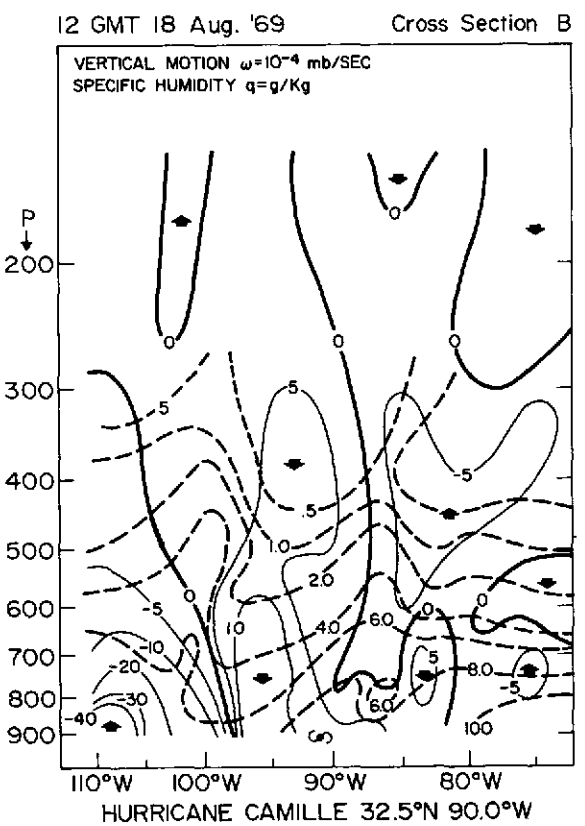

Figure 44. Cross section B, depicting vertical motion (solid lines) and specific humidity (dashed lines) for 1200 GMT on August 18, 1969.

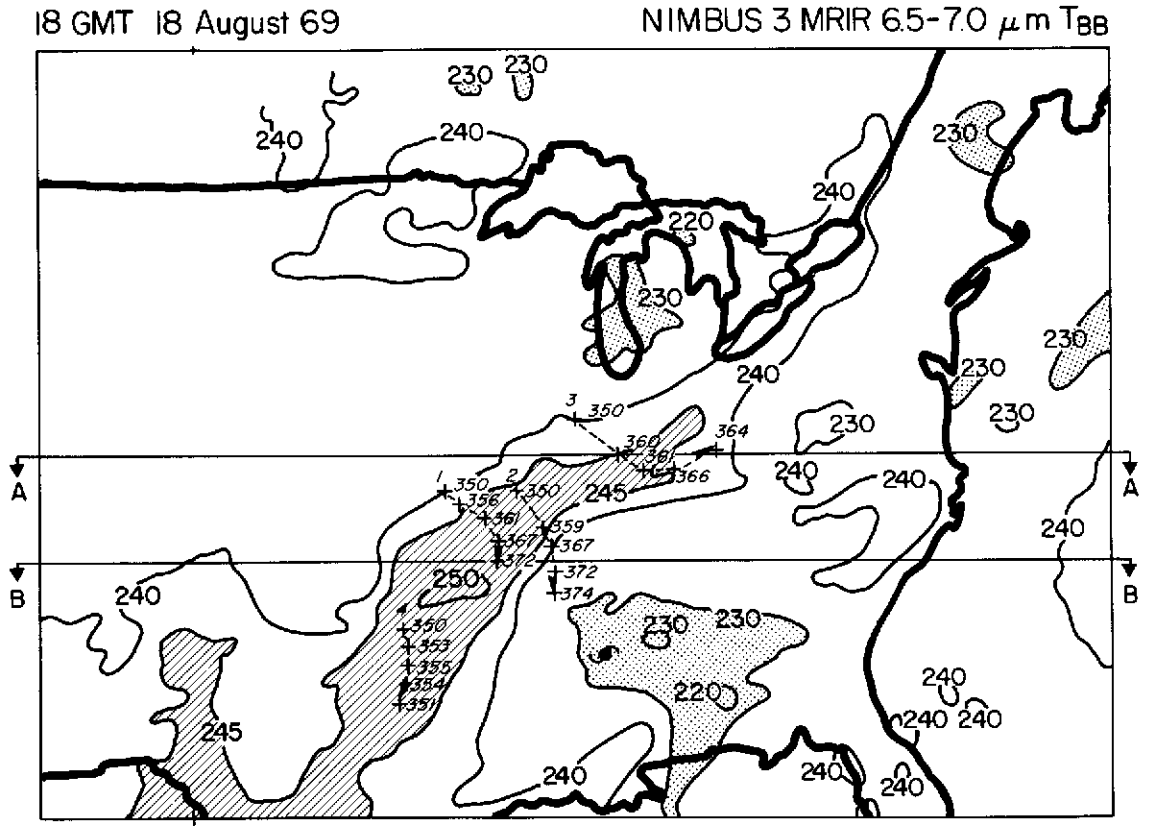

Figure 45. Three-dimensional trajectories between 1200 GMT on August 18, 1969, and 0000 GMT on August 19, 1969, initiated at the 350-mbar level, superimposed upon the 6.5- to 7.0-μm T_{BB}'s at 1600 to 1900 GMT, August 18, 1969, from the MRIR sensor. The crosses represent the position of the air parcels at 3-hr intervals and the number to the side represents the pressure height.

represent these water vapor budget computations for a small segment of cross sections A and B, respectively, at 1200 GMT of August 18. Figure 46 depicts the vertical intersection through the area of warm T_{BB}'s near the trough north of Camille, and Figure 47 depicts the vertical intersection through the area of warm T_{BB}'s in the obstruction effect area northwest of Camille. The graph located above the local change of specific humidity calculation represents the 6.5- to 7.0-μm and 20- to 23-μm T_{BB}'s along the cross section as observed by the MRIR sensor approximately 6 hours later. It can be seen from the local change of specific humidity computations in Figure 46 that the upper troposphere became drier with a maximum decrease of specific humidity of about 5×10^{-5} g/kg s^{-1}. This drying trend is attributed mainly to subsidence and to a lesser extent to the horizontal advection of drier air from behind the trough. This is what is inferred by the 6.5- to 7.0-μm T_{BB} trace along the same segment of cross section A 6 hours later. The location of the maximum T_{BB} corresponds closely to the location of the greatest upper tropospheric drying.

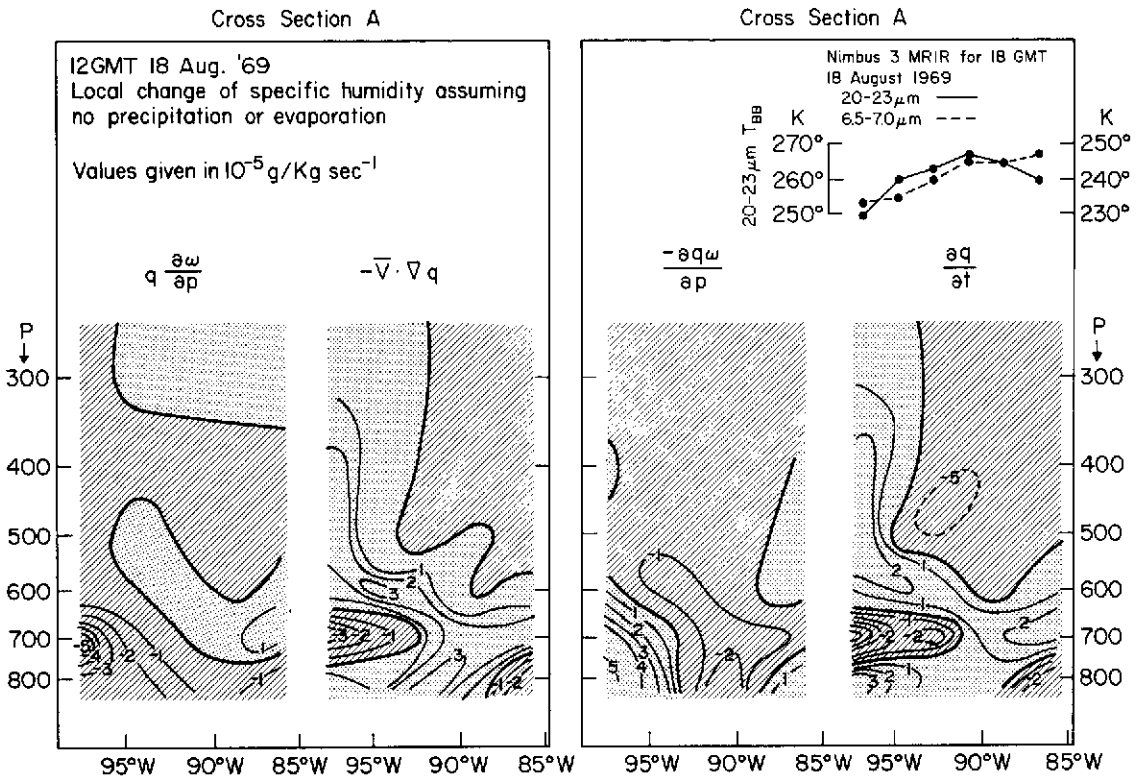

Figure 46. Segment of cross section A depicting the calculations of the local change of specific humidity and its partitioned terms from 1200 GMT, August 18, 1969, data and the 6.5- to 7.0-μm and 20- to 23-μm T_{BB} traces for the same segment of cross section A at 1800 GMT on August 18, 1969.

The same results were found in Figure 47. The upper troposphere also became drier, as seen in the local change of specific humidity calculations, but at a somewhat faster rate as compared to the calculations represented in Figure 46 for the same level. Again this is attributed mainly to subsidence, but as before, horizontal advection of drier air from the northeast, particularly in the middle troposphere, cannot be ignored. The 6.5- to 7.0-μm T_{BB} at 1800 GMT again shows that the location of the maximum T_{BB} corresponded favorably to the position of the upper tropospheric segment that had maximum drying.

From the examination of the upper tropospheric dynamics and water vapor budget, it can be concluded that the dry air that had descended to the west of the trough had moved both northeastward and southwestward. The southwestward moving branch continued to descend under the influence of enhanced subsidence induced by the upper tropospheric convergence between Camille's outflow and the westerlies.

East of Camille there was another area where $T - T_d \geq 15$ K in the middle troposphere. This appears to have been produced by a shear line between two anticyclones east of the storm. The time-lapse movie that showed the shear line sloped from east to west with decreasing altitude as the western anticyclone, probably created by the outflow, weakened and disappeared below the outflow layer. Cirrus overriding the dry air prevented the occurrence

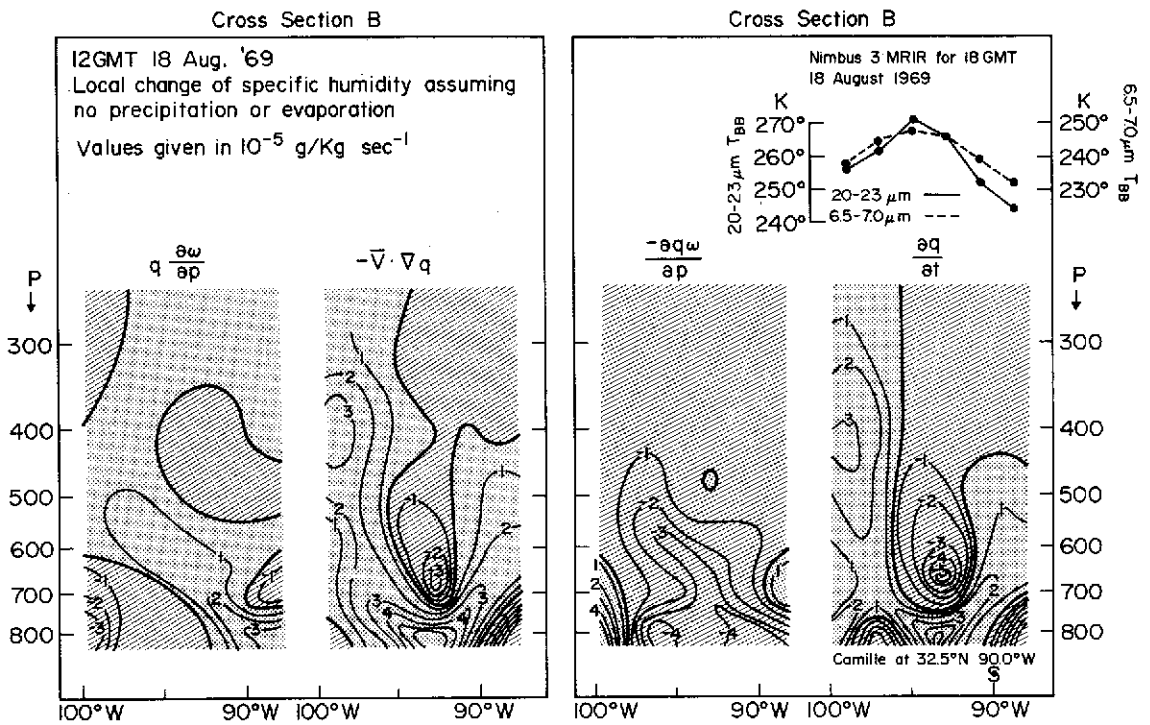

Figure 47. Segment of cross section B depicting the calculations of the local change of specific humidity and its partitioned terms from 1200 GMT, August 18, 1969, data and the 6.5- to 7.0-μm and 20- to 23-μm $\overline{T}_{BB}$ traces for the same segment of cross section A at 1800 GMT on August 18, 1969.

of high T_{BB}'s except for the southern portion where no cirrus was indicated by a few stations over Florida where T_{BB}'s as high as 240 K were observed. Higher T_{BB}'s were not measured because the $T - T_d$ was not consistently large throughout the 300- to 500-mbar layer. Below 300 mbar, $T - T_d$ generally varied between 10 and 15 and the 235 to 240 K measurements compare favorably to the 236 K T_{BB} that would be expected from a clear atmosphere using radiative transfer theory and the 1200 GMT temperature and moisture profile from Tampa.

The superposition of the 500-mbar analysis for August 18 at 1200 GMT on the 20- to 23-μm T_{BB} field is shown in Figure 48. North and west of Camille is the broad dry zone that was observed in the 6.5- to 7.0-μm measurements. Most of the T_{BB}'s of ≥ 265 are within the $T - T_d \geq 20$ isoline. A small 500-mbar anticyclone was located almost underneath the area of maximum horizontal convergence at higher levels. Most of the dry air in the middle troposphere created by the subsidence was transported southwestward by the broad current of northeast winds which was similar to observations in the upper troposphere. The $T - T_d \geq 20$ measurements east of the center, produced by the shear line, were underneath the cirrus moving eastward from Camille. Therefore, this dry area was not detectable with the 20- to 23-μm radiances.

In examining the T_{BB} measurements in the 20- to 23-μm water vapor channel, the same procedures were followed for the examination of the dynamics and the water vapor budget

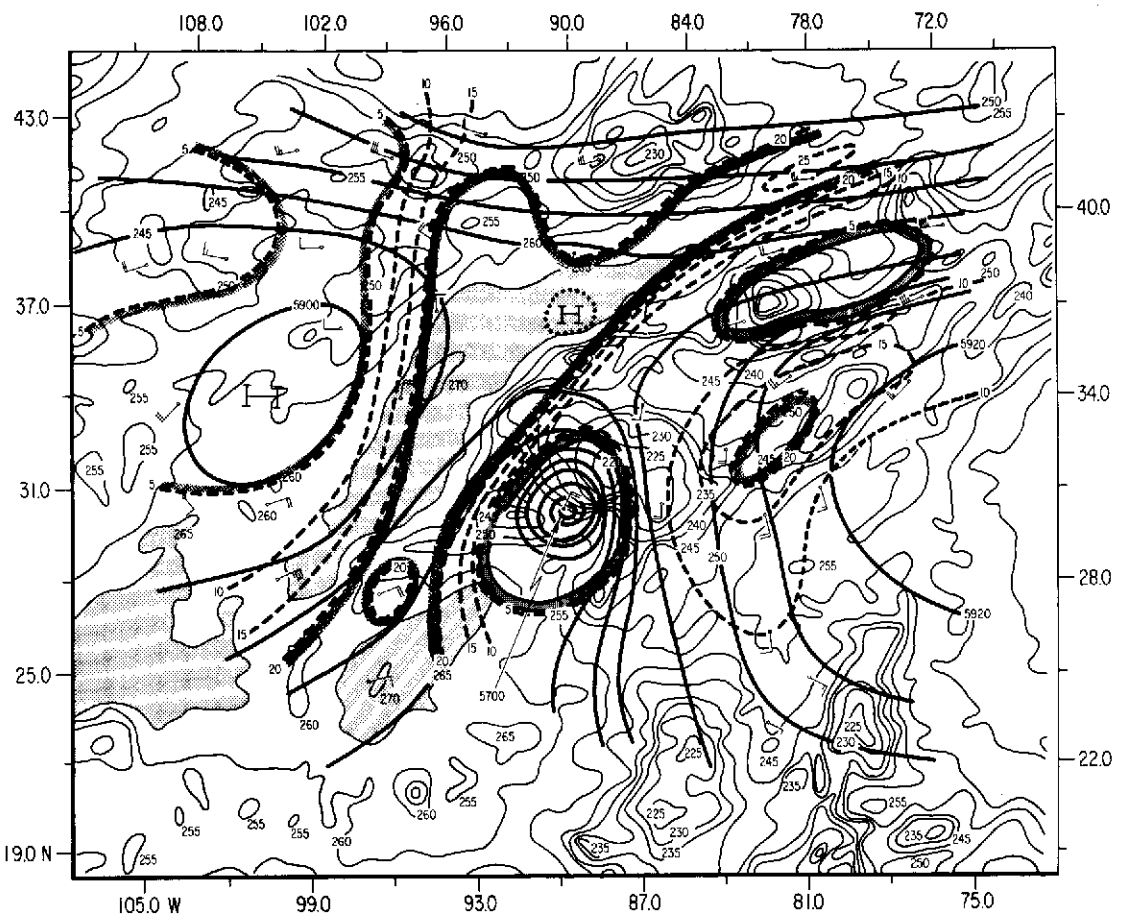

Figure 48. Superposition of the 500-mbar geopotential heights, dewpoint depressions, and winds at 1200 GMT on August 18, 1969, upon the 20- to 23-μm T_{BB}'s from the MRIR sensor at 1600 to 1900 GMT. The 20- to 23-μm (thin solid lines) and dewpoint depression (dashed lines) isotherms are given in K and the geopotential heights are in meters. The areas where the dewpoint depressions are $\leqslant 5$ or $\geqslant 20$ are accentuated with a stippled border. Additional stippling depicts the regions where the 20- to 23-μm T_{BB}'s are $\geqslant 265$ K.

as were used for the measurements in the 6.5- to 7.0-μm channel. However, since the emission measured in the 20- to 23-μm channel emanates mostly from the middle troposphere for clear-sky conditions, the dynamics and water vapor budget must be examined in both the upper and middle troposphere.

The two areas of greatest dynamical interest are the area behind the trough and the area of the obstruction effect. Figure 49 shows the 550-mbar vertical motion field superimposed upon the 500-mbar geopotential heights, radiosonde wind observations, and integrated precipitable water amounts above 800 mbar.

The subsidence associated with the trough in the upper troposphere had created an area of horizontal divergence that can be seen from the 500-mbar wind observation north of Camille. This is the small middle tropospheric anticyclone mentioned in the synoptic discussion. Emanating from this area was a southwest-northeast orientated tongue of

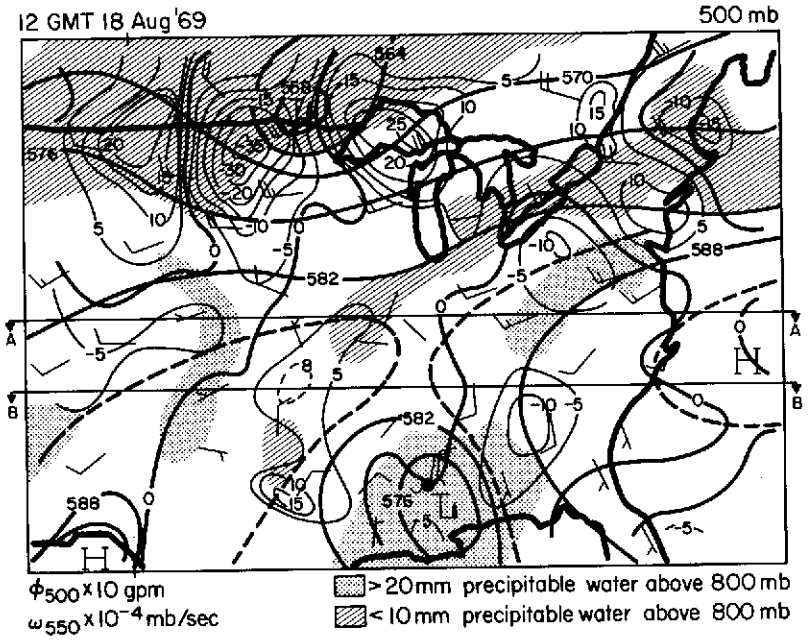

Figure 49. 500-mbar geopotential heights and wind velocities, 550-mbar vertical motions, and integrated precipitable water above 800 mbar for 1200 GMT on August 18, 1969. Lines A and B denote cross sections A and B which are shown in later diagrams.

subsidence of the magnitude of ≥ 0.5 μbar/s. As seen in cross section A (Figure 42), subsidence extended throughout the middle troposphere and was induced by both the differential advection of negative vorticity and the Laplacian of horizontal cold air advection. Further southwestward, under the area of the upper tropospheric obstruction effect, subsidence still existed, but the upper tropospheric convergence was not the dominant reason for its existence. The tongue of maximum subsidence was further west, away from the obstruction effect, and was induced mainly by the Laplacian of horizontal cold air advection from the northeast. Cross section B between longitudes 90° to 100° W in Figure 44 best illustrates the westward displacement of the middle tropospheric subsidence from that in the upper troposphere.

Figure 50 shows four middle tropospheric trajectories superimposed upon the MRIR 20- to 23-μm T_{BB} field for 1800 GMT on August 18. All of the trajectories originated at the 550-mbar level at the same points as those at the upper troposphere level. A descent of nearly 12 mbar in the first 6 hours for trajectory 1 shows that the air that moved out of the trough continued to subside in the middle troposphere. Trajectories 2 and 3 illustrate the middle tropospheric divergence north of Camille. Air moving out of the area of divergence subsided during the first 3 hours, but as seen in trajectory 3, air parcels moving out ahead of the trough moved into an area of ascending motion. Trajectory 4 depicts the subsidence further downstream west of Camille. Here, under the influence of the Laplacian of horizontal cold air advection, the air continued to subside throughout the period. Thus, in the

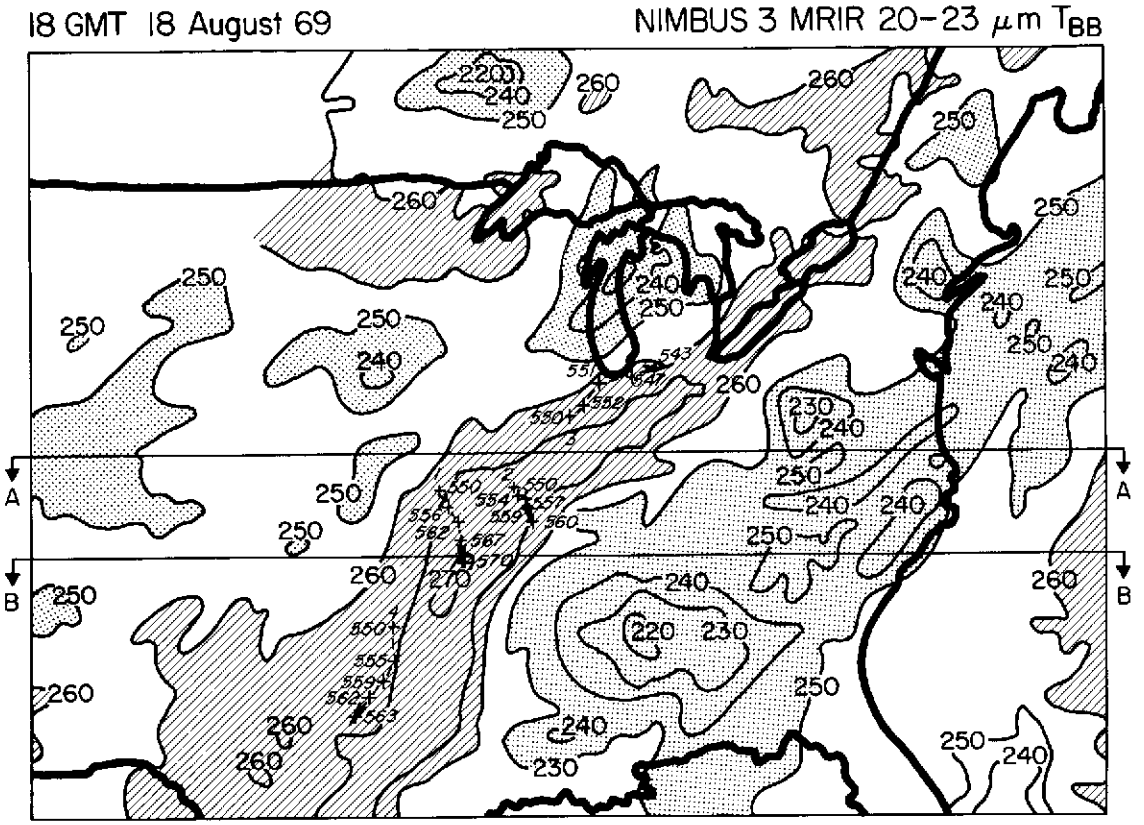

Figure 50. Three-dimensional trajectories between 1200 GMT on August 18, 1969, and 0000 GMT on August 19, 1969, initiated at the 550-mbar level superimposed upon the 20- to 23-μm T_{BB}'s at 1600 to 1900 GMT on August 18, 1969, from the MRIR sensor. The crosses represent the position of the air parcels at 3-hr intervals and the number to the side represents the pressure height.

middle troposphere, the trajectories suggest that there were again two tongues of subsidence that coincided with the warm T_{BB}'s, one moving northeast of the divergent area ahead of the trough and the other moving southwestward out of the trough.

Examining the local change of specific humidity for the same segment of cross sections A and B (Figures 46 and 47) that was examined for the upper troposphere, it is shown in cross section A that dry air extended downward to 600 mbar, where there was dry air resulting from subsidence. However, the horizontal advection of moist air from the northwest below 600 mbar essentially compensated for the drying by subsidence. Figure 47 shows that the loss of moisture in the middle troposphere was contained by both horizontal and vertical advection. As was found in the 6.5- to 7.0-μm T_{BB}'s, the warm 20- to 23-μm T_{BB}'s correspond favorably with the position of maximum middle level subsidence.

There are two regions where $T - T_d \leqslant 5$ K. One is associated with Camille and the other is over a portion of the northeast United States. In the western third of the latter area the low T_{BB}'s show the high clouds associated with thunderstorms over Pennsylvania. In view

of the westerly current, the small $T - T_d$ values east of the thunderstorms were probably the result of these storms and the westerly current that advected the moisture downstream.

Figure 51 indicates the amount of compressional heating caused by the subsidence at the 600-mbar level. In the dry air the temperatures were 277 to 278 K as compared with 274 K

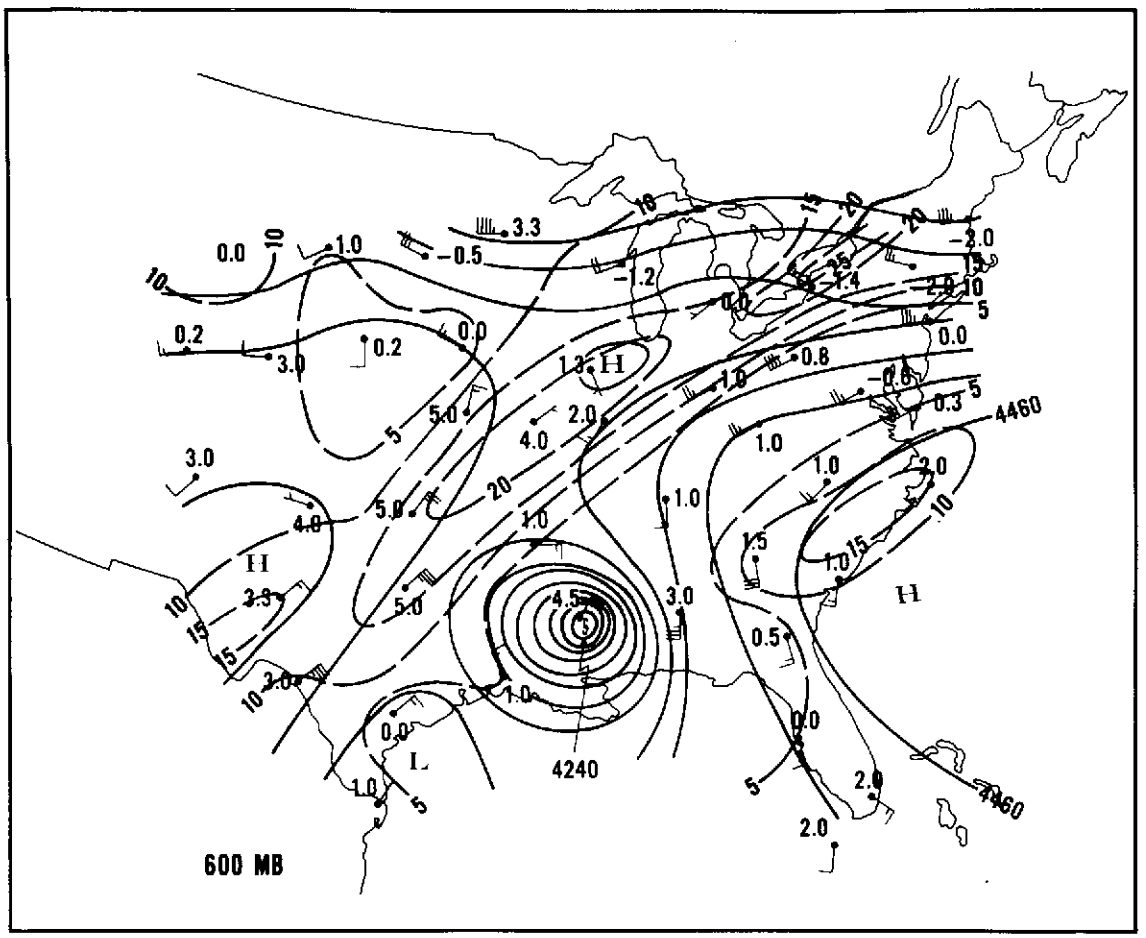

Figure 51. 600-mbar geopotential heights (in meters), dewpoint depression (in K) analyses, and radiosonde stations showing 600-mbar temperature and winds for 1200 GMT on August 18, 1969.

around the periphery of Camille. The dry air extended down to the 850- to 900-mbar layer underneath the region of maximum upper tropospheric horizontal convergence. Camille still appeared to be a warm core system in the middle troposphere, because the 277.5-K temperature measurement at Jackson, Mississippi, was 2 to 4 K warmer than the temperatures near the edge of the circulation. The time-lapse movie showed that the area of $T - T_d \leq 5$ K increased from low to middle levels with the most noticeable effect between 700 and 600 mbar. This could have been caused by the outward transport of moisture in response to high momentum air at low levels moving upward to a region of lower momentum near the center of a warm vortex.

In Figure 51 the 600-mbar wind at Little Rock had a pronounced radial component away from the storm center.

The time-lapse movie of the radiosonde measurements taken at 0000 GMT on August 19 showed that Camille had weakened further by the time the cyclone had reached extreme northern Mississippi. By then Camille had been downgraded to a tropical depression. The strong obstruction effect had almost disappeared, with the ambient upper tropospheric air moving eastward north of the cyclone and an anticyclone west of the center building eastward with a small ridge north of the storm center. These features are seen in the 300-mbar chart for 0000 GMT on August 19 (Figure 52). Despite the substantial reduction of the obstruction effect, the dry air created earlier was still present. With the change to a more zonal circulation north of Camille more of the dry air ($T - T_d \geq 15$) advected

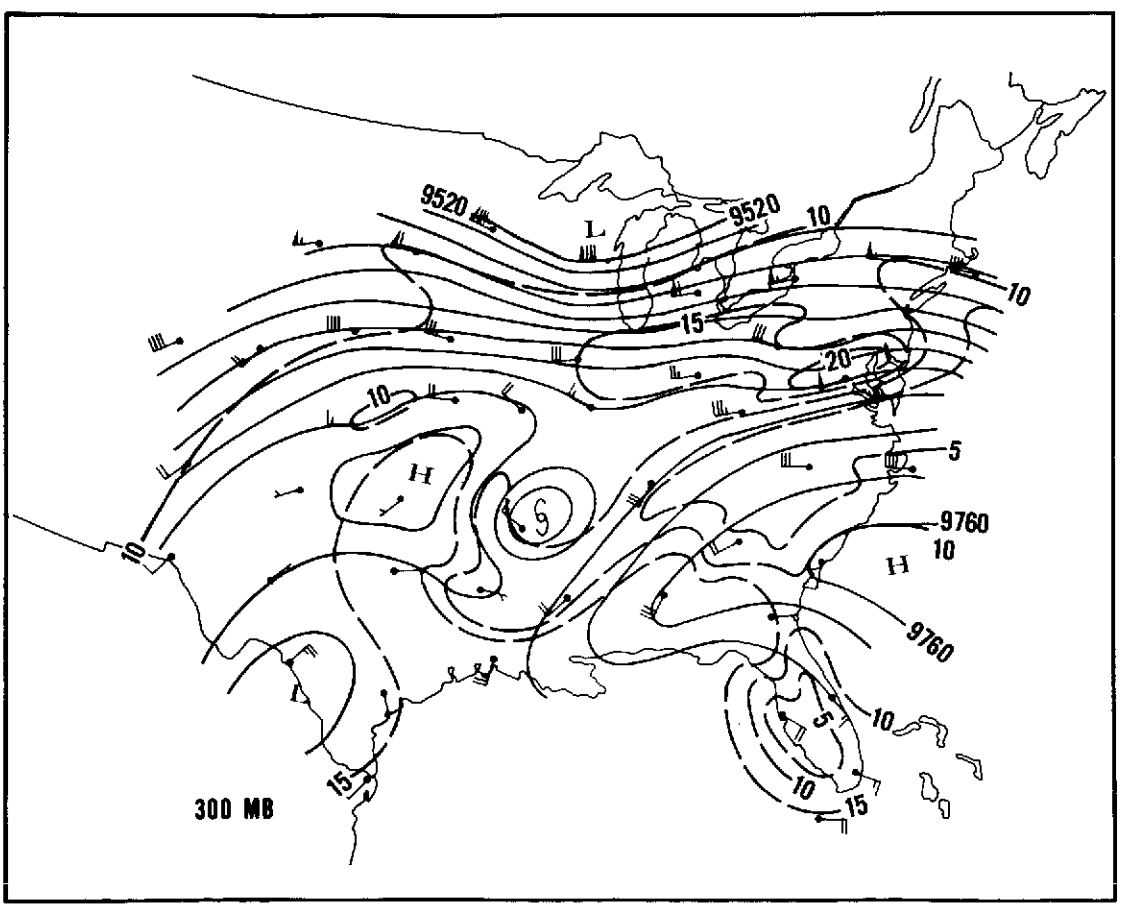

Figure 52. 300-mbar geopotential heights (in meters), dewpoint depression (in K) analyses, and radiosonde stations showing 300-mbar winds for 0000 GMT on August 19, 1969.

eastward over Indiana, Ohio, and some of the Middle Atlantic States. West and southwest of the center there was a large region of dry air which was most pronounced in the middle troposphere. This would indicate that no large-scale upward motion had begun. The 500-mbar chart for August 19 at 0000 GMT (Figure 53) illustrates the extent of this dry air and also that Camille acquired more of the characteristics of a cloud field seen with extratropical cyclones with the cloud mass principally northeast of the center.

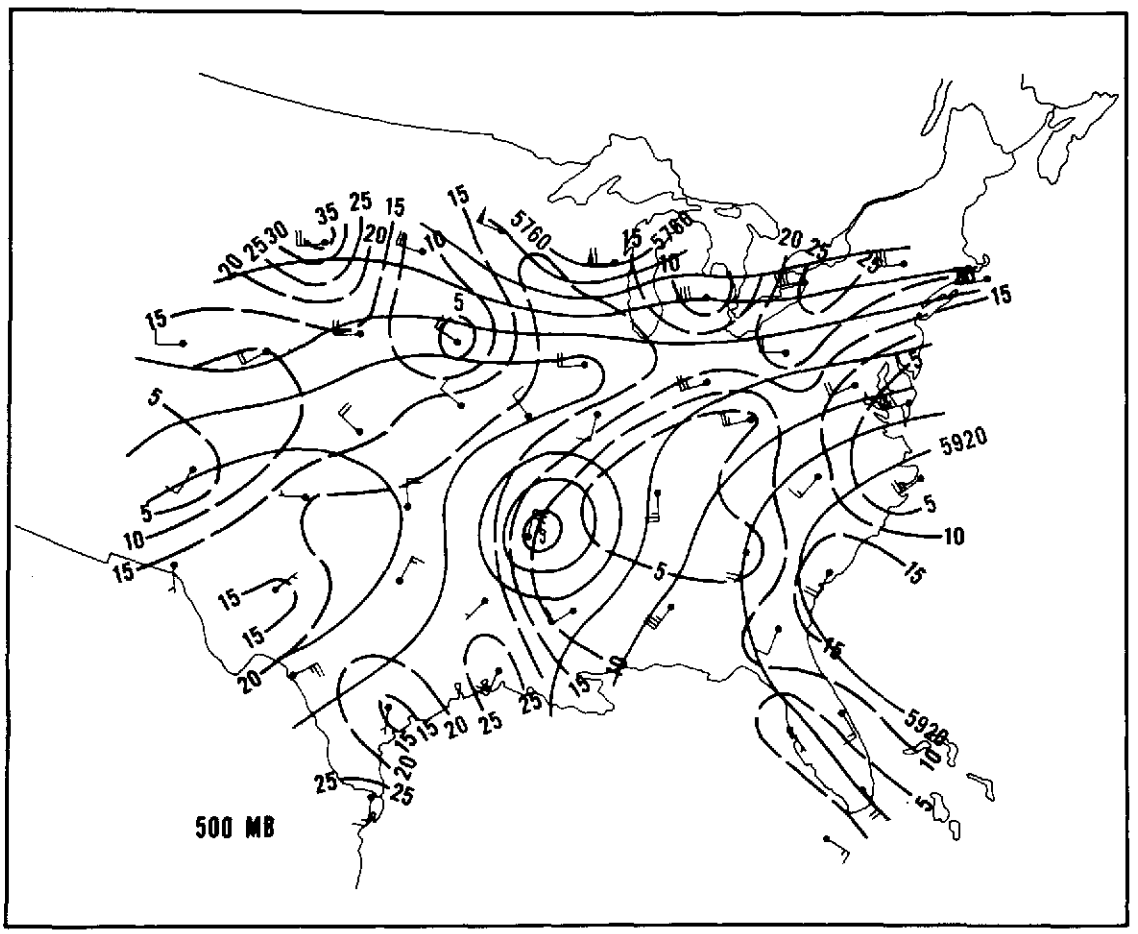

Figure 53. 500-mbar geopotential heights (in meters), dewpoint depression (in K) analyses, and radiosonde stations showing 500-mbar winds for 0000 GMT on August 19, 1969.

At 0000 GMT on August 19, 1969, the dynamics of the upper and middle troposphere had changed. With Camille weakening further and becoming more embedded into a more zonal westerly flow, the interaction between Camille and the westerlies had become weaker. Horizontal divergence calculations at all 10 levels revealed that there was an area of horizontal convergence at the 300-mbar level north of Camille; however, it is not part of the obstruction effect that was seen 12 hours earlier. The vertical motion patterns at 350 mbar as seen in Figure 54 indicate that the subsidence below the area of this maximum upper

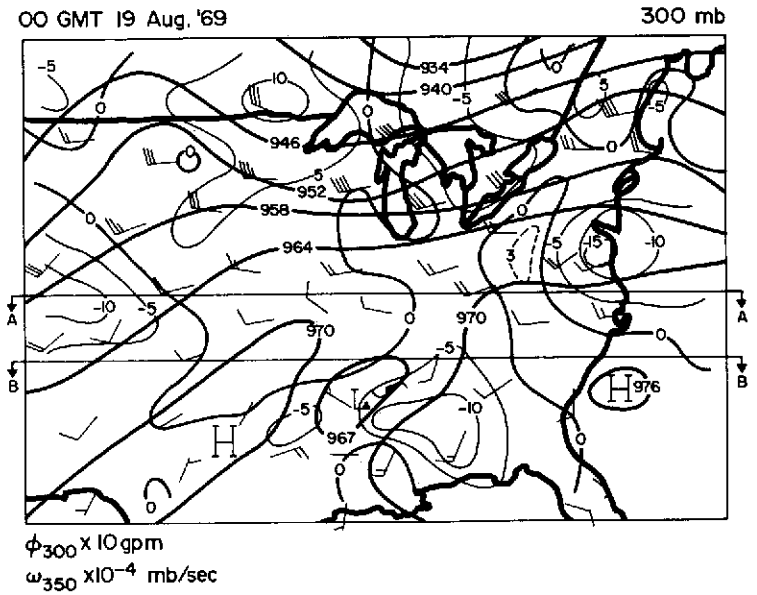

Figure 54. 300-mbar geopotential heights, winds, and 350-mbar vertical motions for 0000 GMT on August 19. Lines A and B denote cross sections A and B.

tropospheric horizontal convergence was quite weak. This subsidence can be attributed mainly to the differential advection of negative vorticity from around the anticyclone to the west. Cross section A (Figure 55)* indicates that the subsidence was considerably weaker and had shifted further west. The vertical extent, however, still extended through the troposphere and as depicted by the isolines of specific humidity, the column was still dry. Futher south, to the west and northwest of Camille (the area of the obstruction effect 12 hours before), subsidence was still present, but was mainly induced by the Laplacian of horizontal cold air advection. This area of subsidence does not extend as far southwestward as it did 12 hours earlier. Cross section B (Figure 56) reveals that the upper tropospheric subsidence had also weakened considerably, which indicates that the obstruction effect has decreased. However, the subsidence extended throughout the troposphere which continued to keep the column dry as seen in the isolines of specific humidity.

In the middle troposphere, vertical motion patterns associated with the interaction of Camille with the westerlies and with the trough north of Camille had also changed. Figure 57 indicates that subsidence at the 550-mbar level associated with the dissipating trough northwest of Camille was still present but had weakened. This subsidence was induced by both the Laplacian of horizontal cold air advection and the differential negative vorticity

*Cross sections A and B in Figures 55 and 56 respectively, intersect the same areas as in Figures 42 and 44.

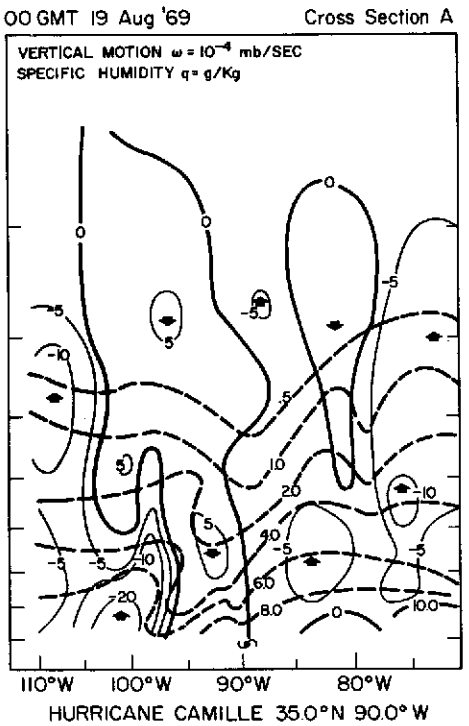

Figure 55. Cross section A, depicting vertical motions (solid lines) and specific humidities (dashed lines) for 0000 GMT, August 19, 1969.

advection. Cross section A (Figure 55) depicts this middle tropospheric subsidence. Further southwestward under the area of the obstruction effect that was present 12 hours earlier, both the vertical motion patterns on Figure 57 and cross section B in Figure 56 reveal that the subsidence had also decreased. The strong subsidence further west that is best seen in cross section B (Figure 56) was not associated with Camille or its interaction with the westerlies but was induced by the Laplacian of horizontal cold air advection from around the ridge west of Camille.

Excessive Rains Over the Central Appalachians

As Camille moved northeast and then east across western Tennessee and Kentucky it was a tropical depression producing moderate to locally heavy rainfall at stations close to the track of the center of 5 to 10 cm. However, as the storm center reached West Virginia, heavy rainfall began in west central Virginia around 0000 GMT on August 20 and continued for approximately 12 hours. Schwarz (Reference 2) has reported that the extreme rainfalls were associated with near record low-level moisture that was not subject to depletion by upwind mountain ridges. The Appalachians contributed to the large local amounts (as high as 69 cm) because the low-level flow was from the southeast, perpendicular to the mountain range. Upper tropospheric horizontal divergence is another important condition that would favor regeneration of the cloud mass and lead to the production of heavier precipitation. A strong field of horizontal divergence is present just

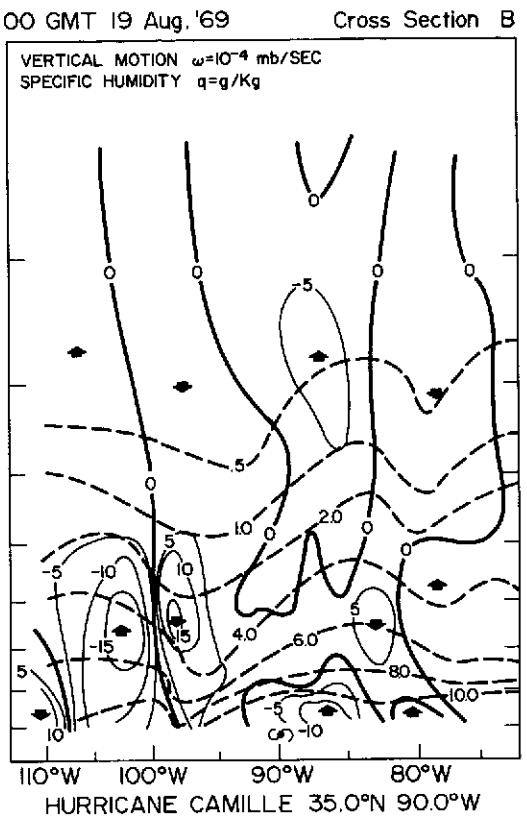

Figure 56. Cross section B, depicting vertical motion (solid lines) and specific humidity for 0000 GMT on August 19, 1969.

northeast of the cyclone center as shown by the 200-mbar chart in Figure 58 for 1200 GMT on August 19 (about 12 hours before the high rainfall rates began). Both speed and direction divergence were present.

The regeneration of the cloud mass was best seen by the Nimbus-3 HRIR which observed Camille's cloud canopy at 24 hour intervals for 2 days before and during the excessive rain period.

Figure 59 provides a standard of reference for the two later HRIR views of Camille as the cyclone was moving ashore on the Mississippi Coast. A large spiral band is seen south of the storm center and the lowest 3.5- to 4.1-μm T_{BB}'s are $\leq$ 210 K over a small area near the center. A maximum cloud-top height of 125 mbar (15.4 km) can be inferred from the minimum T_{BB} and the 0000 GMT, August 18, Lake Charles temperature profile.

Twenty-four hours later the greatly weakened cyclone was over western Tennessee. The HRIR view (Figure 60) indicates that the cloud pattern was more disorganized with the

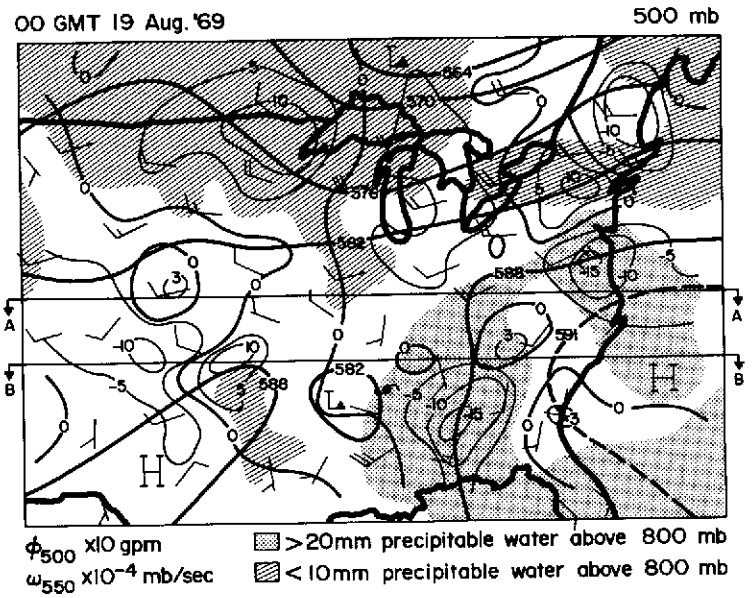

Figure 57. 500-mbar geopotential height, wind, 550-mbar vertical motion, and integrated precipital water above 800 mbar for 0000 GMT on August 19. Lines A and B denote cross sections A and B.

highest clouds (lowest T_{BB}'s) about 300 km northeast of the center. There has been an increase in the minimum T_{BB} to about 215 K. Using the 0000 GMT, August 19 sounding at Nashville, this T_{BB} measurement would mean the maximum cloud top was at 180 mbar (13.2 km). Thus, there was an apparent reduction in the maximum cloud top height of 2.2 km in 24 hours.

The third and final HRIR view of the series (Figure 61) is at the time of the excessive rainfall. Most of the intense cloudiness (as outlined by the area where the T_{BB}'s were $\leqslant$ 230 K) was north and east of the center similar to the position of the cloud shield for an extratropical cyclone. There were several areas where the T_{BB} values were $\leqslant$ 210 K with a minimum of 203 K. Therefore, the maximum cloud top height had returned to the 125-mbar (15.4-km) level which was the maximum cloud top level when Camille was still a severe hurricane, shortly after crossing the Mississippi coast.

Extratropical secondary storm development has occurred when there was a significant vertical cloud growth within a large existing cloud mass; this growth can precede the detection of the new cyclone over the ocean with conventional data (Reference 13). In the case of Camille, the vertical cloud growth to high levels was noticeable when the heavy rains were in progress. Since the HRIR observation interval is 24 hours it is not possible to determine whether or not the clouds reached the observed 0600 GMT, August 20 levels before or at the onset of the period of maximum rainfall rate. If infrared measurements would have been available on a nearly continuous basis from a geosynchronous satellite, it is possible

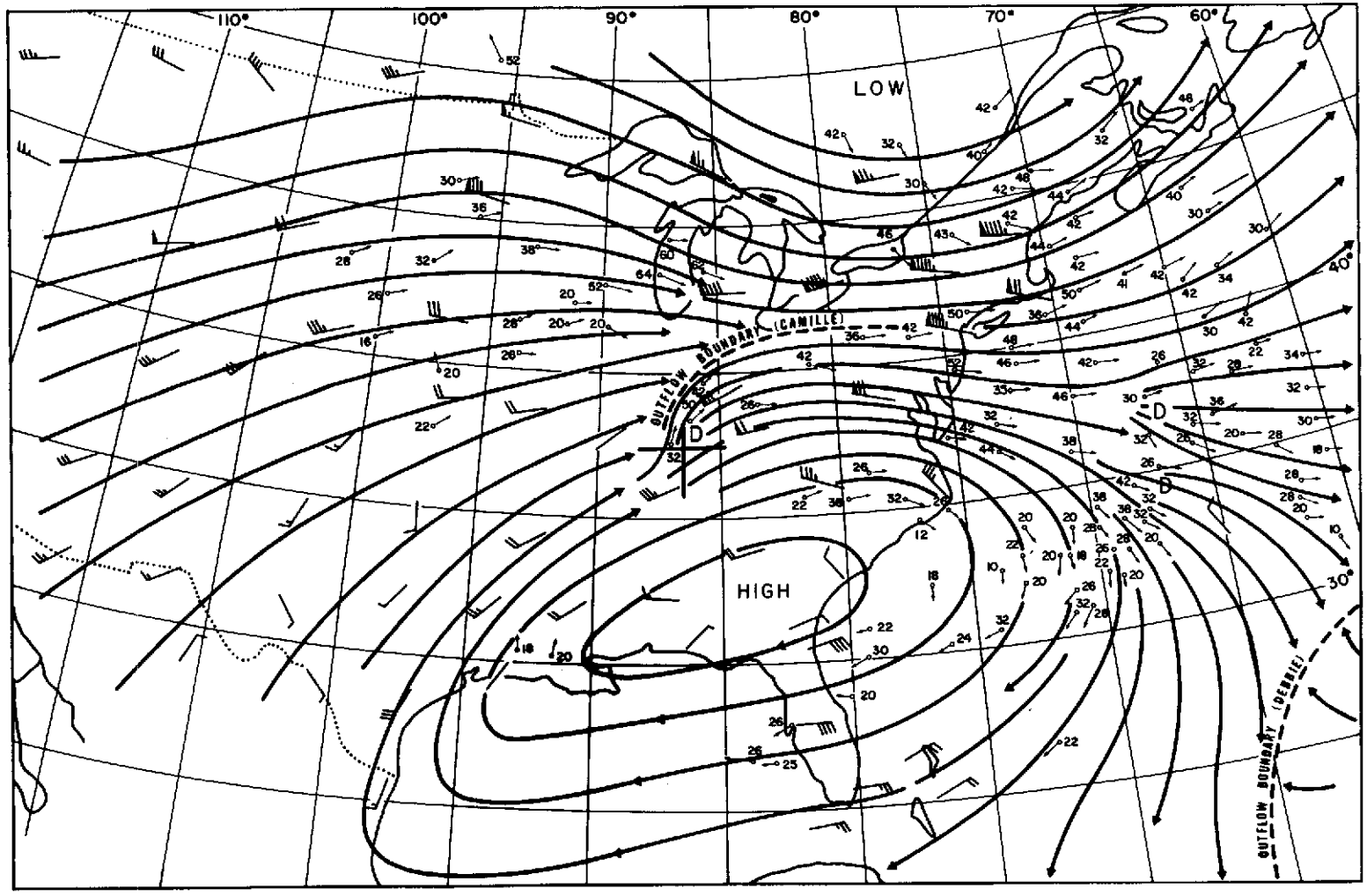

Figure 58. 200-mbar streamlines as derived from radiosonde wind observation and ATS middle and upper cloud motion for 1200 GMT on August 19, 1969. The cloud motion directions are indicated by the arrows and the speeds are given in knots.

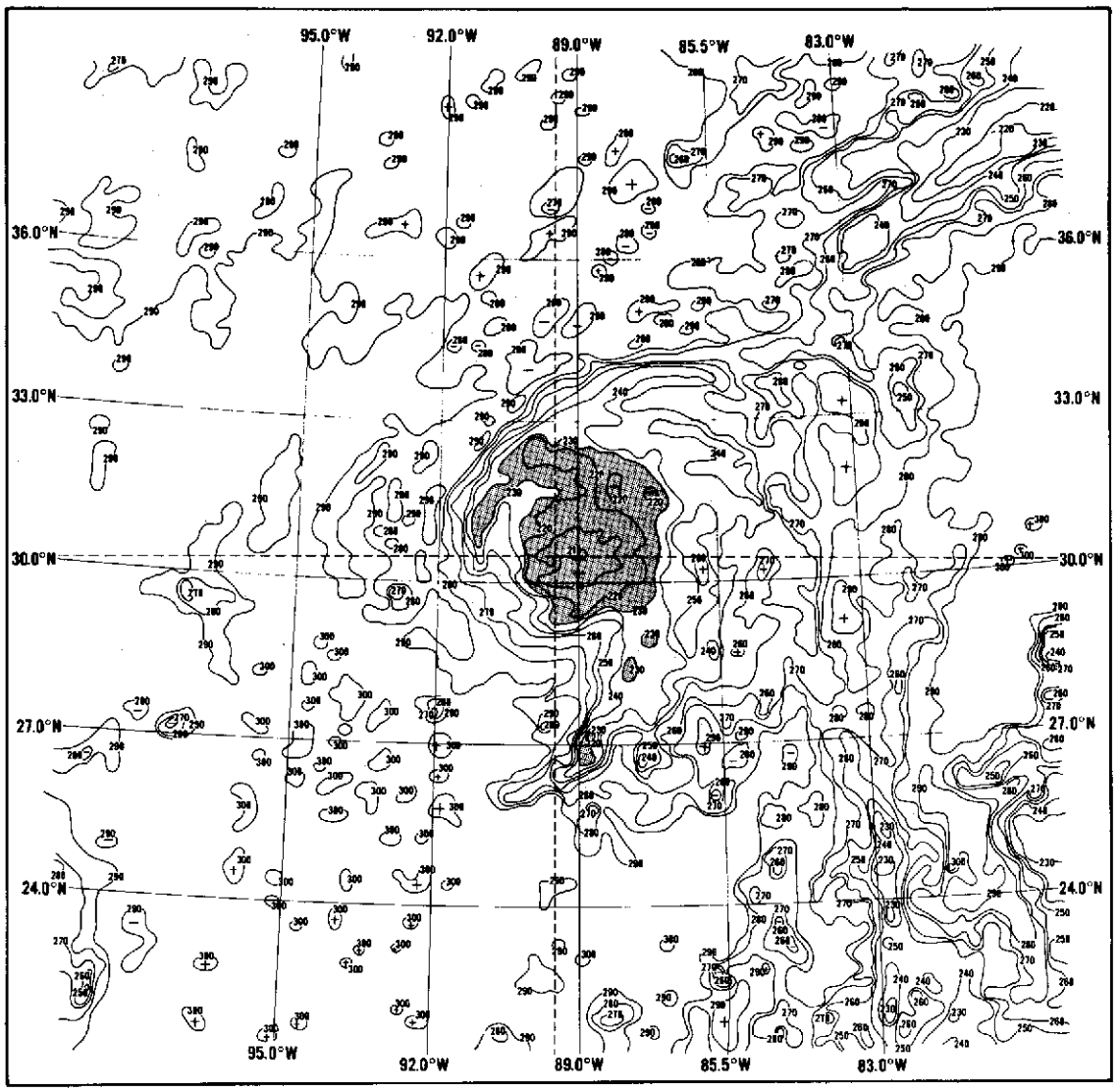

Figure 59. Hurricane Camille at 0540 GMT on August 18, as depicted by 3.5- to 4.1-μm T_{BB}'s from the HRIR. The isotherms are given in K.

that flood warnings could have been issued based on the change in, and/or the absolute levels reached by the cloud tops. Both the Washington and Pittsburgh radars observed the strong echoes at ranges of generally $\geq$ 200 km. Schwarz (Reference 2) concluded that the measurements did indicate the presence of the important vertical motions. However, if the rainfall activity had been outside of effective radar range, then most likely the satellite measurements would have been the only source of information with a timely observation interval.

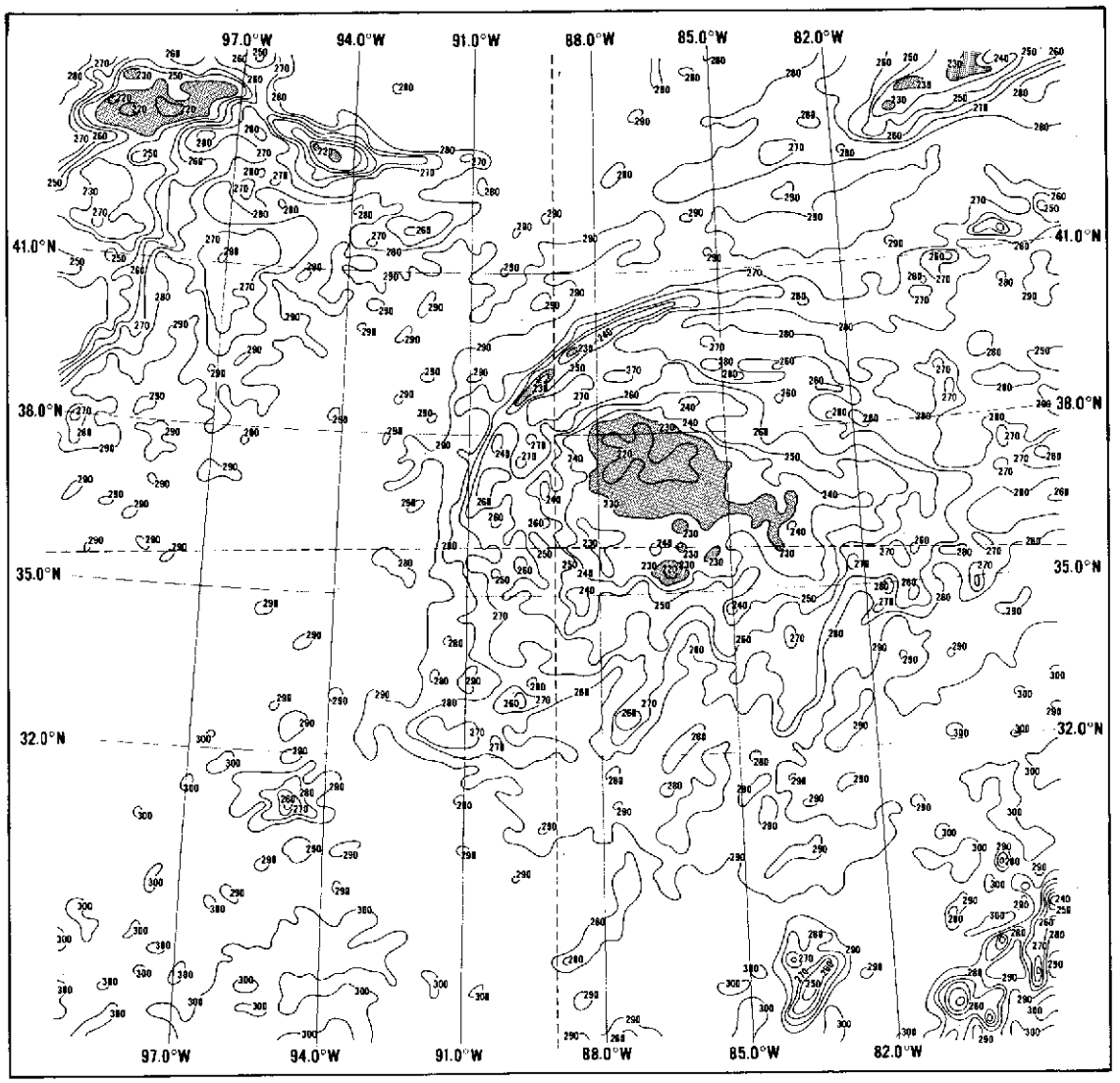

Figure 60. Tropical depression Camille at 0450 GMT on August 19, 1969, as depicted by 3.5- to 4.1-μm T_{BB}'s from the HRIR. The isotherms are given in K.

CONCLUSIONS

Prior to the rapid deepening phase of Camille there was the development of strong low-level inflow of high moisture content air from the region near the ITCZ moving over a sea surface with temperatures 1 to 3 standard deviations above normal. The concurrent development of large-scale cloud bands southeast of the center extending to the cirrus level was the satellite evidence of the inflow. Just before the onset of the rapid deepening, the cloud bands showed a broad connection to the cloudiness within the ITCZ, and the 6.5- to 7.0-μm water vapor channel indicated the outflow of cirrus to the north of the center which was associated with the necessary ventilation of air away from the cyclone. It was possible to ascertain

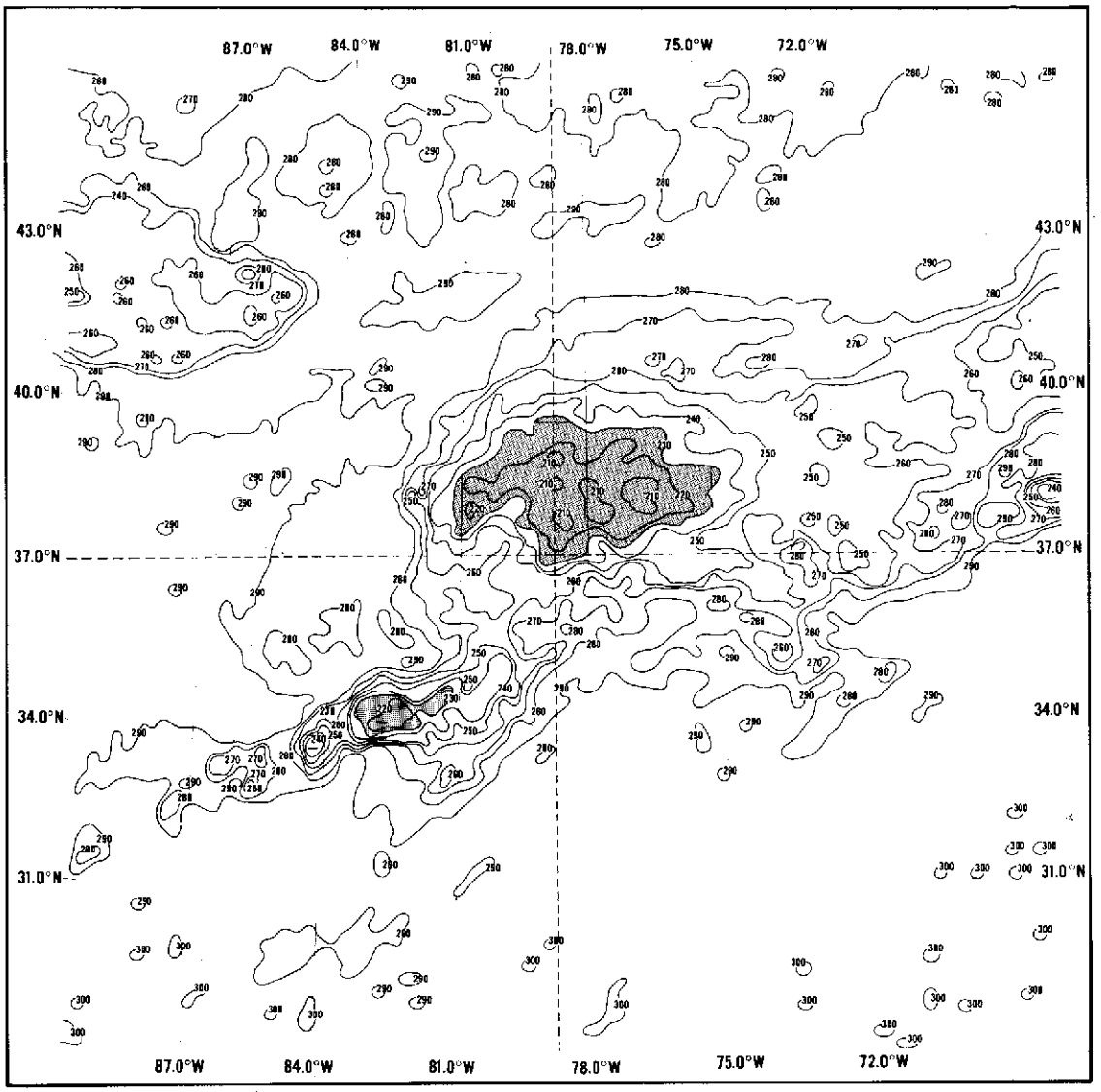

Figure 61. Tropical depression Camille at 0550 GMT on August 20, 1969, as depicted by 3.5- to 4.1-μm T_{BB}'s from the HRIR. The isotherms are given in K.

the relative strength and position of the important features such as upper tropospheric shear lines and easterly waves with the combination of Nimbus-3 MRIR channels and continuity.

During the rapid deepening phase the cloud bands southeast of the center continued to persist. At the beginning of the rapid deepening, the size of the intense cloud region associated with Camille sharply contracted and then expanded again as the maximum deepening rate occurred. Simultaneously, a large area of subsidence developed west and north of the center. The subsidence extended from the upper troposphere vertically downward to at least the low cloud level as inferred from the measurements made by four of the MRIR channels. Neither the expanded cloud shield nor the large subsidence region seemed to

persist for more than 24 hours, leading to the hypothesis that that the rapid deepening was associated with a sudden surge that extended past an energy level that was sustainable. There was a 2- to 3-km reduction in maximum cloud top level about 12 hours after Camille moved inland in response to the probable weakening of the vertical circulation within the inner portion of the cyclone. The outflow acted as an obstruction to the environmental flow in the upper troposphere northwest of the center of Camille. This interaction produced horizontal convergence and subsidence. The effects of the subsidence could be seen in the two water vapor channels where the subsidence areas were demarcated by T_{BB}'s that were initially relatively high and were increasing with time. A smaller region of dry air produced by a shear line east of Camille was not seen as clearly in the satellite measurements as the area northwest of the center due to the cirrus clouds in the outflow region overriding the dry air.

As Camille turned eastward across the lower Ohio valley, the cloud pattern looked like that of a small vigorous extratropical storm with maximum cloud tops at 13 to 14 km, and the interaction between the outflow and the environmental flow had diminished considerably. Speed and direction divergence in the upper tropospheric wind field determined from conventional and cloud motion measurements was an indication that conditions were favorable for renewed vertical cloud development as early as 1200 GMT on August 19. When the excessive rainfall was in progress over Virginia, the cloud tops had risen to 15 to 16 km, which was the level reached when the cyclone was still a severe hurricane just after crossing the Mississippi coast.

This investigation of Camille has attempted to indicate the knowledge that can be gained with (a) multispectral analysis of registered satellite measurements of reflected and emitted infrared radiation; (b) the combination of polar orbiting and geosynchronous satellite and conventional information; and (c) the use of the time domain.

Some of the hypotheses that emanated from the interpretation of the satellite data could not be confirmed due to the lack of supporting conventional information. With the flight of multispectral sensors on future geosynchronous satellites, the increased temporal resolution will undoubtedly improve the understanding of tropical cyclone circulation features beyond what was possible with a 12-hour observation interval. The observations with the spacecraft instrument should be combined with the concurrent collection of in situ, remote earth-based or aircraft measurements of sufficient quality to more effectively interpret the satellite information.

ACKNOWLEDGMENTS

The authors wish to thank Professor Tetsuya T. Fujita, University of Chicago, who computed the cloud motions, performed streamline analyses from the results, and made numerous helpful suggestions. The analyses of the radiation and conventional charts by David Simmes, Allied Research Associates, and Mark Smith, GSFC, are also appreciated.

Goddard Space Flight Center
National Aeronautics and Space Administration
Greenbelt, Maryland, August 10, 1973
039-23-01-01-51

REFERENCES

1. Simpson, R. H., A. L. Sugg, and Staff, "Atlantic Hurricane Season of 1969," *Mo. Weather Review*, **98**, 1970, pp. 307-314.

2. Schwarz, F. K., "The Unprecedented Rains in Virginia Associated with the Remnants of Hurricane Camille," *Mo. Weather Review*, **98**, 1971. pp. 851-859.

3. Nimbus Project, *Nimbus-3 Users Guide,* National Space Science Data Center, Goddard Space Flight Center, Greenbelt, Md., 1969, p. 237.

4. Hubert, L. F., and L. F. Whitney, "Wind Estimation from Geostationary-Satellite Pictures," *Mo. Weather Review*, **99**, 1971, p. 665.

5. Shenk, W. E., H. Powell, V. V. Salomonson, and W. R. Bandeen, "Meteorological Uses of the Stereographic Horizon Map Projection," *J. Appl. Meteor.*, **10**, 1971, pp. 582-589.

6. Rodgers, E. B., and V. V. Salomonson, "Upper Tropospheric Dynamics as Reflected in Nimbus-4 THIR 6.7-μm Data," NASA Technical Note D-7493, 1973, p. 27.

7. Shenk, W. E., and R. J. Holub, "A Multispectral Cloud Type Identification Method Using Nimbus-3 MRIR Measurements," *Preprint Volume of the Conference on Atmospheric Radiation,* 1972.

8. U. S. Naval Oceanographic Office, *Oceanographic Atlas of the North Atlantic Ocean*, Pub. No. 700, Washington, D. C., 1967.

9. Tatehira, Ryozo, "A Study of Rainband," *Japan Meteorological Agency*, **34**, 1967, pp. 115-137.

10. Gentry, Cecil, "A Study of Hurricane Rainbands," National Hurricane Research Project No. 69, 1964, p. 85.

11. Barr, S., P. E. Long, and I. A. Miller, "Atmospheric Sensing and Prediction Projection Project," Scientific Report No. 2, Air Force Cambridge Research Laboratories, Air Force Systems Command, U. S. A. F., Bedford, Mass., 1970.

12. Palmen, E., and C. W. Newton, *Atmospheric Circulation Systems,* Academic Press, New York and London, 1969, pp. 379-386.

13. Shenk, W. E., "Meteorological Satellite Infrared Views of Cloud Growth Associated with the Development of Secondary Cyclones," *Mo. Weather Review,* **98**, 1971, pp. 861-868.

APPENDIX

RELATIONSHIP BETWEEN BRIGHTNESS AND CLOUD-TOP TEMPERATURE

From the comparison of the 0.2- to 4.0-μm normalized reflectances and the 10- to 11-μm T_{BB}'s on August 18 over the Camille cloud canopy, it was observed that when the reflectances were near 70 the T_{BB}'s were around 230 K, whereas when the reflectances were near 60 they were concomitant with T_{BB}'s from 225 to 260 K. From these observations it was hypothesized that there might be a relationship between reflectance and the range of 10- to 11-μm T_{BB}'s, where, at extremely high reflectances, this range might be small. When reflected energy channel spatial resolution is much higher than that of the infrared window channel, a relationship could be useful in isolating the regions where the highest clouds occur and for the interpretation of a registered infrared measurement. A specific example of a large resolution difference between these two channels will be on the Synchronous Meteorological Satellite (SMS) where the visible and infrared channel spatial resolutions will be 0.9 and 9.0 km, respectively.

The MRIR reflectance window channel relationship shown in Figure A-1 was established through the use of daytime data for August 18 that was associated with the ITCZ south of Camille. This region was chosen because a relatively large percentage of the data samples had normalized reflectances of $\geqslant 60$. Figure A-1 indicates that the spread of the 10- to 11-μm measurements decreases as reflectance increases. The range of T_{BB}'s when $R \geqslant 73$ is only 15 K and the maximum T_{BB} was 212 K. An upper boundary could be drawn in Figure A-1 that would connect the highest T_{BB}'s for a given reflectance. Thus, these data suggest that extremely high reflectances can provide some estimate of the window T_{BB}'s in regions of deep convection.

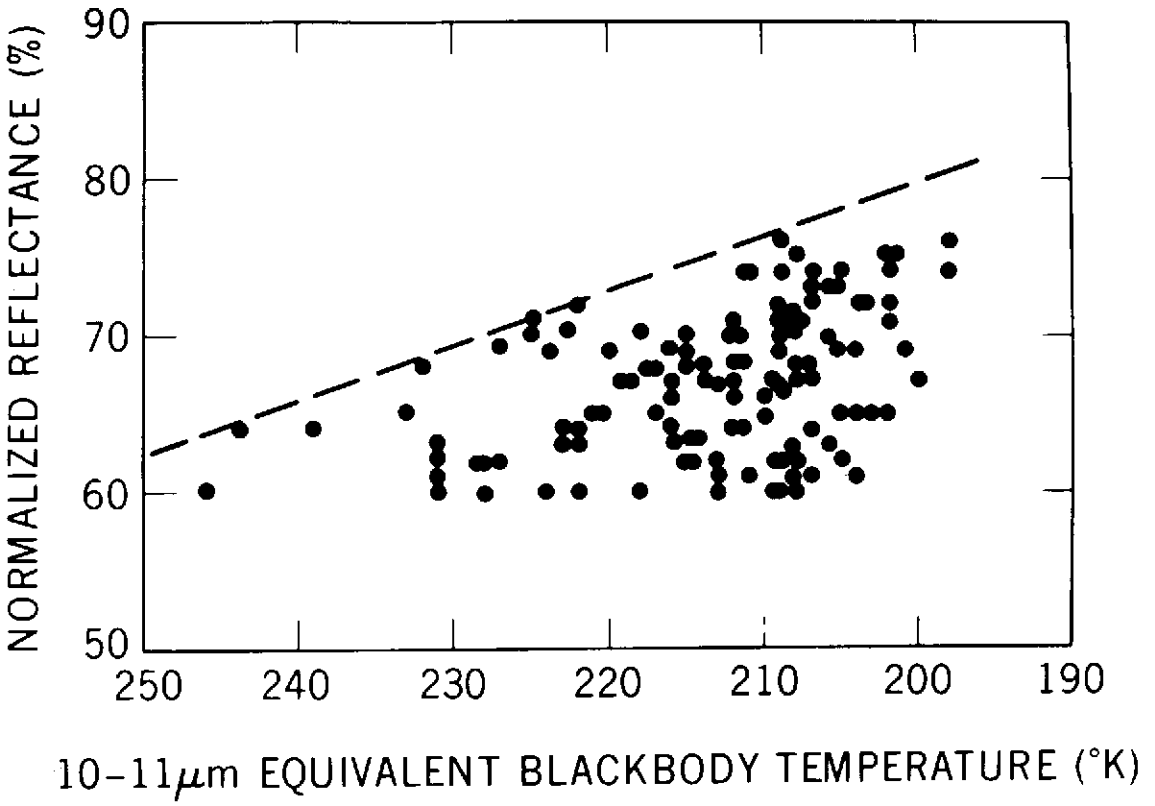

Figure A-1. Plot of concurrent normalized reflectance measurements and 10- to 11-μm T_{BB}'s in the Intertropical Convergence Zone south of Hurricane Camille during the daytime on August 18, 1969.